Power-to-heat integration in a combined heat and power installation to provide flexibility to the Dutch grid.

Femke Mirjam van Deursen

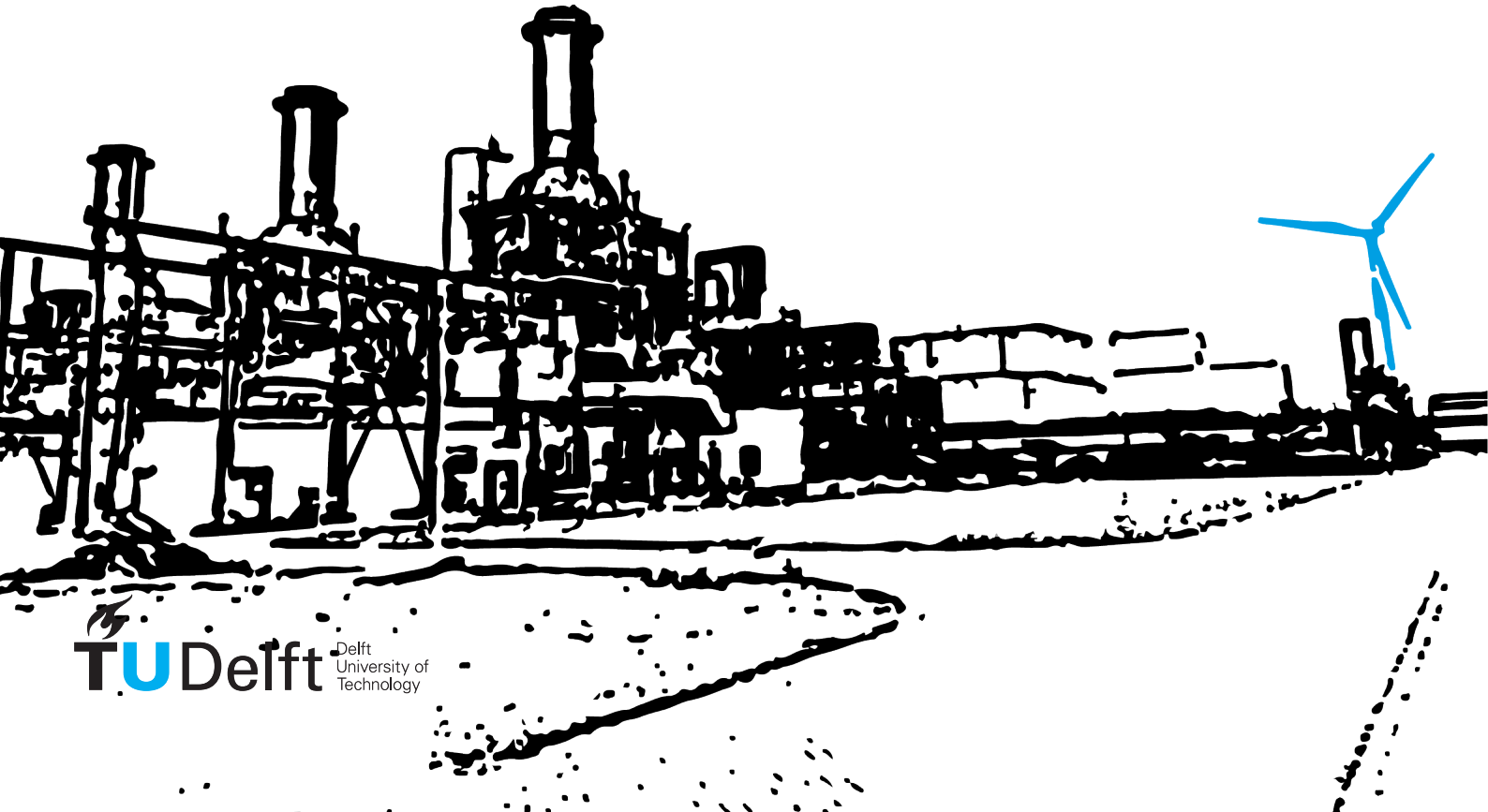

TU Delft Delft University of Technology

Power-to-heat integration in a combined heat and power installation to provide flexibility to the Dutch grid.

by

Femke Mirjam van Deursen

to obtain the degree of Master of Science
at the Delft University of Technology,
to be defended publicly on Friday November 23, 2019 at 9:00 AM.

Student number:	4010744	
Project duration:	April 1, 2017 – November 23, 2018	
Thesis committee:	Prof. dr. ir. S. Klein,	TU Delft, supervisor
	Dr. ir. R. M. Stikkelman,	TU Delft
	ir. D. Berghuis,	Nouryon
	ir. N. Dijkstra,	Stork Thermeq

This thesis is confidential and cannot be made public until November 23, 2024.

TU Delft Delft University of Technology

"Failure is unimportant. It takes courage to make a fool of yourself."
- *Charlie Chaplin* -

Abstract

The increase in the share of renewable energy sources in the Dutch energy mix, requires an increase in flexibility from the power consumers and producers. A key issue in the availability of wind and solar power that it is independent of the power demand. Fortunately, the liberalised power market provides a financial incentive to increase both upward and downward flexibility.

Delesto is a company that supplies process steam at ChemiePark Delfzijl. They are looking into the possibility to integrate power-to-heat (P2H) in their Combined Heat and Power installation (CHP). This would open up the possibility to decrease the power output of the plant beyond deep part load conditions, and to save on overall fuel consumption. This would be beneficial for periods where profits made from power production drops below the cost of fuel consumption. For this research it is assumed that the power used is emission free, as it originates from renewable energy sources.

In this study, the technical and financial feasibility of an hybrid configured combined heat and power plant, in which both gas and power are used to produce process heat, is researched. The CHP consists of a gas turbine (GT), a dual pressure heat recovery steam generator (HRSG) and a steam turbine (ST). Eight different configurations that offer P2H functionality to the CHP are being assessed. The electric heater concepts are compared to the 'conventional' part-load of the CHP. Their steady state behaviour is evaluated using parameters such as Additional Flexibility (AF) and Effectiveness of fuel saving (ε). A duct heater inside the HRSG offers the greatest AF, whereas an air preheater upstream of the GT performs best in terms of effectiveness. Additional to the initial eight electric heater concepts, the combinations of air preheater with other promising electric heater concepts are evaluated.

A dynamic study of (a part of) the HRSG including an electric heater is performed. Only the most promising electric heater concepts in terms of the steady state behaviour are reviewed. From this dynamic study it can be concluded that the minimum ramp time is of the HRSG is well within the requirements of the grid operator. However, a high pressure boiler parallel to the high pressure evaporator of the HRSG results in relative high temperature drop in the system compared to the other electric heater concepts, and is therefore removed from further consideration.

From a financial analysis, a business case is constructed for an air preheater, a duct heater, a stand-alone boiler and their combinations. It is apparent that the profits obtained at the spot market are negligible compared to the profits obtained at the imbalance market. Transportation costs are relatively high and have a damaging effect on the business case. The payback period of the air preheater is the shortest and the payback period of the duct heater the largest.

Acknowledgements

I am very glad that I got the opportunity to work at Delesto. It was very helpful to be able to study the technology so close to the actual plant. I would like to thank Gerard van de Putte and David Berghuis of Delesto, for making me feel welcome in their engineering team. They provided me with the practical knowledge I needed to start my research with confidence.

I would like to thank my supervising professor, Sikke Klein, for providing me with guidance throughout the entire project. I thank you for your patience and the time you have invested. I am very grateful that I got a chance to collaborate in writing a paper.

Thank you, Nutte Dijkstra for the pleasant conversations at Stork Thermeq. You have acted as a sounding board for my thoughts on the project. During our meetings you provided me with useful insights for the further development of my research.

I would like to thank Boudewijn, for being there with me on my personal journey. I would like to thank my friends for making my many years as a student worthwhile. Last, but not least, I would like to thank my parents, who taught me the skills of curiosity and kindness. Both skills were essential throughout my study.

Femke Mirjam van Deursen
Delft, November 2018

"Failure is unimportant. It takes courage to make a fool of yourself."
- *Charlie Chaplin* -

Contents

List of Figures

List of Tables

Nomenclature

Abbreviations

AF	Additional flexibility
AFS	Absolute fuel savings [MW]
AP	Air preheater
CAPEX	Capital expenditure
CHP	Combined heat and power installation
CO_2	Carbon dioxide
CPD	Chemie Park Delfzijl
DH	Duct heater
EH	Electric heater
EU ETS	European Union Emission Trading System
FHDB	Fuel heater in duct burner
FHGT	Fuel heater in gas turbine
GT	Gas turbine
GT-HRSG	The combination of a gas turbine and an heat recovery steam generator
HP	High pressure level (88.0 bar)
HPB	High pressure boiler
HPP	High pressure pump
HRSG	Heat recovery steam generator
IP	Intermediate pressure level (30.5 bar)
LP	Low pressure level (4.2 bar)
LPB	Low pressure boiler
NO_x	Nitrogen Oxides
NPO	Net power output
O_2	Dioxide
ODE	Ordinary differential equations
OPEX	Operational expenditure
P2H	Power-to-heat
PI	Proportional Integral
PTU	Programme Time Unit (1 PTU = 15 minutes)

RES	Renewable energy sources
SB	Stand-alone boiler
ST	Steam turbine

Greek Letters

α	Heat transfer coefficient [W/(m^{2}K)]
Δ	Difference between two points of a certain quantity [1]
ϵ	Strain [1]
ε	Effectiveness of electric heater [1]
η_{th}	Thermal efficiency [1]
ρ	Density [kg/m^3]

Symbols

A	Heat transfer area [m^2]
C	Cost [€]
c_p	Specific heat capacity [J/kg]
CR	Circulation ratio of the HP evaporator [1]
E	Energy [J]
ε	Tolerance [1]
V	Gravitational acceleration [m^2/s]
H	Fuel consumption [MW]
h	Enthalpy [J/kg]
I	Electric current [A]
KE	Kinetic energy [J]
$\dot{m}$	Mass flow [kg/s]
M	Mass [kg]
n	Time step [1]
p	Pressure [Pa]
p	Solution of the system
PE	Potential energy [J]
P	Electrical power [MW$_e$]
p	Price [€/MWh]
$\dot{Q}$	Heat [W]
R	Resistance [Ω]
RFS	Relative fuel savings [1]

RSL	Relative stack losses [1]
T	Temperature [K]
TEC	Thermal expansion coefficient [K^{-1}]
$\tilde{t}$	Characteristic time scale [s]
t	Time [s]
U	Internal energy [J]
u	Specific internal energy [J/kg]
v	Velocity [m/s]
$\dot{W}$	Work [W]
z	Elevation [m]

Subscripts

1	Operation mode 1 (see table 5.2)
1	Operation mode 2 (see table 5.2)
E	Entering
fg	Flue gas path
HE	Heat exchanger
i	Cell number
inj	Flow is injected in the desuperheater
L	Leaving
c2c	Coil-to-coil
r2r	Row-to-row
tot	Total
w	Water/steam path
$tube$	Tube wall material

1 Introduction

As a result of the Paris agreement (2015, COP21) and the antecedent European 20-20-20 targets for 2020 and its additional mid- and long term objectives for respectively 2030 and 2050, renewable energy sources (RES) such as wind and solar energy will obtain a more prominent role in the Dutch energy mix in the upcoming years. Up until now the Netherlands had difficulties staying on track for the targets on renewable energy [1]. To show the world and the Dutch citizens that the Netherlands is serious about contributing to a sustainable energy infrastructure, the government published new policy that surpasses the agreements of the European Union [2]. In 2030 the emission of carbon dioxide has to be reduced with 49% with reference to the emissions in 1990. The government only steers in the direction of carbon dioxide reductions, as it believes that energy savings will result from that [3].

Among other things, the new policy includes plans for expending the off-shore wind power capacity. The North Sea strategy for 2023 and later is shown in figure 1.1. The total growth of capacity in the North Sea between 2024 and 2030 will roughly be 7 GW, compared to a operational capacity of 957 MW in 2016. This increase is a great deal and a big step towards a more RES dominated power system. However an increase in the share of RES in the energy mix brings along some complexity and the produced power could even be perceived as undesired. In section 1.1 this phenomenon is explained and the importance of flexibility is stretched.

Another component of the policy is to stimulate industries to increase the yearly energy savings rate from 1.1 % to 1.5% [4]. In the Netherlands, two-third of the final energy usage by companies is used by the industry, while the industry only makes up for 4% of the companies. Almost half of the energy used in the industry is used for heating purposes [5]. One can imagine that the energy intensive industries are the focus of the Dutch government in its efforts to reach the targets regarding the sustainable growth. The basic assumption is that the energy saving agreements with a return on investment smaller than 5 years are already in operation. The energy intensive industries (1100 companies) set up energy-efficiency plans with a return on investment of more than 5 years. These measurements became a necessity when it became apparent that the original agreements from 2013, Energieakkoord (Agreement on Energy for Sustainable Growth), were not enough. The energy intensive industries have the mere motion to make individual agreements with the government. Amongst these large scale consumers is AkzoNobel, which is further introduced in section 1.3.

1.1. Flexibility

In the year 2016, the total energy consumption of the Netherlands was for 5.9 % from renewable sources [6]. This has to increase to 14 % in 2020 and 16% in 2023 as is agreed upon in the Energieakkoord [4]. With conventional power systems the demand and supply of electricity were more or less coupled. Electricity was only generated if there was a demand for it. The cheaper means of producing electricity were deployed first, and with the increase in demand, more expensive producers went online. The price of electricity reflected these market forces. However, RES have relatively low operational costs, therefore the generation of electricity from wind and solar are to a great extent unaffected towards electricity prices on the market [7]. Production takes place regardless of the demand. Hence, the increasing share of RES in the energy mix has some implications on the fluctuations of load on the grid.

Models can help to predict the generation from RES. Conventional power systems could react on the

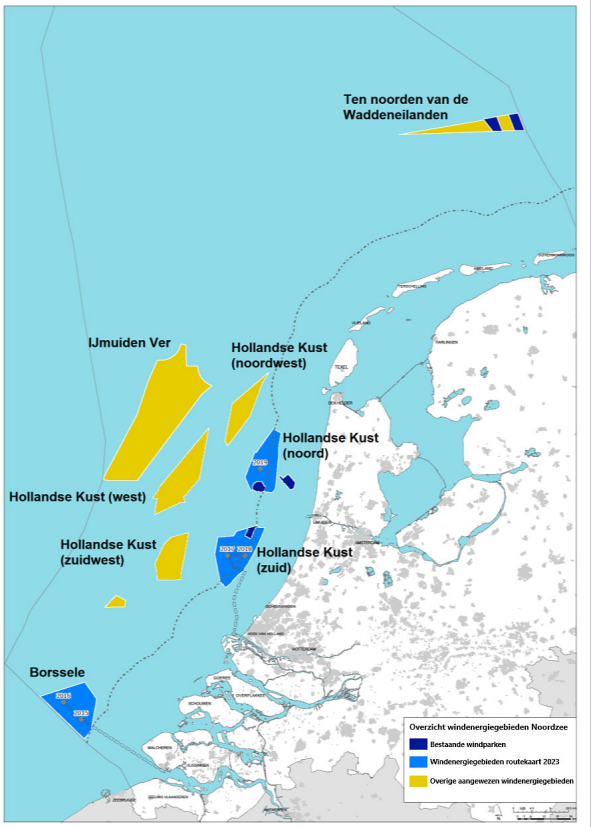

Figure 1.1: North Sea Strategy for Wind at Sea 2030

prospected supply, by shifting its load the opposite way. However, contingent imbalances in supply and demand of electricity will still arise, due to the error made in forecasting the generation of renewable electricity [8]. This error makes it complex to anticipate on events accurately.

1.1.1. Fluctuations on the power grid

The reason that these fluctuations are a problem is that the input and output power on the power grid have to be equal in order to maintain a grid frequency of 50 Hz. The power grid of European countries is interconnected to a great extent. The international grid has a big inertia, which dampens the effect of fluctuations. Every country has one or more Transmission System Operators (TSO), which are collaborating to oversee the healthy operation of the grid. TenneT-NL, the Dutch TSO, is in charge of the High-Voltage grid (220 kV and 380 kV) of the Netherlands. Its main focus is balancing the load on the grid, and securing a safe and reliable electricity supply. This is done by managing the TSO's of the Low-Voltage grid, and importing or exporting electricity when necessary [9]. Upon till now Tennet-NL has a good track record: the reliability of the electricity grid is 99.994 % [3]. Market forces, interconnection and the contracting of Regulating and Reserve Power are means to achieve this. But there are clear signs that the task of balancing is getting more complex. The two examples given below:

- In Germany, which has a renewable share in electricity of 33% [10], prices have dropped below zero several times, an example is shown in figure 1.2. This was the fourth day in a row negative prices occurred. At these instances it is profitable to consume electricity. However, for the power producer it could still be worth to produce power to avoid ramping down and unnecessary stresses in their system [11].

- In the Netherlands, in May 2018, a shortage in load on the grid was present, both the reserve capacities and the weather conditions failed to comply to the requirements on the grid. TenneT-NL managed to keep the grid online, but only by buying expensive power from international suppliers. The TenneT-NL paid €300 /MWh during this emergency [13], compared to an average price for energy intensive industries of €32 /MWh [14] [15].

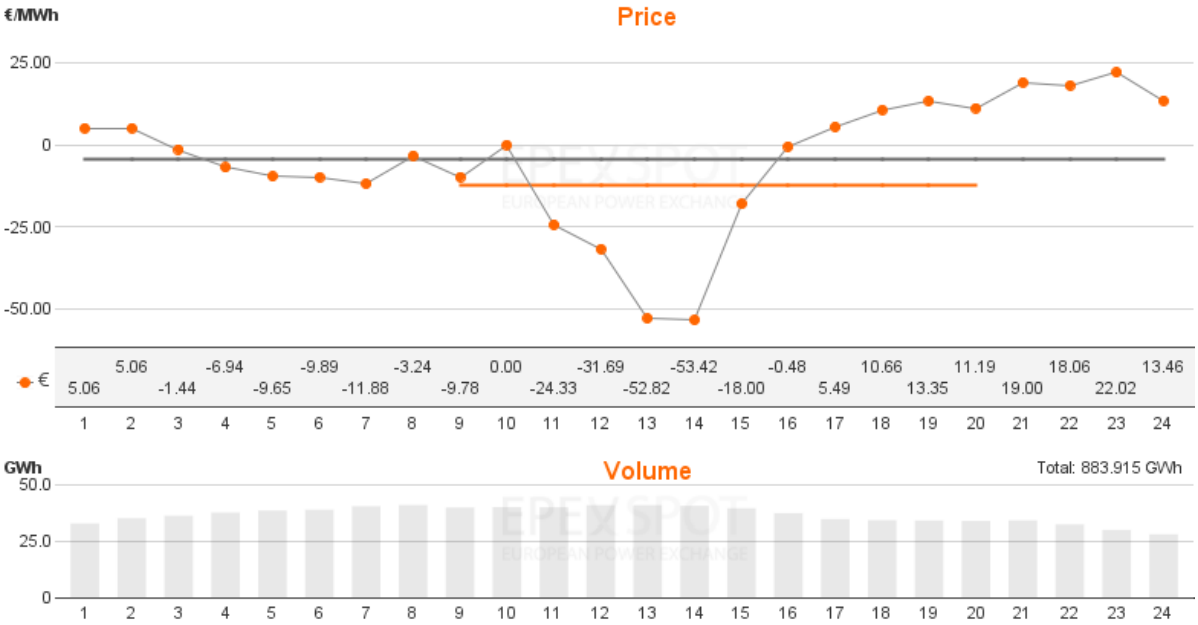

Figure 1.2: Day-ahead auction 26-12-2017 [12]

1.1.2. Flexibility

The examples in the previous section show, not only the essential role of flexibility in the future power infrastructure, but also that there is financial incentive to be an active player on the electricity market to provide in flexibility either upward or downward.

Within this context flexibility can be described as follows: (ECN,[8])

A measure of flexibility is the change in dispatch-able generation from one hour to the next hour. Total demand for flexibility can then be defined as the sum of the change in generation from one hour to the next over a year plus the total curtailment of demand in a year .

According to Energy research Center of the Netherlands (ECN), the prospective total demand for flexibility increases with 46 % between 2012 and 2023. The increase is to a great extent due to the expected increase in wind power production (20%) and the corresponding volatility [8].

If a system operates at full load it can only contribute to downward ramping flexibility. The same holds true for a system that is offline or operates in the deepest part load possible; it could only contribute to the upward ramping flexibility. Most conventional power plants are not well suited for flexible operation. But besides shifting the operational load, other methods to provide flexibility exist: storage and demand side response. Industries are watching the developments in storage capacity closely, as this could potentially uncouple the availability of electricity from the demand. Demand response could bring about the demand peak shifts, with the sole purpose that it is more attuned with the instantaneous available capacity. Demand response calls for smart and integrated systems. Key to these systems is the electrification of processes and subsystems: the more of these processes have electricity as energy source, the more they can participate in the bigger 'smart' system.

1.1.3. Electrification

In 2016, the RES share in the electricity generation was 11% [14]. To be prepared for a future energy mix where a bigger share of RES (in particular wind- and solar energy) is part of the energy mix, electrification of a lot of processes is necessary. An example of electrification could be the use of electric cars, or on a somewhat bigger scale the use of electricity instead of gas to produce the process heat used for chemical processes. Depending on the exact scenario, it is expected that by 2030 13 to 26% of the end usage in the Netherlands is going to be electricity.

Power to heat

In the Netherlands, the heat demand result for 44% from industries [16]. This is approximately 520 PJ. Most of this heat is produced by burning fuel. Heating with electricity is called 'Power to Heat' (P2H). The heat used can be either lower-grade or high-grade: the temperatures vary from lower than 100 °C to above 1000 °C. Especially the lower grade heat is assumed to be suitable for electrification [3], but there are High voltage Electrode Boilers commercially available that produce 45 bar steam of 260 °C. The potential role of P2H as role in the demand for flexibility and is very high. Not only is the potential capacity big, but costs are relatively low compared to other electrification methods (such as Power to gas, hydrogen and batteries) [7]. In Denmark a big share of the power production comes from Combined Heat and Power plants (CHP), and most of its corresponding heat is used for district heating (low-grade heat) [17].

1.2. Power Market

On account of the liberalised electricity market alternations in availability and load on the grid, whether or not desirable, translate into variations of the electricity price. These fluctuations are an incentive for large share energy consumers to think of better ways to respond to them. Price fluctuations are an important mechanism to the stabilisation of the grid. The participants in the electricity market are producers, energy intensive industries/bulk consumers, traders, energy brokers and energy suppliers. These stakeholders can trade electricity on a spot market platform: the European power exchange SE (EPEX SPOT SE). There are three important markets in place:

Future market

At the future or forward market, contracts for long term are concluded. The majority of power is traded on the future market. Maximum three years in advance agreements on quantities and prices are made. If the prospected consumption changes, the purchaser could trade the expected shortage or overage on the day-ahead market.

Day-ahead market

About 20% of the trades are done on the day-ahead auction [5]. Companies that need to purchase power bid on this auction: they indicate per hour the desired quantity/volume and the price (between -500 and 3000 euro's per MW) they are willing to pay per unit of quantity for the upcoming day. Instead of hourly bids, a buyer can choose to make an all-or-none bid on a block of a few hours. Just like the buyers, sellers of electricity will provide information on the quantities they are selling and the price for which they are willing to sell, on an hourly basis. This results in a aggregated curve, shown in figure 1.3. The final price per MW arises from the point where the two curves intersect. Customers that bid less than this final price won't have access to the electricity. Suppliers that overpriced their electricity won't be able to sell.

Intraday market

A rather small part of the transactions take place on the intraday continuous market, where a participant can indicate until 30 minutes in advance that they are interested in trading. Prices are between -9999 and 9999 €/MW, which differs significantly with the price range from the day-ahead market. Another kind of intraday market is active in Germany, which is on a 15 minute basis. The price range is smaller (-3000 €/MWh to 3000 €/MWh), and will stimulate flexible energy consumption that follows the intermittent power availability.

Over the counter

Is is possible to trade power between two parties. A bilateral contract states the agreements on quantities and price. This is called 'over the counter'.

The day-ahead and the intraday market are both part of the spot market. Where the day-ahead market is fit to deal with the forecast diurnal variations of wind power, the intraday market will be used to maintain the balance when the production of wind power deviates from forecasts.When the market forces are inadequate for balancing the power grid, TenneT could contract regulating and reserve power (RRP).

It is expected that both the price as the volatility of the price for electricity are increasing in the (near) future [8], see figure 1.4. The increase in price is expected because of higher fossil fuel costs and a decline in production capacity relative to the power demand. The price volatility will increase due to the fact that the infrastructure will be more complex to address the increased fluctuations caused by wind power.

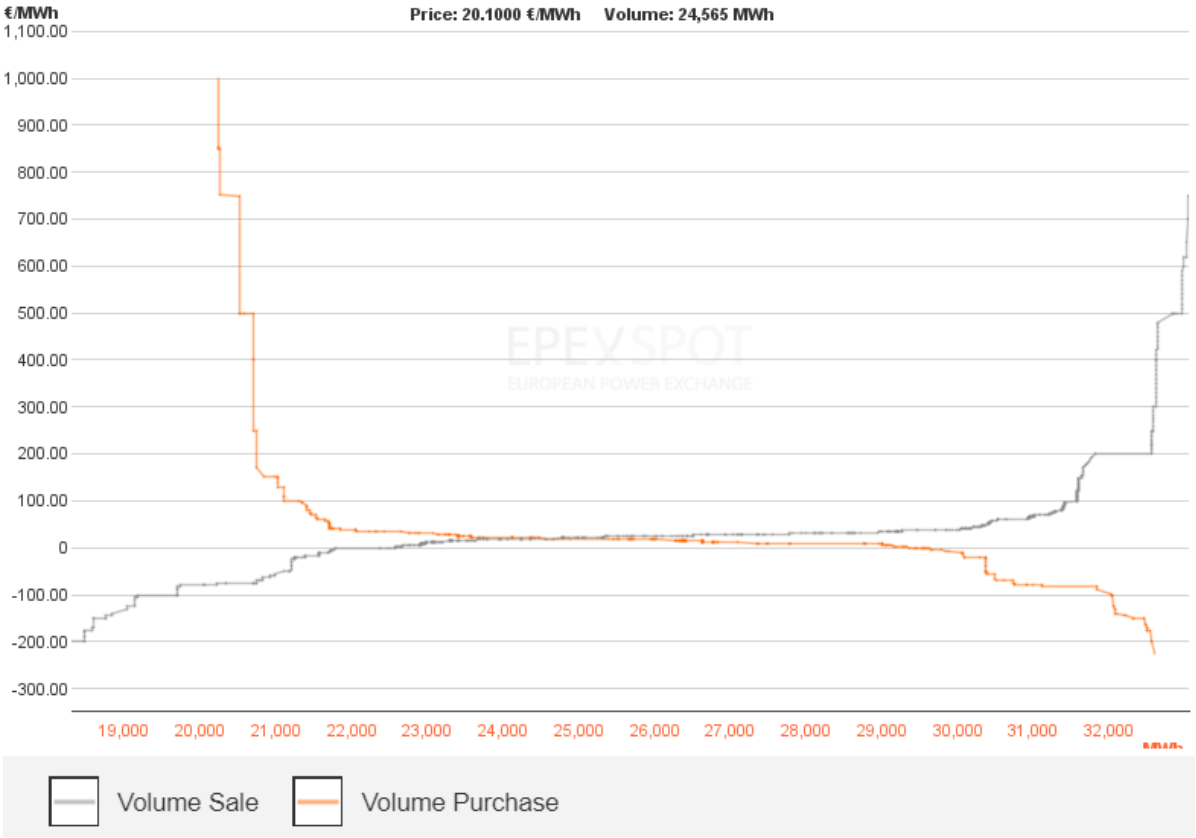

Figure 1.3: Example of an aggregated curve constructed for the day-ahead power market (01-05-2016) [18]

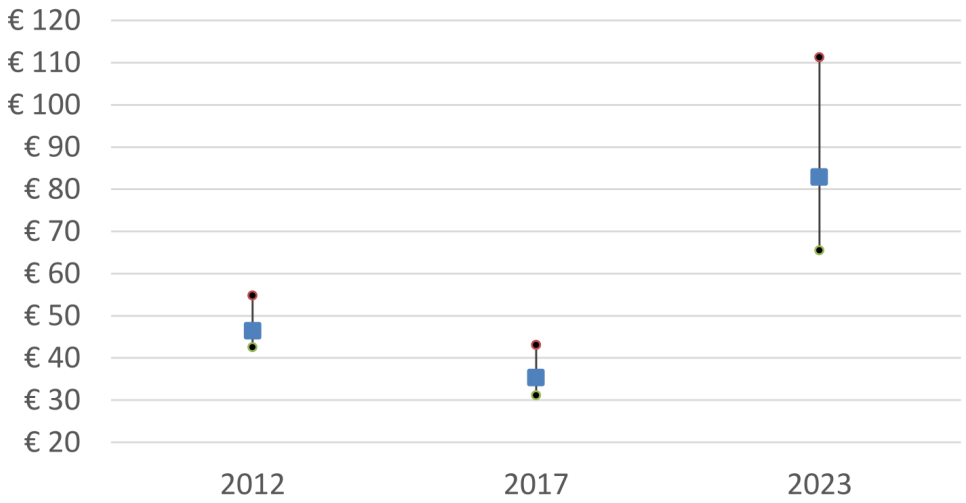

Figure 1.4: Price volatility on the day-ahead market in the Netherlands in 2012 and 2017, and a prediction for 2023[8]

The forecast error of wind power generation results in an increased price volatility in the intraday market. In case of upward demand the price will be higher and in case of downward demand the price will be lower than the day-ahead market. This interaction will become more extreme in 2023, see figure 1.5a and 1.5b.

In particular, the increased price volatility stimulates the incentive for companies to take advantage of the price peaks and troughs.

In collaboration with TenneT, industries are exploring the possibilities of flexible generation and demand response. The former option could be realised by implementing flexible electricity generators to quickly respond to differences in demand and supply in order to diminish the imbalance. In the case of power excess

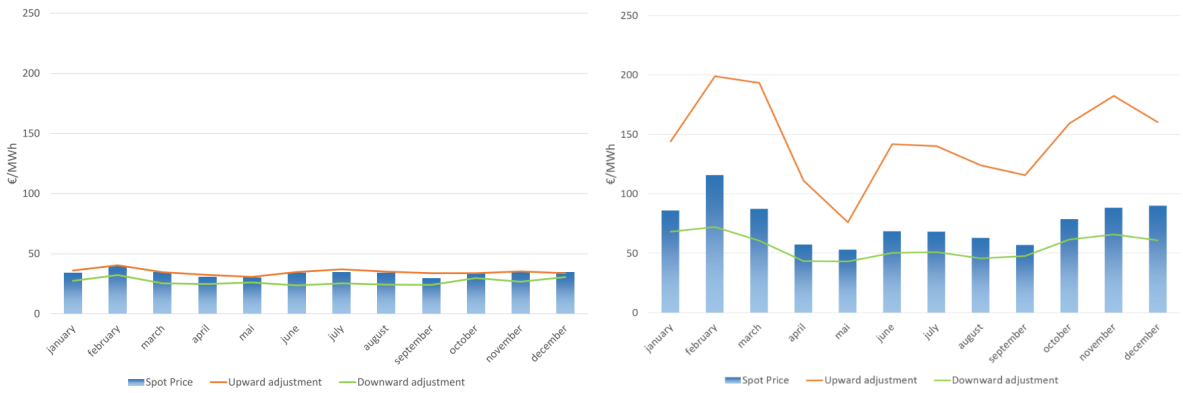

(a) 2017

(b) 2023

Figure 1.5: Monthly spot and intraday prices in the Netherlands [8]

on the grid these generators can be operated in part-load to damp the imbalance. The latter method, demand response, is not yet explored thoroughly.

One of the companies that would like to capitalise on the price volatility is AkzoNobel.

1.3. AkzoNobel

The Dutch company AkzoNobel is specialised in paints, coatings and specialty chemicals. It has an annual energy input of 98 000 TJ and is good for 9.7 Mt CO_2 globally. It finds itself amongst the most energy intensive companies of the Netherlands. The company set great store by sustainability and has committed to use 100 % renewable energy and become carbon neutral by 2050 [19]. It was one of the energy intensive companies eligible to set targets with the government.

In the light of its own vision, the price volatility on the market, and the goals of both the Dutch government and TenneT-NL, AkzoNobel is researching the possibilities to operate one of the company's Combined Heat and Power (CHP) Installation in hybrid mode. This particular CHP is located in Delfzijl at the industry site ChemiePark and is the focus of this report. A short introduction is given in the next section .

1.3.1. Meet AkzoNobel Delesto

Chemiepark Delfzijl (CPD) is located in Groningen in the Netherlands near the German border. Multiple industries are housed at this industry site. AkzoNobel has a relatively big share in the amount of these industries. One of these companies is the power facility of ChemiePark: AkzoNobel Delesto, operational since 1987. It has two combined heat and power installations (CHP), named Delesto 1 and Delesto 2, in which process steam and electricity are produced simultaneously. Since March 2012 the biggest CHP, Delesto 2, is taken out of operation in response to a deterioration in the energy market.

Since the shut down of Delesto 2, a part of the steam demand on SPD is fulfilled by the EEW Energy from Waste plant, and by the Eneco Bio Golden Raand biomass plant.

Delesto 1 is still in operation. It consist of three gas turbines (GTs), three dual pressure Heat Recovery Steam Generators (HRSGs) and one steam turbine (ST). This configuration is called a Combined Heat and Power plant (CHP) as it has the ability to cogenerate electricity and steam in a very efficient matter. The hot flue gases from the gas turbine are led into the HRSG, which is in principle a counter flow heat exchanger consisting of a gas path and a dual pressure water-steam path. Auxiliary firing is used to control the steam generation. More detailed information on Delesto 1 can be found in chapter 2.

AkzoNobel Delesto is always adapting to a continuously evolving energy market. Even though their own production of steam and electricity decreased throughout the years, the Delesto system will continue to have a key role as distributors of energy flows in Chemiepark Delfzijl. Their job is to supply reliable and sustainable steam against low tariffs. The production of electricity is a by-product in this process.

One way to achieve this is to play an active role on the electricity market. Flexibility is key to participate effectively. Ramping the load of the gas turbine is already a common flexibility tool. During periods in which it is not economical attractive to produce electricity, due to low tariffs, the gas turbine will be operated in part-load. This will reduce the fuel consumption in the gas turbine. To keep the steam supply sufficient, auxiliary firing will increase, but at a lower rate than the decrease the fuel consumption in the gas turbine. This process results in gas savings. These gas savings are where it gets interesting for AkzoNobel to formulate a business case.

1.3.2. Potential business case

The gas turbines would already have the flexible characteristics that are required in a system that is reliant on quick responses. One can operate in part load when electricity prices are low. But the heat recovery steam generator opposes this flexibility as specific exhaust temperatures are needed for the HRSG to perform well. This is often remedied with the use of supplementary firing, which enables you to control the temperatures of the exhaust gases within the HRSG, and consequently the steam flow output. Delesto is interested in taking it one step further. The company is already assessing the possibility of placing an electric boiler that operates parallel to the HRSG. Electricity is used to meet the steam demand, instead of the combustion of gaseous fuel. Another option would be an hybrid configuration, in which an electric heater is integrated in Delesto 1. Depending on the location, size and kind of electric intervention an hybrid configuration could save gas input in the duct burner. This report will assess the possibilities of implementing an electric heater in the CHP system.

1.4. The destruction of exergy

One could argue that the electrical generation of steam is a destruction of exergy. Of course they are right to note the thermodynamic sin. In a conventional power plant coal is burnt to heat water. The resulting steam is led through a steam turbine where it condenses to generate electricity. In figure 1.6, the energy flows are summarised in a Sankey diagram. The heat losses in figure 1.6a correspond with the energy in the condensed steam. Utilising the generated electricity to, once again, generate steam is indeed a waste of coal and exergy. This does not change the case of the Delesto system. There are probably more elegant ways of electrification and demand response. But where this case is different is that theoretically the electricity does not come from a fossil source. It comes from the excess of electricity on the grid due to the generation of electricity in wind turbines. No greenhouse gases were emitted during the generation of the electricity and it allows AkzoNobel to save on fuel consumption, resulting in lower emissions.

Whether or not the exergy destruction of the electric heater is justified, will not be discussed any further in this report.

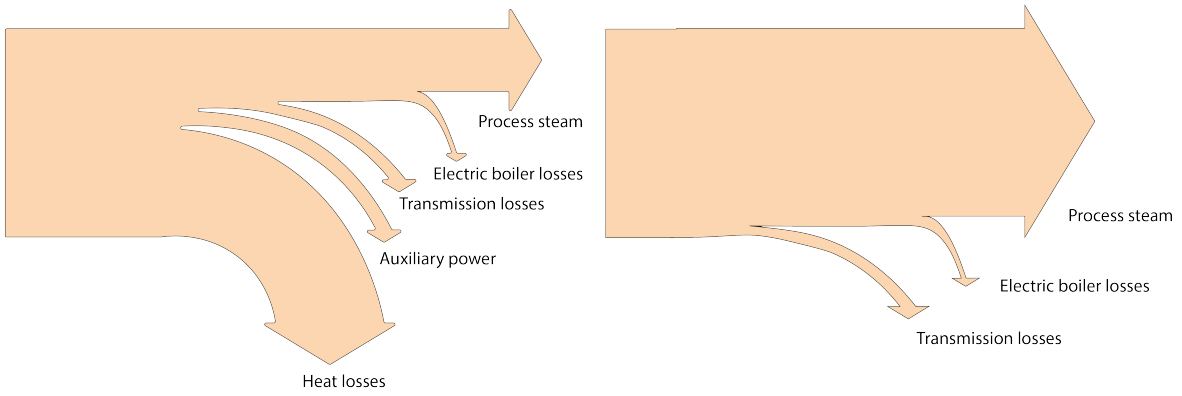

(a) From fossil to power to process steam

(b) From wind power to process steam

Figure 1.6: Sankey diagram

1.5. Research approach

The research objective of this thesis is to contribute to the flexibility of CHP's to make it fit for the future energy mix. This is achieved by developing a new configuration for the CHP at Delfzijl, in which excess electricity from the grid could be used to produce part of the steam required for industrial processes.

1.5.1. Research Question

What is the technical and financial feasibility of an hybrid configured combined heat and power plant, in which both gas and power could be used to produce process heat?

1.5.2. Central questions

To end up with useful results, a systematic approach will be taken. To steer in the right direction, some central questions are formed. It is important to get a good overview of the framework of the project and its design requirements. Knowledge of CHPs in general and the system of Delesto 1 in particular must be obtained.

- What are the possibilities to adjust the HRSG of a CHP in such a way that it can respond to the excess electricity on the grid?
  - What are the relevant parameters in the existing industrial CHP installation in Delfzijl?
  - Which methods are currently being used to convert power into steam?
  - How could these methods contribute to a hybrid configuration of the HRSG?

As this project is about retrofitting an existing system, the possibilities for P2H methods are restricted to the characteristics of the current installation. A model will be constructed of the GT-HRSG-ST combination in THERMOFLEX Thermoflow. This model will be validated, after which it the model will be used to evaluate the design cases. The assessment of the technical feasibility, will be subdivided into two parts; the thermodynamic and dynamic behaviour of the design cases.

- What is the steady state behaviour of the numerous electric heater concepts?
  - Which configurations are the most promising in terms of thermodynamic performance?

The most promising design cases are inspected further in a transient analysis. A design case is only of true value if the system is able to ramp up and down fast enough to fit the way the energy market operates. Obeying a maximum rate of temperature change to prevent the material of failing, while ramping down would gives an idea of the dynamic feasibility of the system.

- What is the dynamic behaviour of each of the 'high potential' design cases?
  - What is the steady state at which the system settles expected when a electric heater is set in operation mode?
  - Where are the weak links in the system?
  - What is the time needed to reach the steady state value, taking into account the material limitations regarding thermal stresses?

In chapter 6 the steady state model of THERMOFLEX is used to find the significant changes in the system. Using this information the system boundary is set up. The transient model will be simulated in Matlab. With the constructed model the critical ramping time that is required for safe operation is analysed, in chapter 7.

Naturally, the business case is very important. Without some financial feasibility there is no incentive to research the possibility further. In chapter 8 historical data from the energy market is used to simulate the profits on account of the electric heater.

- What is the expected financial performance of the remaining electric heater concepts?
  - In which ways could a power to heat system contribute to this market?
  - Which criteria are suitable to determine the financial feasibility?
  - Which of these methods have the potential to be financial feasible?

Lastly, one important question remains to be answered in the chapter 9.

- What would be the preferred concept design for further development, according to the results of the techno-economic analysis?

2

The characteristics and design requirements of the Delesto system

Before discussing the possible design options for the hybrid configuration in chapter 3, an overview of the existing system and its requirements is given. In this chapter an answer to the following question will be formulated: *What are the relevant parameters in the existing industrial CHP installation in Delfzijl?*

As was mentioned in chapter 1, the world of energy trading is a dynamic world. Due to changing insights and regulations AkzoNobel is forced to continuously reconsider their strategy. To be able to determine if a Power 2 Heat (P2H) application is attractive, it is first necessary to set up a framework in which this application will operate in. We will assess the potentials in the light of a scenario that would reflect Delesto's probable future (2019) situation. By this time Delesto 1 has a single gas turbine - heat recovery steam generator combination (GT-HRSG) operational in combination with a single Steam Turbine (ST). The overall system schematic of this combined heat and power(CHP) unit is shown in figure 2.1.

First the steam supply requirements are discussed in section 2.1.

2.1. Steam Demand

The industries at the CPD urge for a steam supply with a pressure of 4.2 bar and 30.5 bar absolute. In this context, these are referred to as low pressure (LP) level and intermediate pressure (IP) level respectively. The focus on the production of IP steam is diminished, as the generation of its complete demand is covered by external parties. However, as Delesto's more critical customers demand this pressure level, it requires the capability to produce the IP steam itself to secure the availability for the processes at CPD. The low pressure steam flow to be produced by the Delesto system is approximately 120 t/h.

The process steam needs a certain degree of superheat for transportation to the industries. The minimum LP steam temperature is 165 °C, and the minimum IP steam temperature is 275 °C, which is respectively 37 °C and 41 °C superheated.

The design steam production of the Delesto system is summarised in table 2.1.

Table 2.1: Design steam production of the Delesto CHP unit (2019)

Design Steam Production			
	Pressure [bar]	Temperature [°C]	Mass flow [t/h]
Intermediate Pressure	30.5	275	0
Low Pressure	4.2	165	120

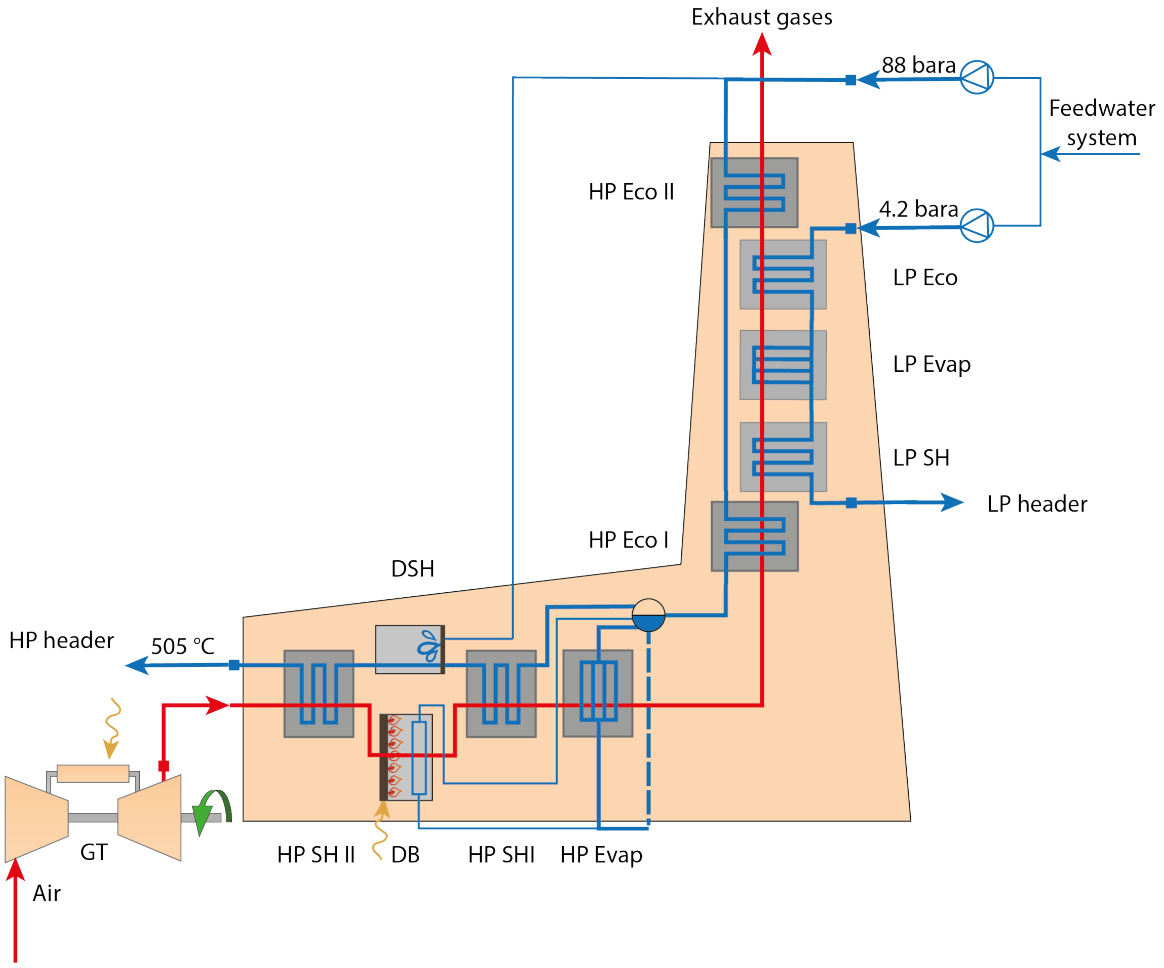

Figure 2.1: Schematic of the gas turbine and Dual Pressure HRSG. Heat from the flue gases (red) from the gas turbine is transferred to the water-steam cycle (blue). Auxiliary firing (DB) is present to control the steam output flow.

2.2. Dual Pressure Cycle

The HRSG of Delesto is a dual pressure system. Having two pressure levels increases the amount of heat that can be recovered from the flue gases, making the system more efficient than a single pressure system. Preheated feedwater coming from a deaerator enters the HRSG and is divided into two streams, (top right in figure 2.1). Both streams are pressurised by feedwater pumps: One to a pressure level just over 88 bar, the other to just over 4.2 bar, respectively the high pressure (HP) and the low pressure cycle (LP).

The LP cycle has a maximum flow rate of 16 t/h, and is small in comparison to the HP cycle, which has a maximum flow rate of 160 t/h.

In figure 2.2 the QT-diagram of the HRSG is shown. The characteristics of each component are explained in the corresponding sections.

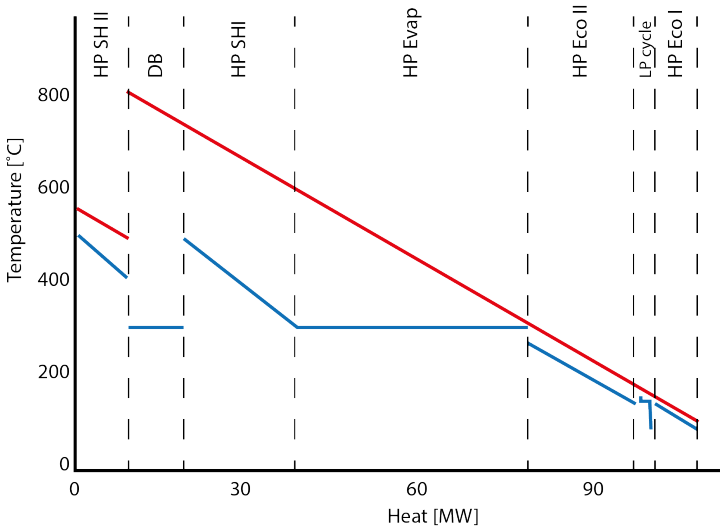

Figure 2.2: Q-T diagram of the HRSG, the red line indicates the temperature of the flue gases throughout the HRSG, and the blue line indicates the temperature development in the water/steam path

2.3. Combined heat and power components

In this section several components of the Delesto 1 are discussed.

The gas turbine in section 2.3.1, the Duct Burner in section 2.3.2, the heat exchangers in sections 2.3.3 to 2.3.6, the steam turbine in section 2.3.9.

2.3.1. The gas turbine

The gas turbine is the heart of the CHP, which in this case is a General Electric Frame 6 gas turbine. Air is compressed in the compressor with a pressure ratio of 12. High calorific gas is combusted to heat the compressed air. The flue gases resulting from the combustion enter a turbine, where the pressure of the flue gases is reduced. Approximately 37 MW_e electric power is generated in the turbine's Full Load operation. The flue gas mass flow at this load is 140 kg/s. The gas turbine is equipped with a Dry Low NO_x system (DLN), which function is to minimise the formation of NO_x [20]. Prior to the combustion the fuel and air are premixed. The DLN restricts the part load to a minimum of 80% of the full load, generating 29 MW_e. Its 'by-product' is heat carried by the flue gas flow with a temperature of 544 °C. This waste heat is fed to the HRSG. The HRSG consist of multiple heat exchangers that transfer the heat from the flue gases to the dual pressure water/steam cycle.

In figure 2.3 one can see the flue gas conditions as a function of the Gas Turbine Load. A maximum flue gas temperature of 575 °C occurs at a load of 80 %. The flue gas mass flow is rapidly increasing with an increase in load. A decrease in load results in a linearly decrease in flue gas temperature and a moderate decrease in exhaust mass flow.

The exhaust conditions of the GT are determining for the behaviour of the HRSG. In figure 2.4 one can see the maximum allowable steam flow under certain conditions. It can be seen that the steam pressure of 88 bar and the steam temperature of 505 °C can be sustained from 70% part load to full load. However, the DLN requires a minimum part load of 80 %. This is the deepest part load considered in this case study.

2.3.2. Auxiliary Firing

The HRSG is equipped with duct burners, located between the two superheaters of the high pressure cycle. The main advantage of auxiliary firing is the control over the steam output of the plant, see figure 2.4. It enables the fulfilment of the steam flow demand up to 160 t/h, at this production rate the firing is maximum and the Gas Turbine runs at full load. To decrease the supply to 120 t/h one could decrease the firing. When the GT runs at 90 % load the maximum steam supply is lower than at full load; 130 t/h. When the GT operates in deep part load, a maximum HP steam demand of 120 t/h is possible. This could be beneficial when the costs of producing electricity in the Delesto system surpass the costs of buying the same amount of electricity. If no auxiliary firing is present, the steam production characteristics (mass flow, degree of superheat and pressure) depend on the temperature of the exhaust gases and thus on the gas turbine load.

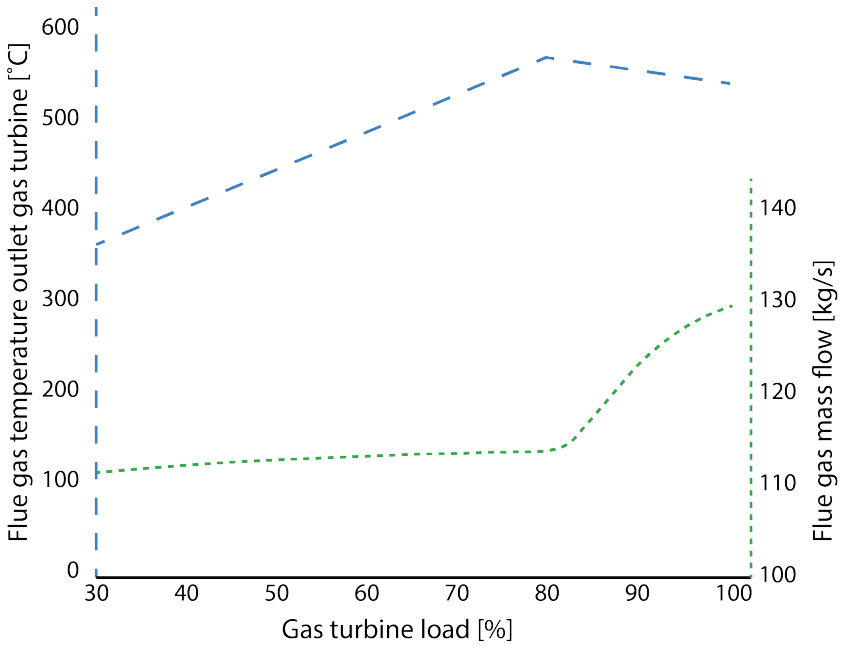

Figure 2.3: Gas turbine exhaust conditions as function of Gas Turbine Load [21].

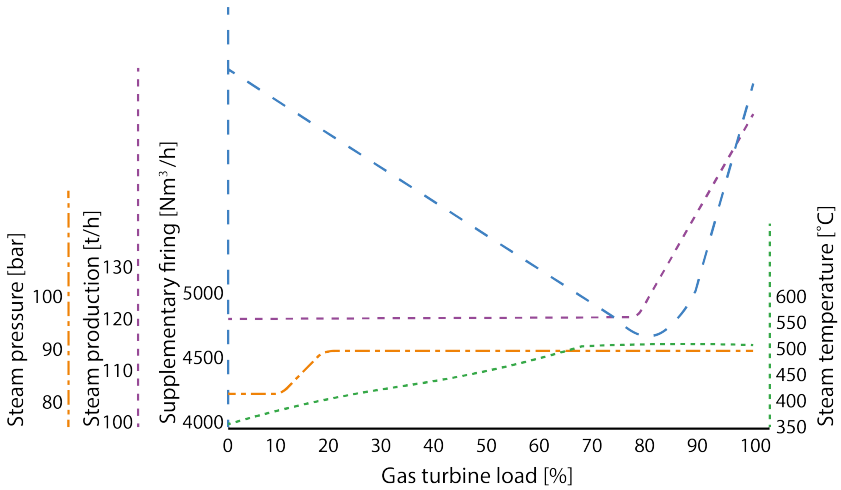

Figure 2.4: Maximum allowable steam production as function of the gas turbine Load.

The duct burner is cooled by water cooled walls and an evaporation screen. The water cooled walls are tubes surrounding the circumference of the duct burner to protect it from the heat that is produced. The evaporation screen is a tube bank of two rows in staggered configuration. It prevents radiation from reaching the adjacent heat exchangers, and consequently damaging them. The steam produced in these tubes contribute to the HP evaporation process.

In reality the minimum HP mass flow is set to insure that all the on-site available hydrogen could be used as fuel in the duct burner. This will not be taken into account in this study as it is believed that other use cases could be developed for the excess hydrogen. This assumption will simplify the task ahead.

2.3.3. Economisers

From the water flow path's perspective, the economisers are the first heat exchangers it encounters, see HP Eco I, HP Eco II and LP Eco in figure 2.1. The function of the economiser is to bring the temperature from the water up to just below saturation temperature to avoid steaming in the economiser tubes. The differ-

ence is called "approach temperature". The HP cycle consists of two Economisers, HP Economiser I and HP Economiser II, the LP cycle has one Economiser: LP Economiser I. The remaining energy content in the flue gases is relatively small. Therefore the tubes of the economisers are all finned to maximise the heat exchanging contact area. The tube rows are all staggered. The pressure drop in staggered tube banks is increased compared to in-line arrangements, but so is the overall heat transfer coefficient [22].

2.3.4. Drum

The subcooled water from the economisers will enter a drum, see figure 2.1. In this drum vapour and water are in equilibrium. The prevailing temperature is the saturated temperature. It will act as storage for the evaporators, to prevent "dry-boiling" from happening. The drum separates the water from the vapour by means of difference in density. The water flows into the evaporators (section 2.3.5) and the vapour will go to the superheaters (section 2.3.6).

2.3.5. Evaporators

Water will flow into the down comers, which lead to the evaporator tubes. The evaporator is the heat exchanger in which the saturated liquid absorbs heat under constant temperature. In this process, part of the liquid evaporates, resulting in a two-phase flow. The HP Evaporator and LP Evaporator have both finned tubes and are staggered, but differ from each other in orientation and by means of circulation driving force. After the evaporators the two-phase water returns to the drum via risers.

HP Evaporator

The HP evaporator has a vertical orientation. Water in the down comers becomes slightly subcooled, due to a static pressure increase. When it enters the evaporation tubes the density gradually decreases as the amount of vapour increases. The gravitational force on the fluid in the down comers, is higher than the one on the liquid-vapour mixture in the evaporator tubes. This makes the fluid circulate. The driving force is called thermal head and is also known as natural circulation. The HP evaporator consist of 1092 parallel tubes. The circulation rate (CR) is 7, which means that the vapour quality is 1/7 at the end of the riser tubes [23].

LP Evaporator

In the LP Evaporator the tubes are oriented horizontally. The mass in the LP evaporator tubes is much smaller than in the HP evaporator tubes. The difference in density is no longer a relevant driving force. Therefore a pump induces a pressure gradient that will act as the driving force.

2.3.6. Superheaters

The vapour in the drum flows to the superheaters. In the superheater, the temperature can increase beyond the saturation temperature. Because of the relative high energy content of the flue gases, the tubes of the superheaters are not equipped with fins. Without the fins there is already a sufficient amount of heat transferred to the steam. The HP superheater II is staggered, whereas the HP Superheater I and the LP Superheater are not.

2.3.7. Desuperheater

Parallel to the duct burner, but integrated in the steam path, a desuperheater is located. This unit controls the temperature at the outlet of superheater II, with a set-point of 505 °C. Superheated steam from Superheater I is injected with water directly coming from the high pressure feedwater pump. Two principles are working together. Injecting the cooling water, decreases the temperature at the inlet of SH II. Obviously the decrease in temperature at the inlet of the SHII will have an effect on the exit temperature of the SHII. Concurrently, the increase in the steam flow will cause a smaller overall temperature increase, assuming the same amount of heat transferred in the heat exchanger.

2.3.8. Feedwater supply system

Not shown in the pictures is the feedwater supply system. It consists of a deaerator, and a feedwater preheater. The main purpose of the deaerator is to remove the non-condensable gases carbon dioxide CO_2 and oxide O_2. O_2 causes corrosion in the boiler, and CO_2 aggravate this effect. Two other key functions of the deaerator are the heating and storage of the feedwater. Demineralised water from the processes at Chemiepark is fed back to the deaerator.

2.3.9. Steam turbine system

The superheated HP steam exiting the HRSG is collected in an HP header, and the superheated LP steam is collected in a LP header, see figure 2.5. The superheated steam of 88 bar generated in the superheater is not of particular interest for processes, but is needed for the power generation in the steam turbines. In the ST's it is not important how much heat the steam can transfer, but how much work it can do. An advantage of using superheated steam over saturated steam during expansion is that a large enthalpy difference can be achieved without wetting the steam.

The superheated HP steam is guided from the HP header to the ST. The ST assembly consists of a HP turbine and an IP turbine. Between these two steam turbines it is possible to extract part of steam at a pressure of 30.5 bar. The extracted steam enters an IP header. The remaining steam will enter the Intermediate Pressure turbine. At the exit of this turbine the steam has a pressure of 4.2 bar, and is added to the LP header.

A minimum flow is necessary to prevent overheating of the steam turbine. The lower limit of mass flow is fixed by the maximum allowable temperatures at the turbine exits: 420 °C and 350 °C for the IP and LP turbine respectively. Downstream of the steam turbine outlets desuperheating stations are located to control the temperature of the steam. The IP steam outlet is controlled with a set point temperature of 280 °C, as a rule of thumb 10% of the exiting flow is additionally injected. The LP exit stream is kept at a temperature of maximum 185 °C, the injection stream is limited to 3.2 t/h. The maximum output of the steam turbines are 125 t/h at LP and 110 t/h at IP. At full load the HP turbine and IP turbine produce 15 MW_e and 14 MW_e respectively.

Pressure reducing stations/ Steam turbine bypass stations

It is possible to partly bypass the steam turbine, either because the steam entering the HP header exceeds the maximum capacity of the steam turbines, in case of failure, or there exists no financial incentive to produce electricity. The HP, IP and LP headers are connected by means of pressure reducing stations that form this bypass.

In a reducing station the prevailing pressure is reduced. The saturation temperature of water decreases with this decrease in pressure. To produce steam at the required conditions a desuperheater is installed downstream to the reducing station. Injection water comes from the deaerator after which it is pressurised to 70 bar. This injection water is also used as cooling water at the outlets of steam turbine.

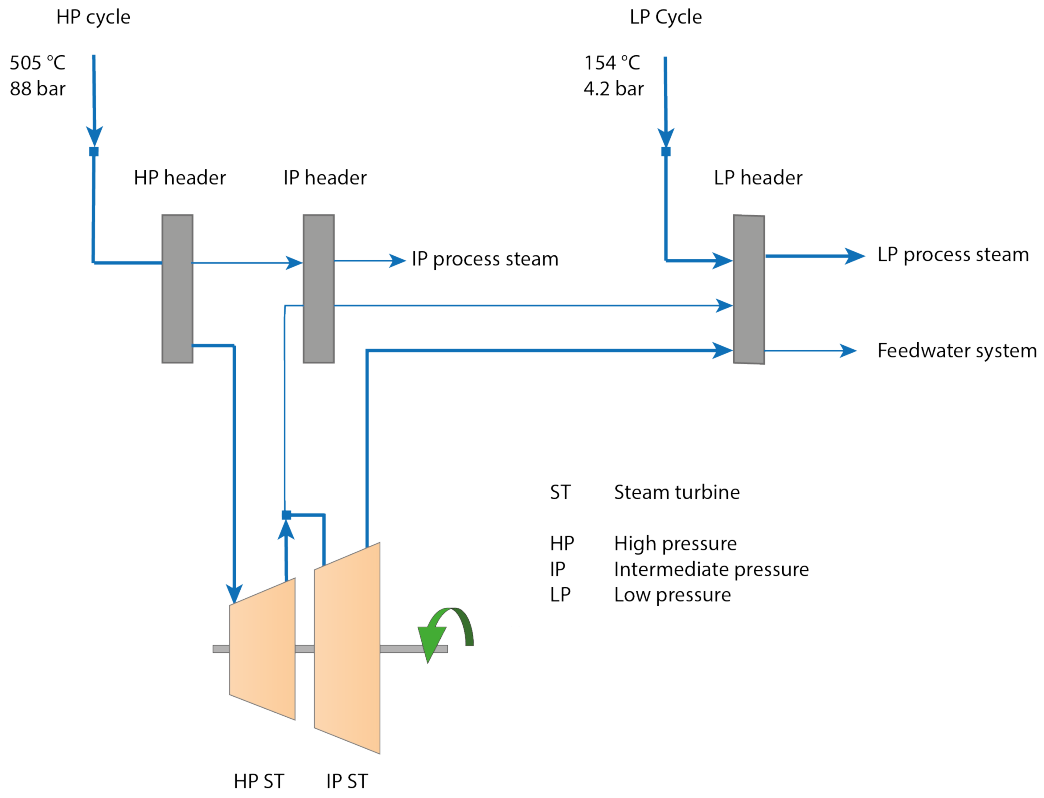

Figure 2.5: Schematic of the steam turbine system

3

Potential configurations

In chapter 2 a better understanding on the Delesto plant is gained. In this chapter, an answer is given on the questions *Which methods are currently being used to convert power into steam?* and *How could these methods contribute to a hybrid configuration of the HRSG?*

The opportunities to implement power to heat in this existing plant are researched. In section 3.1 two of the existing power to heat (P2H) applications and their characteristics are described. In section 3.2 eight design cases are set up. The theoretical principle is briefly explained.

3.1. Power 2 Heat applications

The collaboration of CHP plants and P2H heat is not a new idea. For example in Denmark, a country that utilises CHP's for district heating, a lot of research has been done on the topic [17] [24] [25] [26]. The studies are done on the production of low grade heat, which is up to 100 °C. Process heat is considered to be high grade heat. Obviously, low grade heat is easier to obtain than high grade heat.

There are several methods to convert power into heat. In this section the working principles of immersion heaters and electrode boilers are discussed. Other methods, like heat pumps, and trace heating are not considered in this report. The indirect path from power to gas to heat is not considered here.

3.1.1. Immersion heater

An example of the immersion heater could be found in many house holds: the electric tea kettle. The immersion heater consists of an electrical resistance 'immersed' in the medium subjected to heating. It is in direct contact with the fluid to be heated. When a voltage potential over the resistance exists, a current will flow through. This current causes Joule heating to occur, which relationship is described with equation 3.1. Depending on the magnitude of the resistance R of the resistor and the current flowing through it I, a certain amount of heat will be dissipated. This heat will be transferred by means of convection to the medium the resistor is immersed in. In the light of this study, that medium could be air, fuel or water.

$$Q \propto I^2 R \tag{3.1}$$

The temperature increase this process induces depends on the heat capacity of the system. The specific isobaric heat capacity c_p is a measure of the amount of heat added to a system to increase the temperature of the system with 1 °C, it is a function of temperature and it has different values for air, fuel and water. The efficiency of immersion heating is approximately 100 %, as all electricity input is 'lost' or converted into heat.

3.1.2. Electrode boiler

The electrode boiler utilises the conductive property of water to produce heat. A schematic of the configuration of the electrode boiler is shown in figure 3.1. Three electrodes are suspended in a container of water. Three phase alternating current (3-phase) is fed to the electrodes to agitate the water molecules to produce steam. The steam will move upward. The water is supplemented with the water contained in the bottom part of the vessel. If the amount of steam produced surpasses the demand, the pressure in the vessel increases. The supply of feedwater to the container with electrodes is controlled using this pressure.

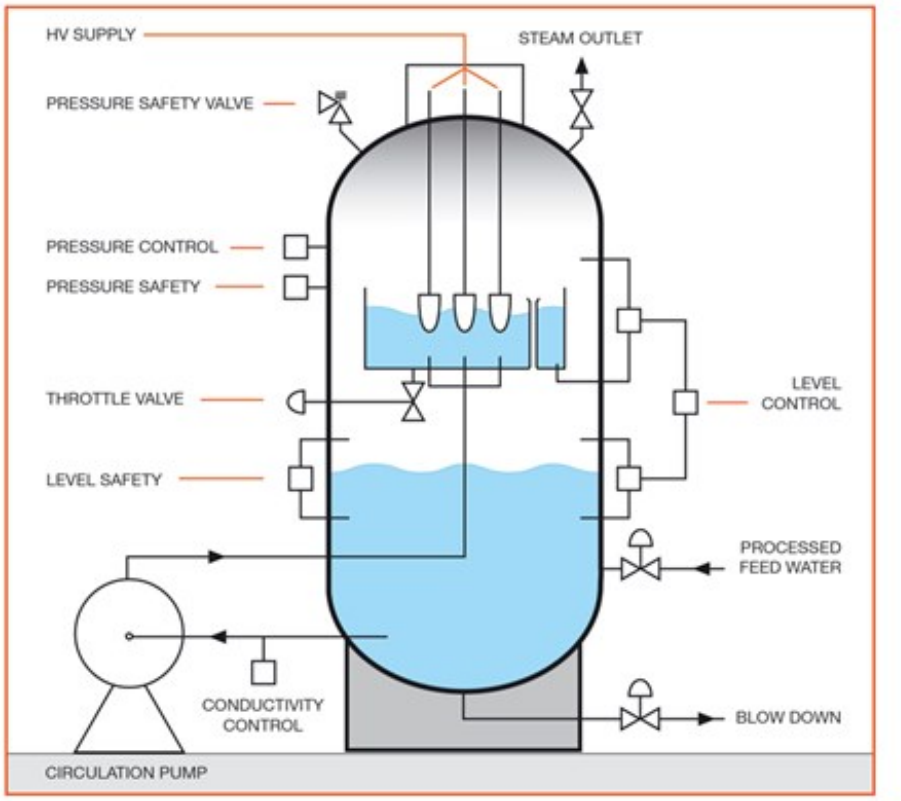

Figure 3.1: Schematic representation of the Electrode Boiler Steam generation system [27]

The conductivity of the water is essential to the performance of the electrode boiler. This conductivity of the water is thanks to the presence of certain minerals in the water, which might be undesired for the feedwater of the HRSG itself. It is possible to control the concentration of these minerals by adding them to the water. As these minerals are non-condensables, they won't leave the vessel with the steam. Accumulation of the minerals should be prevented, this is done with the blow down at the bottom of the vessel.

The electrode boiler is appreciated for its applicability in a energy mix with high share in renewable energy sources. Typically, they have a capacity of 50-70 MW, and a steam output of 45 bar at 260 °C [7] [28]. With some modifications it is also possible to superheat the steam. The efficiency is 99.9 %. The ramp up time from zero to full load of minutes enables quick response to always changing electricity prices [27]. In Denmark it is already complementing CHP's in their function for district heating [28].

3.2. Electric heater concept designs

Eight optional design cases came up after several discussions with AkzoNobel Delesto and Stork Thermeq. The working principle of the several options are shortly discussed in this section. The methods could be categorised by the medium on which they act. They are intervening on the fuel entry, on the air/exhaust path or on the water/steam path. In table 3.1 the different cases are summarised, the locations of each method is shown in figure 3.2. Although there is one device, the High Pressure Pump, that does not function on the heating principle, the collective term used in this report for the electric intervening devices is Electric Heater (EH).

3.2.1. Air preheater (AP)

The performance of the gas turbine can be described with the With an increase in compressor inlet temperature of the gas turbine, the density of the working fluid air decreases. This decrease in air density induces a decrease in thermal efficiency, specific work and an increase in specific fuel consumption. It is said that for every 1 °C a reduction of power output of 0.5 - 0.9 % is to be expected [29] [20].

The increase of temperature at the compressor inlet can be achieved with the implementation of an Air preheater, located in front of the gas turbine, see (1) in figure 3.2. It should be noted that the composition

Table 3.1: Potential design cases for the hybrid configuration of the CHP

	Device	Symbol	Location	
1.	Air preheater	AP	Gas Turbine	gas path
2.	Duct heater	DH	Duct burner	
3.	High pressure boiler	HPB	Bypass high pressure evaporator	water/steam path
4.	Low pressure boiler	LPB	Bypass low pressure evaporator	
5.	High Pressure Pump	HPP	Integrated with high pressure feedwater pump	
6.	Fuel Heater Gas Turbine	FHGT	Fuel inlet GT	fuel entry
7.	Fuel Heater Duct Burner	FHDB	Fuel inlet DB	
8.	Stand-alone boiler	SB	Parallel to the HRSG	

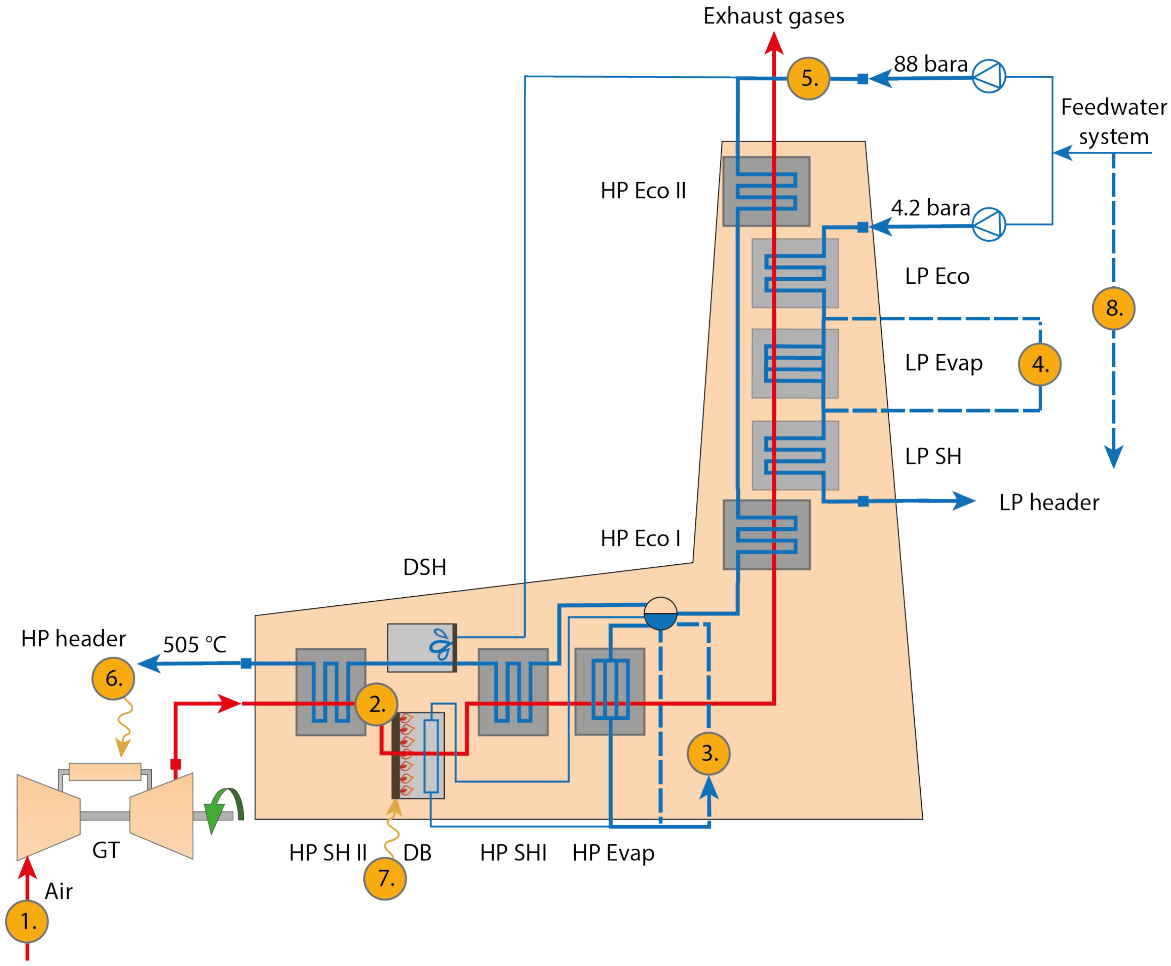

Figure 3.2: Different locations of the electric heaters, the numbers correspond to the numbering used in table 5.2

of the exhaust gases will differ from the composition during standard operation. The oxygen content is less, thus firing in the duct burner could be influenced by this method.

It is common practice to cool the inlet air of the gas turbine to enhance the power production in the gas turbine, especially in tropical areas. Less common is the preheating of air, at best this is used during cold seasons as anti-icing practice. This makes that there has not yet been a real incentive to raise the temperature limit at the compressor inlet, which is currently around 45 °C. Technologies such as exhaust gas recirculation will help to grow this incentive. In this report it is assumed that it is within the technical possibilities to raise this temperature, and that development will follow the incentive. Therefore the temperature limit at the inlet of the compressor is set at 90 °C.

3.2.2. Duct heater (DH)

To shift part of the load from the duct burner, a flue gas heater could be placed upstream in the gas path of the duct burner, see (2) in figure 3.2. In this way the heater replaces directly (partly) the function of the duct burner. This will affect the radiation temperature in the duct burner.

3.2.3. High pressure boiler (HPB)

Parallel to the HP evaporator an electric boiler can be operated to partly substitute the function of the evaporator, (3) in figure 3.2. The main reason for auxiliary firing in the duct burner is supplying the right amount of energy in the flue gas flow to enable the production of the right amount of high pressure steam. The bottle neck is the pinch point. This pinch-point demands a certain flue gas temperature at the exit of the evaporator so that enough heat can be transferred to the steam to overcome the latent heat.

In figure 3.3 one could see the Q,T-diagram of the dual pressure steam cycle of interest. Part of the heat transferred to the saturated water comes from electricity. The evaporation process is no longer restricted by the flue gas temperature at the pinch point and is less depending on the auxiliary firing. A smaller temperature rise over the duct burner is required and consequently less gas is burned. Note that the part of water conventionally evaporated in the DB has shifted to the HP evaporator component.

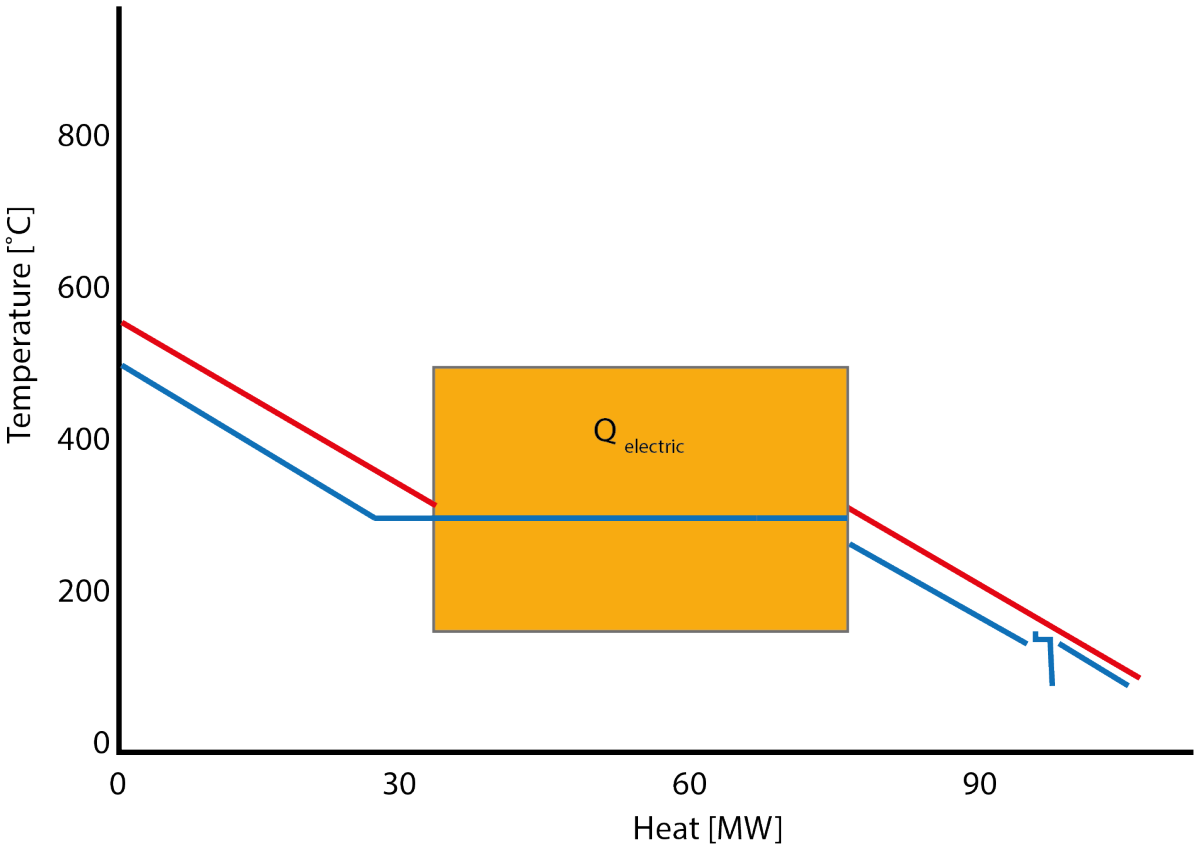

Figure 3.3: QT-diagram of the heat transfer inside the HRSG. P2H is used to evaporate part of the water flowing into the drum. The need for duct firing dissappears.

3.2.4. Low pressure boiler (LPB)

Just like the previous mentioned high pressure boiler, a low pressure boiler could be placed parallel to the evaporator of the low pressure cycle, see (4) in figure 3.2. Unfortunately, the LP cycle has a maximum capacity of 'only' 16 t/h and is less defined by its pinch-point than the HP cycle, which limits the potential saved gas input. This can be seen by looking to the LP cycle in figure 3.3.

3.2.5. High pressure pump (HPP)

One could decide to increase the pressure of the high pressure cycle, see (5) in figure 3.2. The theory behind this method is as follows:
The latent heat decreases with increasing pressure. This could mean that the temperature of the flue gases does not have to be elevated to the usual/normal level. One side note is that the saturation temperature also increases with increasing pressure, which could diminish the net effect. Both effects are linear around the high pressure level of 88 bar, see figures 3.4a and 3.4b . An advantage of this method is that the pump is already present in the installation, it only has to switch from operation mode. The pressure design limit for the high pressure cycle is 102 bar.

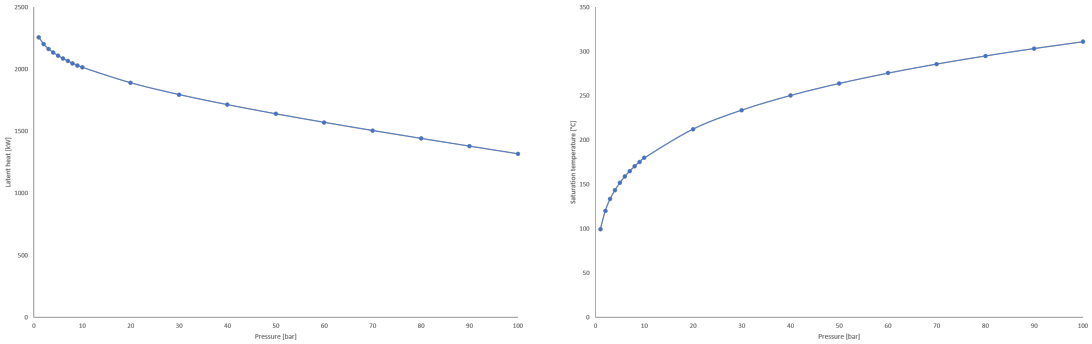

(a) Latent heat with respect to water pressure

(b) Saturation temperature with respect to water pressure

Figure 3.4: An increase in the pressure of the High Pressure cycle would induce an increase in latent heat,this would result in a decrease in duct firing needed. However, the saturation temperature also increases for increase in pressure. Elevation in saturation temperature would result in an increase in duct firing. If the HPP is successful depends on both.

3.2.6. Fuel heaters in gas turbine and duct burner (FHGT & FHDB)

During combustion part of the heat released is used to elevate the temperature of the gaseous fuel to ignition temperatures. One way to increase combustion efficiency is to preheat the natural gas, so that less energy is required to bring it up to combustion temperature. In theory one would want to bring it as close to auto-ignition temperature of natural gas [30], which is 580 °C [31] (or 537 °C [32]) as possible. In practise temperatures of 185 °C are typical [33]. In conventional systems the heating is done using heat extracted from the boiler. Using electric heaters would not be convenient in these systems, but could be interested in perspective to a hybrid CHP and could be implemented in both the fuel input of the gas turbine and of the duct burner, see (6) and (7) in figure 3.2.

3.2.7. Stand-alone boiler (SB)

Last but not least, one important option should be considered, this case will function as the "control group". It is an electric boiler that is not integrated in the CHP, but runs parallel to it, see (8) in figure 3.2. It is decided to operate it at the pressure level of the IP Header to ensure the supply security at this level demanded at CPD. To produce superheated steam, one should pressurise the steam to a level where the saturation temperature corresponds with the desired temperature of the superheated steam. Afterwards the pressure is reduced to the desired pressure level.

4

Steady State Model of Delesto

To assess the potential value of the concepts discussed in chapter 3, a model is created in THERMOFLEX (programme of Thermoflow). This program is component based software for industrial applications. An advantage of the software is that it allows the user to over define the system, by prioritising the input of the model. It is extremely suitable to compute steady state behaviour of thermodynamic systems.

In this chapter some basic information is given on the developed model. The gas turbine and steam turbine are modelled and tuned separately, in respectively section 4.2 and section 4.3. The tuning is done by comparing the outcome of the model to some available measurement data from DNV-GL, section 4.1.

4.1. Data

There are two sets of measurement data available. One set is on the Gas Turbine - Heat Recovery Steam Generator combination (GT-HRSG) and the other is on the Steam Turbine (ST) performance. These data sets are used to tune the THERMOFLEX models from section 4.2 and 4.3.

The measurements on the GT-HRSG combination has been done by varying the load of the gas turbine and the duct burner. The data points used are shown in table 4.1. The GT load and the DB fuel consumption and HP mass flow obtained during the DNV-GL measurements are used as input of the new model.

Table 4.1: Measurement Programme of the data set

Data Point	GT Load [%]	Duct Burner Load [%]
1		100
2		75
3	100	50
4		25
5		0
6		50
7	80	25
8		0

The data on the ST system is obtained by running through the operating range of the ST to map its characteristics. The result is detailed information about pressures, temperatures and generated power for several LP and IP mass flows.

4.2. Gas Turbine and Heat Recovery Steam Generator

The model of the GT-HRSG inside the THERMOFLEX environment is shown in figure 4.1. This model includes the HP and LP cycle, and the duct burner, which are shown in figure 4.2, 4.3 and 4.4 respectively. In the component input structure, specific characteristics can be indicated, such as the contact area and the overall design heat transfer coefficient for the heat exchangers.

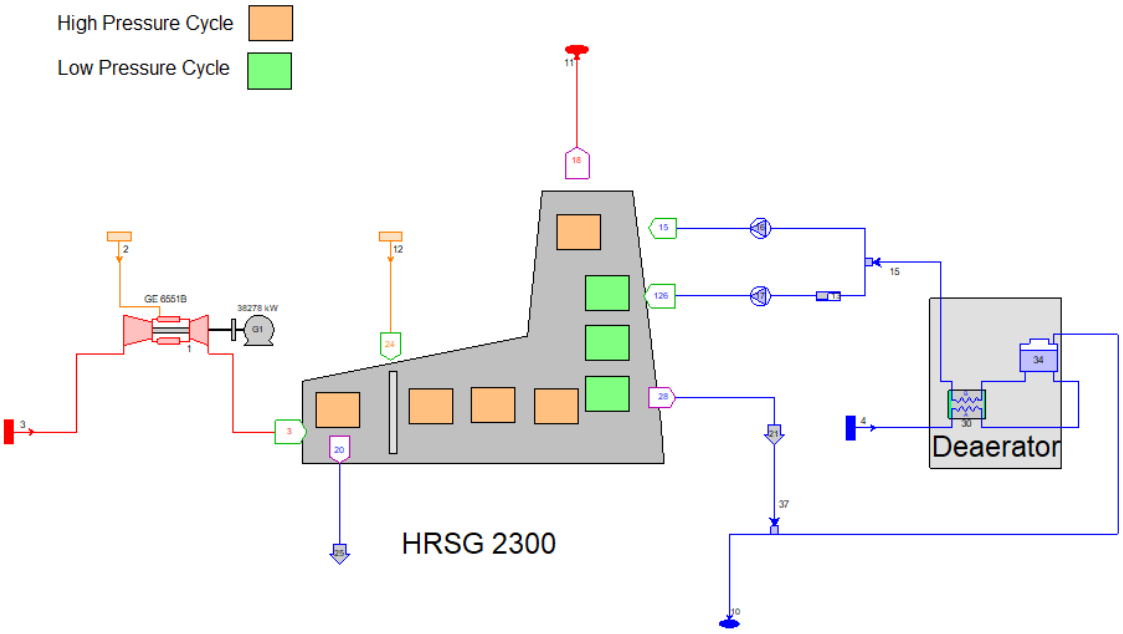

Figure 4.1: Combination of the gas turbine and Heat Recovery Steam Generator in the THERMOFLEX environment.

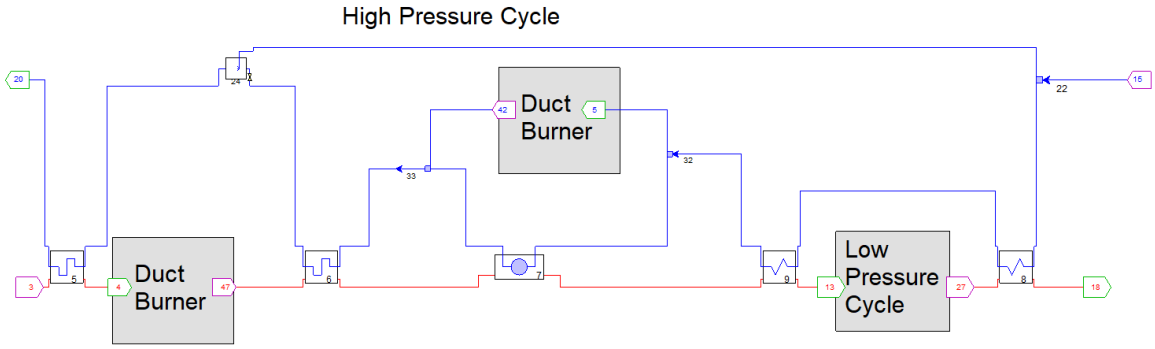

Figure 4.2: High pressure cycle in the THERMOFLEX environment

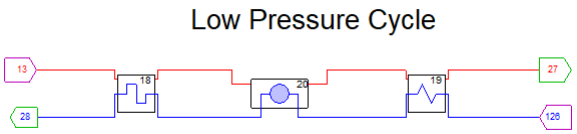

Figure 4.3: Low pressure cycle in the THERMOFLEX environment

4.2.1. Tuning

The tuning of the GT-HRSG is done by adjusting the operation parameters of the Gas Turbine, such as efficiency reduction for the compressor and turbine, TIT control, turbine nozzle area, and inlet guide vanes parameters. Additionally, some correction factors of the heat exchangers are modified.

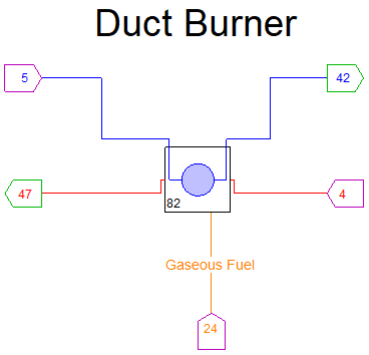

Figure 4.4: Duct Burner in the THERMOFLEX environment

4.2.2. Validation

To validate this part of the model, the characteristics of the gas turbine (compressor discharge pressure and temperature, power output, inlet air flow, fuel consumption and the exhaust temperature) are compared for an old model, the DNV-GL data and the new model. The comparison of the power output and the fuel consumption of the GT are shown in figure 4.5 and 4.6. The power output according to the new model is slightly (2%) more than the measured power output. The fuel consumption in the new model stays within the 1% of the measured data.

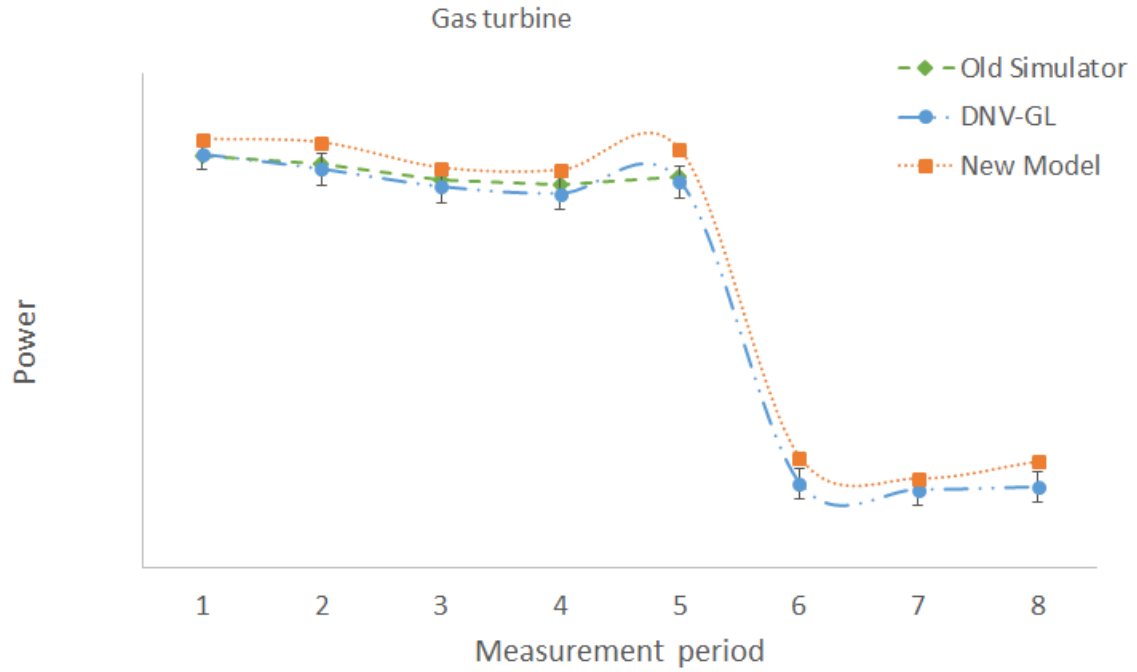

Figure 4.5: Power output of the GT for the conditions described in table 4.1. The error bars show a 2 % deviation from the maximum value of the data obtained from measurements

Additional to the behaviour of the GT, the behaviour of the HRSG is looked into. The characteristics mass flows of the model's HRSG are compared with the DNV-GL measurements and the old simulator. The mass flow of the LP cycle and the injected water in the desuperheater are shown in figure 4.7 and figure 4.8 respectively.

It is seen that the LP mass flow more or less stays within a 1% deviation from the maximum HP mass flow measured.

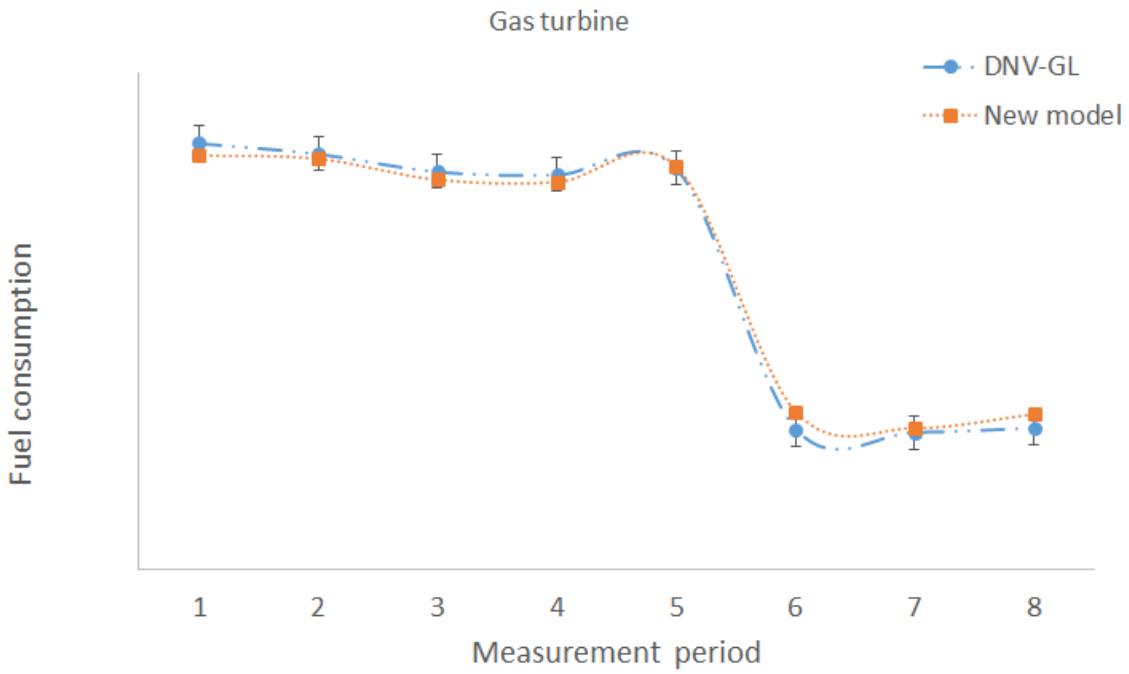

Figure 4.6: Fuel consumption of the GT for the conditions described in table 4.1. The error bars show a 1 % deviation from the maximum value of the data obtained from measurements

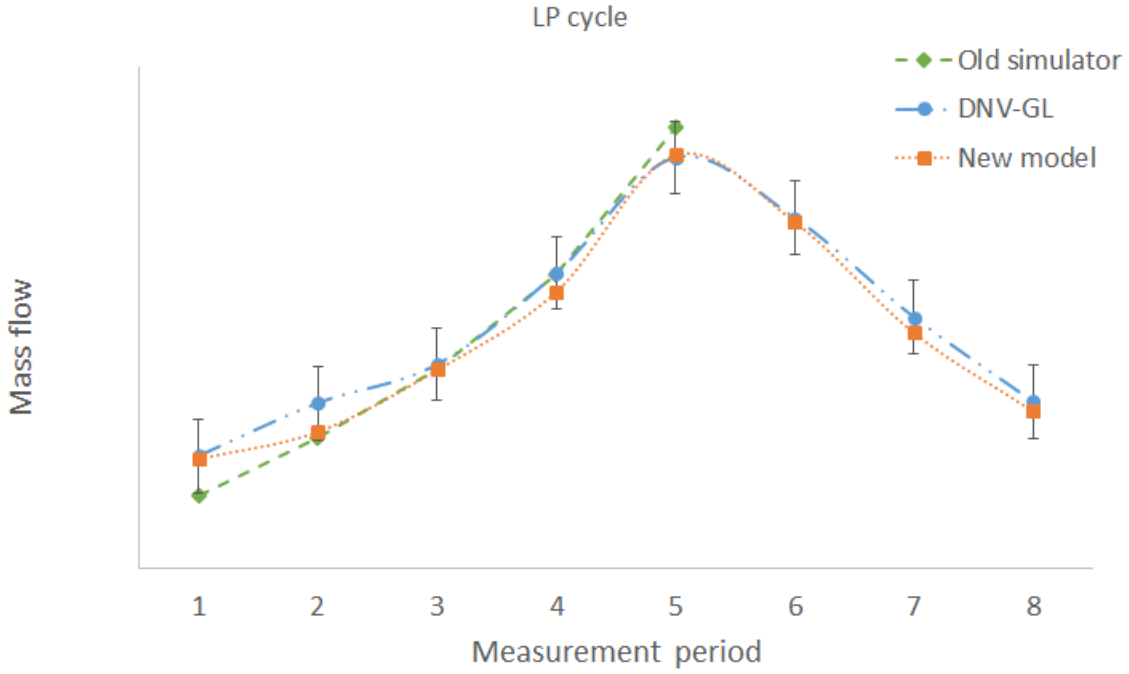

Figure 4.7: Mass flow of the low pressure cycle for the conditions described in table 4.1. The error bars show a 1 % deviation from the maximum value of the HP mass flow according to data obtained from measurements

At first glance, the injected mass flow in the desuperheater does not fit the measured data. However, as one can readily see, the new model has values that corresponds better to the real behaviour than the old simulator. If one compares the deviation relative to the entire mass flow of the HP cycle most data points stay

within the 1% error, and all of them within the 2%.

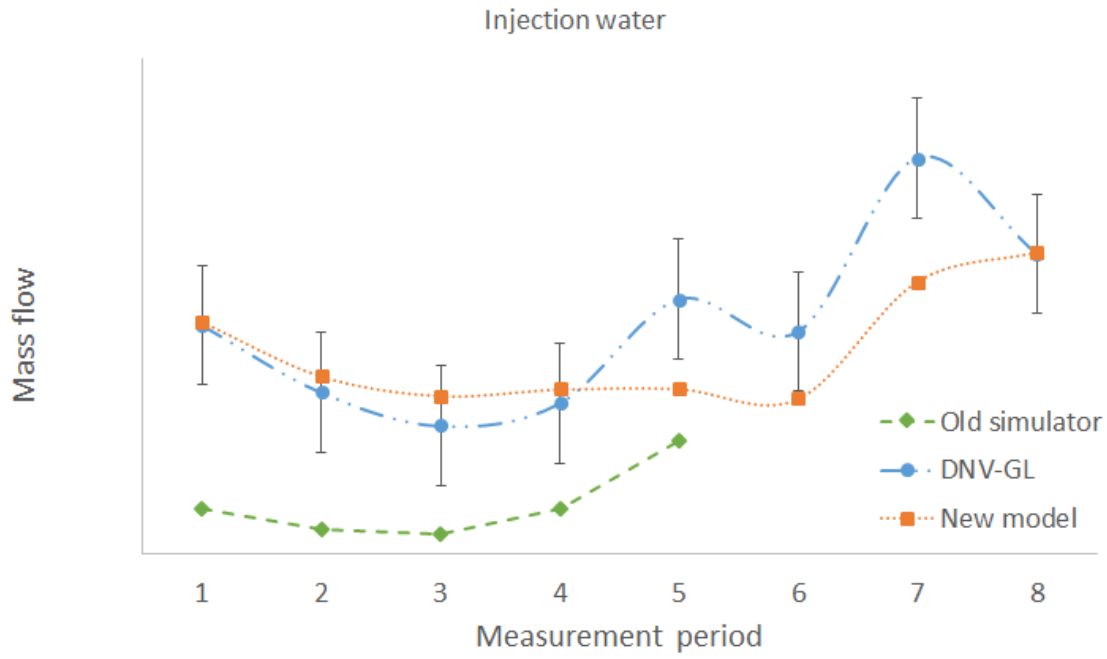

Figure 4.8: Injected mass flow in the desuperheater for the conditions described in table 4.1. The error bars show a 1 % deviation from the maximum value of the HP mass flow according to data obtained from measurements

4.3. Steam turbine

The model of the steam turbine inside the THERMOFLEX environment is shown in figure 4.9. Results from the DNV-GL measurements, such as the entering amount of superheated steam and the delivered process steam at MP and LP level are used as inputs of the model.

4.3.1. Tuning

To tune the model the isentropic efficiencies, the temperature at the turbine exits and the power output of the turbines are compared. To fit the model to the available performance data, a value for the inlet nozzle adjusted area is chosen and the overall the model is tuned by specifying an exhaust loss curve of the steam turbine assembly. It represents the loss of kinetic energy and enthalpy still present in the stream after the turbines [34].

4.3.2. Validation

In this section some important graphs are shown to compare the results of the THERMOFLEX model of the steam turbine system with the measurement data from DNV-GL. The temperature, isentropic efficiency and the power output against the entering mass flow are compared.

In figure 4.10 one could see that the modelled temperatures at the outlet of the HP an IP turbine fit the data well. The error bars indicate a deviation of 1% of the maximum temperature on Kelvin scale. In figure 4.11 the power output of the complete steam turbine assembly is shown. The power output of the modelled steam turbine is in accordance with the data. The error bars show a deviation of 2 % with respect to the maximum power output, in almost all the cases the power output stays within that 2%.

In figure 4.12 the power output of the steam turbines is shown separately. The trend of the two turbines in the model is in accordance with the trend in the data. In the HP turbine the error increase for increasing mass flow.

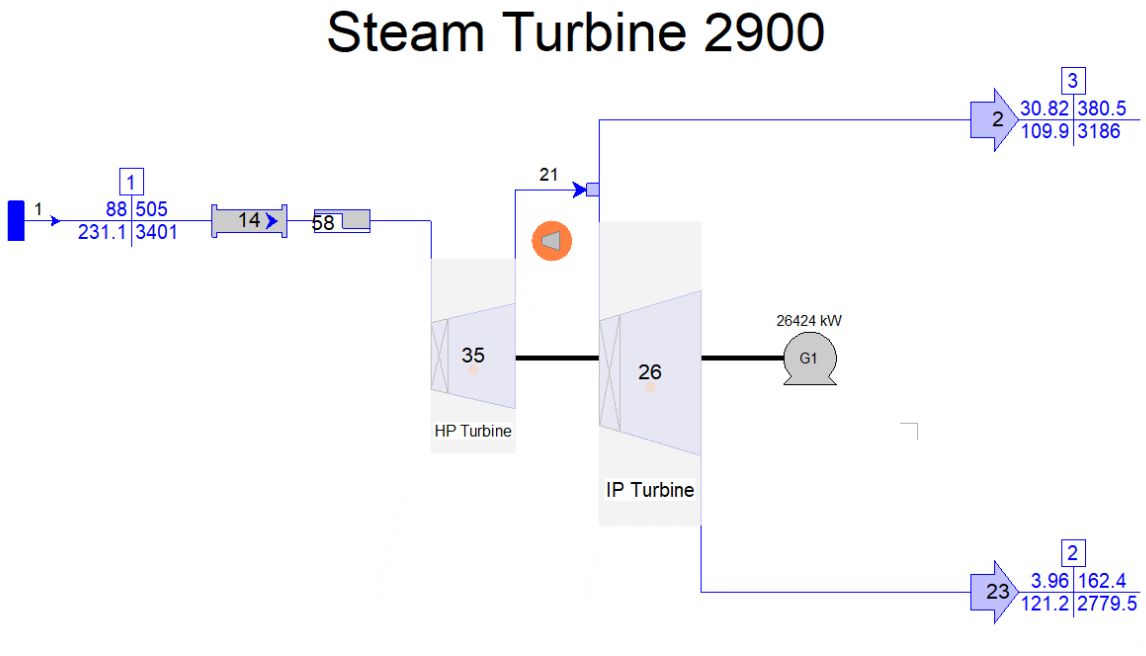

Figure 4.9: Steam turbine assembly in the THERMOFLEX environment

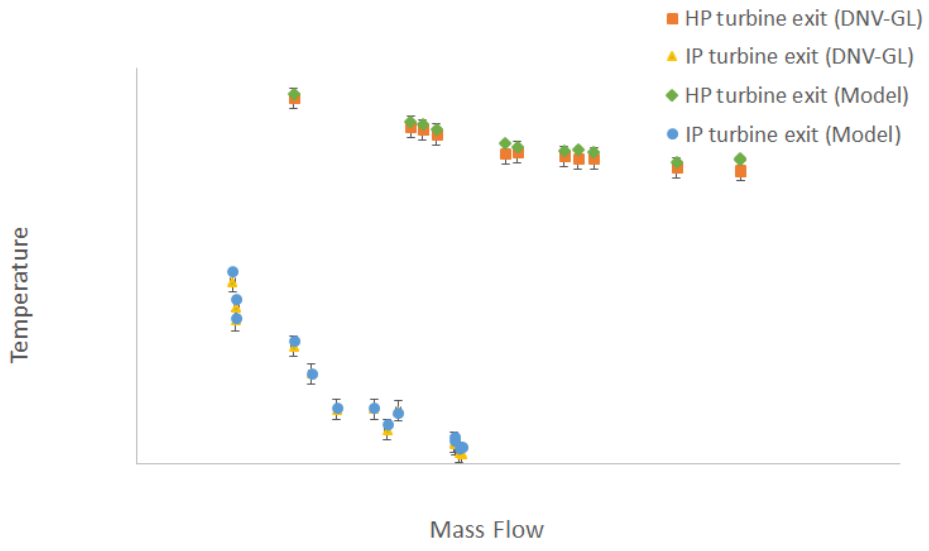

Figure 4.10: Temperature at the outlet of HP and IP Steam Turbine at varying process steam supply. The error bars show a 1 % deviation from the maximum absolute temperature of the HP inlet from the measured data.

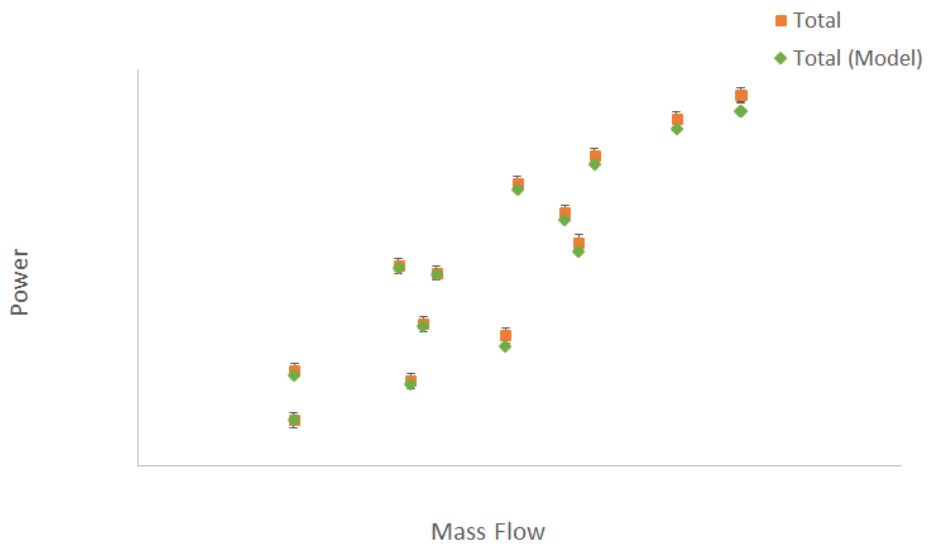

Figure 4.11: Combined power output of the entire steam turbine assembly. The error bars show a 2 % deviation from the highest total power output from the measured data.

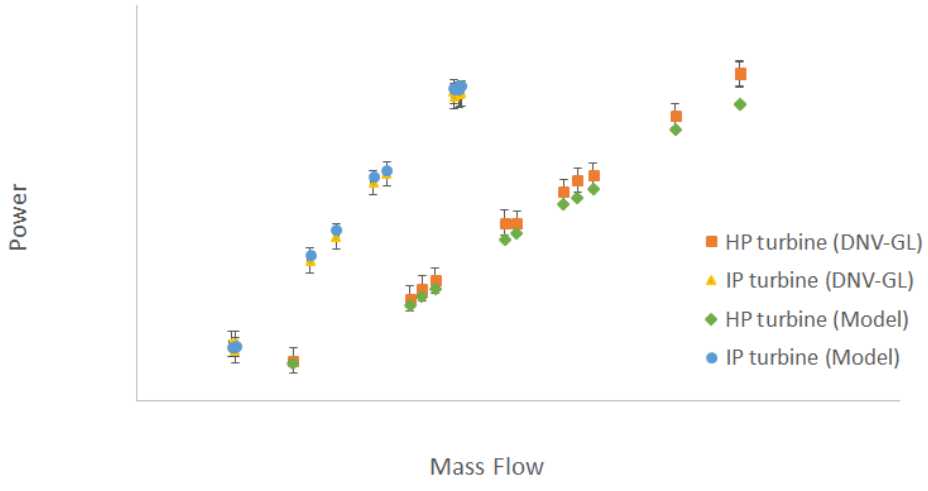

Figure 4.12: Power output of the HP and IP steam turbine separately. The error bars show a 2 % deviation from the maximum total power output from the measured data.

4.4. Coupling of the GT-HRSG and the ST model

Both the model of the GT-HRSG and the model of the ST give results that are able to simulate approximately the same behaviour as the actual system. To obtain a model to simulate the entire system these two models will be coupled, figure 4.13. The superheated steam outlet of the HP cycle in figure 4.1 is connected to the steam turbine assembly inlet of figure 4.9. Additionally, an infrastructure of HP, IP, and LP headers is implemented to enable (partly) bypassing of the ST. At last the EH's from chapter 3 are added.

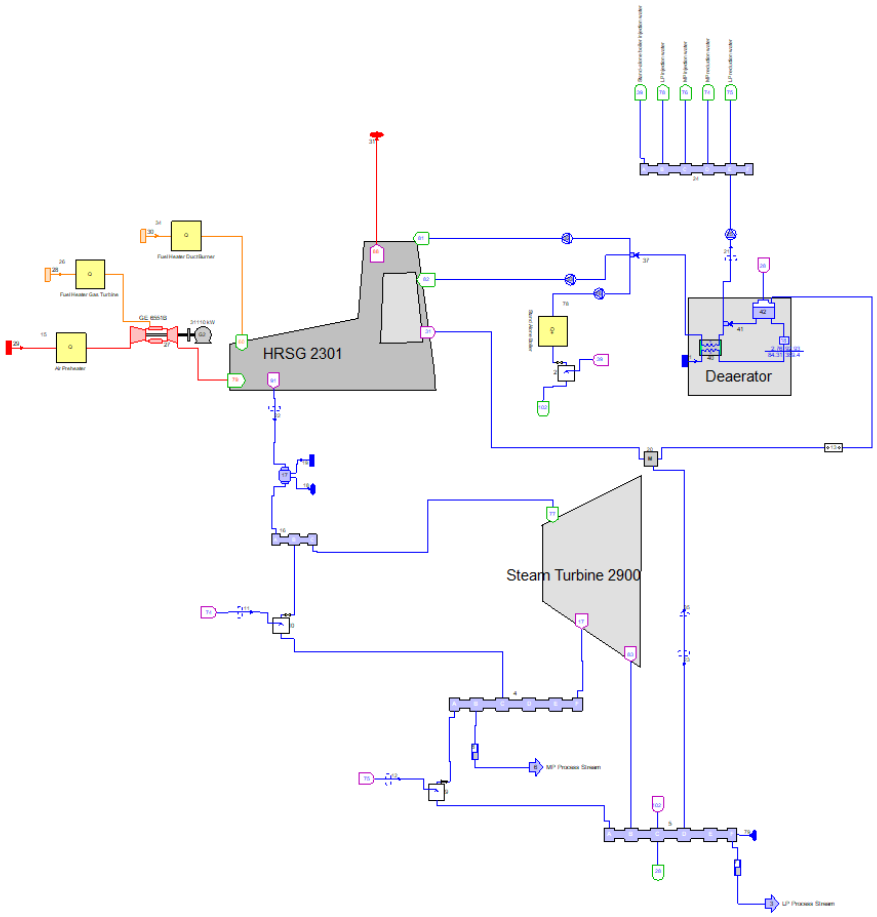

Figure 4.13: Final model of the combination GT, HRSG and ST in the THERMOFLEX environment. The yellow boxes have the function of the EH's. In this overview only the AP, GHGT, GHDB, and the SB can be seen.

This model will be used to analyse the steady state response to the deployment of the EH's described in chapter 3. The analysis is described in chapter 5.

5

Analysis of steady state performance of the electric heaters

After the conceptual cases of chapter 3 have been implemented in the model constructed in chapter 4, the performance of the concepts of electric heaters (EHs) can be evaluated. This will result in an answer to the question: *What is the steady state behaviour of the numerous electric heater concepts?* As was discussed earlier (table 2.1), the desired steam supply of the Delesto system is 120 t/h. In this chapter the performance of the EHs is reviewed for this process steam supply. Additionally, the performance of the EHs at a steam demand of 100 t/h and 140 t/h are researched to obtain a view of the steady state performance over a wider operating window considering that the steam demand might deviate from the design objective. The evaluation in this section only covers the steady state behaviour of the plant; the dynamic response is discussed in chapter 7.

Dependent on the location and the medium the EH is acting upon, the maximum load of the device differs. The limits are discussed in section 5.2. The performance of each of the devices will be assessed against several criteria, these criteria are discussed in section 5.3. Obviously, one of the key criteria in this study is the increased flexibility in terms of electricity output and the savings in gas consumption. The results from the analysis are discussed in section 5.4. From the results it shows that a few concepts are very promising, in section 5.5 the performance of a combination of the concepts is reviewed.

5.1. Operation modes

The conventional practise of ramping down the power production of the CHP is to first bring the GT to part load, the continuous steam demand is fulfilled by increasing the auxiliary firing. The minimum load the GT can operate at for each of the different process steam demands is summarised in table 5.1. As a second measure, to further reduce the power output, the steam turbine will be partially bypassed. As the ST is a very efficient method of producing electricity and it takes a lot of time to heat up, this only occurs in the event of longer periods of low electricity prices or when TenneT called off for reserve capacity.

Table 5.1: Minimum operation load of the gas turbine for some of the values of process steam demand.

Minimum operation load of the GT				
Process steam demand	100	**120**	140	[t/h]
Minimum GT Load	80	**80**	89	[%]
Air mass flow	114	**114**	125	[t/h]

The several modes of operation for the CHP including the EH are specified and shown in table 5.2. As with the conventional operational modes first the GT will be backed off from full load. Secondly, the EH will be turned on. Finally, in case there is still need for an additional decrease in electricity production, the ST will be ramped down.

Table 5.2: Operation modes of the CHP equipped with EH from full load to part load

	Modes of operation load of the CHP		
Mode	Gas turbine	Steam turbine	Electric heater
1	100%	100%	0%
2	min.	100%	0%
3	min.	100%	max.
4	min.	min.	max.

5.2. Limitations of electric heaters

The electric devices are all constrained by certain limits. Before analyses of the EHs, these limitations and how they will affect the performance needs to be understood. Furthermore, the conversion of electricity into heat is only useful until the point that the fuel consumption in the DB becomes zero. In table 5.3, an overview of the maximum power input of the EHs and their limiting factor at operation mode 3 are listed for a process steam demand of 100 t/h and 140 t/h. Besides that, the limits are described separately.

Air preheater

The AP heats the air entering the compressor of the gas turbine, figure 3.2. It is not able to bring the fuel consumption in the duct burner down to zero. Therefore the AP is only restricted by the maximum allowable compressor inlet temperature. The air flow in the GT depends on the load that the GT is operated at, figure 2.3. The mass flow corresponding to the minimum GT load of operation mode 2 are contained in table 5.1.

Duct heater

The DH can completely substitute the duct burner combustion. The radiative heat transfer to the evaporation screen and water walls will decrease, so that will not cause any problems. Zero gas consumption will limit the DH.

High pressure boiler

In case of the 100 t/h and 140 t/h the HPB is limited to the zero fuel consumption in the duct burner. The HPB at a process steam demand of 120 t/h is limited by the requirement that the LP process steam temperature should not drop below 165 °C. The decrease in temperature after the duct burner causes a decrease in heat transferred to the superheated steam in the superheater I. A decrease in the amount of injection water can mitigate this. Obviously, the amount of injection water cannot drop below zero. In this instance the superheater cannot maintain an outlet temperature of 505 °C. When the outlet temperature of the SHII decreases to much, the process steam temperature demand can't be fulfilled.

Low pressure boiler

The LPB would have a significant range, were it not for the mass flow restriction in the LP cycle.

High Pressure Pump

The maximum power input of the HPP is prescribed by the maximum design pressure of the HP cycle. As one can see in table 5.3 it is significantly less than the potential input of the other EHs.

Fuel Heaters

The fuel heaters are restricted by the maximum allowable natural gas temperature. The maximum electricity input of the FHGT is like the AP dependent on the load of the GT. The FHDB has a smaller maximum power input, as the fuel mass flow to the DB is smaller than to the GT.

Stand-alone Boiler

The SB is limited by a minimum mass flow through the system. When the EH load is set higher, the water/steam mass flow through the HRSG to low and the thermodynamic laws will be disobeyed in the model. The maximum input is significantly lower than the maximum input of the DH and HPB, but it is still amongst the larger capacity EHs.

Table 5.3: Overview of maximum power input of operation mode 3

	Overview				
Process steam demand	100	**120**	140	[t/h]	Limit
Air Preheater (AP)	7,167	**7,167**	7,561	[kW]	The compressor inlet temperature should not exceed 90 °C.
Duct Heater (DH)	29,688	**45,780**	58,220	[kW]	Converting electricity into heat is useful until the point that the fuel consumption in the DB becomes zero.
High Pressure Boiler (HPB)	28,489	**44,388**	55,123	[kW]	For 100 t/h and 140 t/h: Converting electricity into heat is useful until the point that the fuel consumption in the DB becomes zero. For 120 t/h: A LP steam temperature of 165 °C should be maintained
Low Pressure Boiler (LPB)	8,394	**8,391**	8,634	[kW]	The maximum mass flow of the LP cycle is 16 t/h.
High Pressure Pump (HPP)	0.321	**0.574**	0.530	[kW]	The pressure of the HP cycle should not exceed the design pressure of 102 bar.
Fuel Heater Gas Turbine (FHGT)	2,873	**2,874**	3,088	[kW]	The natural gas temperature should stay well below the limit of auto-ignition. For safety reasons a maximum of 500 °C is taken.
Fuel Heater Duct Burner (FHDB)	873	**1,352**	1,709	[kW]	The natural gas temperature should stay well below the limit of auto-ignition. For safety reasons a maximum of 500 °C is taken.
Stand-alone Boiler (SB)	16,136	**29,244**	43,416	[kW]	A minimum water mass flow through the heat exchangers is required.

5.3. Analysis of interest

As the performance of the several EHs is being assessed. To obtain quantitative results some metrics are defined. The purpose of the EHs is to create flexibility in terms of the net power output and to save gas in this process.

5.3.1. Additional Flexibility

The main purpose of the Electric Heater is to induce a change in the net power output of the plant. The Net Power Output (NPO) is defined as in equation 5.1. With P being the electric power produced, and subscripts GT, ST,aux and EH respectively for the gas turbine, steam turbine, auxiliaries and the electric heater. The negative sign in the term of the auxiliaries and electric heater indicates that power is consumed.

$$\text{NPO} = P_{GT} + P_{ST} - P_{aux} - P_{EH} \tag{5.1}$$

The Additional Flexibility (AF) is a measure of the flexibility obtained. It is expressed as the change in NPO due to the deployment of the EH, see equation 5.2. The subscripts 2 and 3 stand for that particular operation mode (see table 5.2).

$$\text{AF} = \text{NPO}_2 - \text{NPO}_3 \tag{5.2}$$

5.3.2. Relative Fuel Savings

Another interesting study is how much gas is saved with the flexibility obtained from the EH. A measure, the relative fuel savings, is defined in equation 5.3. Taking the conventional plant, with the gas turbine in part-load (mode 2 from table table 5.2) as reference plant. This shows a clear view of the additional fuel savings next to the fuel savings already obtained from the ramping down to part-load operation is achieved. The measure will be referred to as Relative Fuel Savings (RFS), equation 5.3. H_3 stands for the fuel energy input of the system with EH, H_2 stands for the one of the reference plant with part-load conditions.

$$RFS = 1 - \frac{H_3}{H_2} \tag{5.3}$$

Another interesting study would be the CO_2 emission savings[35]. However, in this study the CO_2 emissions are one-to-one related to the AFSs in the plant, as the electricity used is assumed to come from CO_2-free wind power.

5.3.3. Effectiveness

The Absolute Fuel Savings (AFS) are defined as the absolute fuel saved thanks to the deployment of the EH, equation 5.4.

$$\text{AFS} = H_2 - H_3 \tag{5.4}$$

The effectiveness ϵ of an EH will be defined as the ratio between the fuel saved and the flexibility obtained due to the deployment of the EH.

$$\varepsilon = \frac{\text{Absolute Fuel Savings}}{\text{Additional Flexibility}} = \frac{AFS}{AF} \tag{5.5}$$

5.3.4. Thermal Efficiency

The thermal efficiency η_{th} of a CHP plant is described with equation 5.6. The efficiency in a system could also be described using the energy loss in the stack, (second equality in equation 5.6). It is the energy not absorbed by the water-steam cycle from the flue gases. The less the energy content at the outlet of the stack flow differs from the ambient energy content, the smaller the losses.

$$\eta_{\text{th}} = \frac{\text{Useful output}}{\text{Energy input}} = 1 - \frac{\text{Heat losses}}{\text{Energy input}} \tag{5.6}$$

By looking at the energy present in the flue gases at the outlet of the stack, one can get an idea on how efficient the plant is. Dividing this by the stack losses that exist at the conventional part load operation gives an indication of the relative efficiency performance.

$$\text{Relative Stack Losses} = \frac{\text{Stack Losses}}{\text{Stack Losses}_2} \tag{5.7}$$

5.4. Results

Bearing in mind the maxima established in section 5.2, the analysis of interest described in section 5.3 can be performed. For increments of one-fifth of the maximum power input of the EH, performance data has been collected.

The results will be plotted against the additional flexibility achieved (equation 5.2). It is the change of the net power output caused by the deployment of the EH. The greater the domain of a certain EH is, the more flexibility this EH can provide.

The case of a process steam demand of 120 t/h will be discussed first (section 5.4.1), after which deviations to the design process steam demand will be looked into (section 5.4.2).

Before the more specific results are discussed, some general numbers could be helpful in gaining an understanding of the order of magnitude of the fuel consumption and electricity generation. In table 5.4 one can find the values of electricity generation, steam production and fuel usage when no electric intervention is considered.

Table 5.4: Relevant energy flows in the CHP at full- and part-load conditions

	Energy Flows				
	Process steam demand	100	**120**	140	[t/h]
Mode 1	Electricity Generation GT	37	37	37	[MW]
	Electricity Generation ST	13	18	20	[MW]
	Fuel Consumption GT	117	117	117	[MW]
	Fuel Consumption DB	22	39	54	[MW]
	LP Steam Production	77	93	108	[MW]
	Stack Losses	12	11	10	[MW]
Mode 2	Electricity Generation GT	29	29	32	[MW]
	Electricity Generation ST	13	18	20	[MW]
	Fuel Consumption GT	99	99	107	[MW]
	Fuel Consumption DB	30	46	58	[MW]
	LP Steam Production	77	93	108	[MW]
	Stack Losses	9	8	8	[MW]

The total amount of electricity produced is from the GT and the ST. The increase in production at full-load conditions for a higher steam demand is attributed to the increased amount of steam expanding in the turbine. The fuel usage increases with an increase in steam demand in both part- and full-load conditions, which is solely attributed to the increased fuel usage in the duct burner.

5.4.1. 120 t/h

As could already have been deduced from table 5.3 the maximum load of each EH differs from almost nil (HPP) to 44 MW (DH). This maximum load cannot directly be translated to the maximum additional flexibility and fuel savings offered by the EH. From the graph in figure 5.1 it can be seen that the maximum amount of fuel saved is the same for the HPB and DH. Obviously, this is the limit of fuel saving due to the zero fuel consumption of the duct burner at this point. The steeper the slope of the curve, the more efficient fuel is saved. One can see that the AP is the most efficient EH to save fuel, and the SB and LPB the least efficient EHs. The HPP adds no significant RFS, the FH's of the GT and DB and the LPB save a limited amount of fuel, mainly due to the limited operating range of the EHs.

In figure 5.2 practically the same information can be found. But now a clear distinction between the numerous EH curves can be made. It can be seen that the FHGT, FHDB, DH, HPB and SB have more or less a constant effectiveness throughout their operating range. The HPB having the greatest, and the SB having the worst effectiveness of this selection. The effectiveness of the HPP alternates rapidly for an increase in

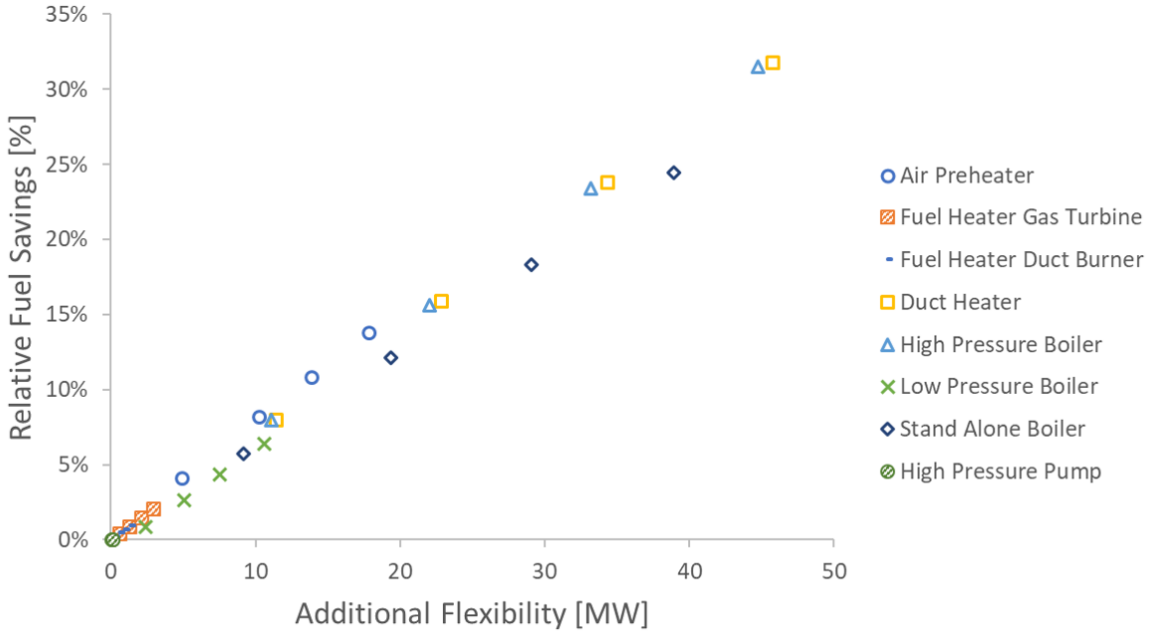

Figure 5.1: Relative fuel savings of the electric heaters at design process steam demand (120 t/h)

load. The LPB effectiveness increases with an increase in load and AF. The AP becomes less effective over its operating range. However, it is still more effective than the other devices.

It is readily understood that one would prefer a device with high AF and great ε, (in this graph the upper right corner). On the contrary, low AF and small ε is the least favourable region to operate in, (the lower left corner in the graph). From that view, the AP can be praised for its high effectiveness, and the HPB, DH and HPB for their range.

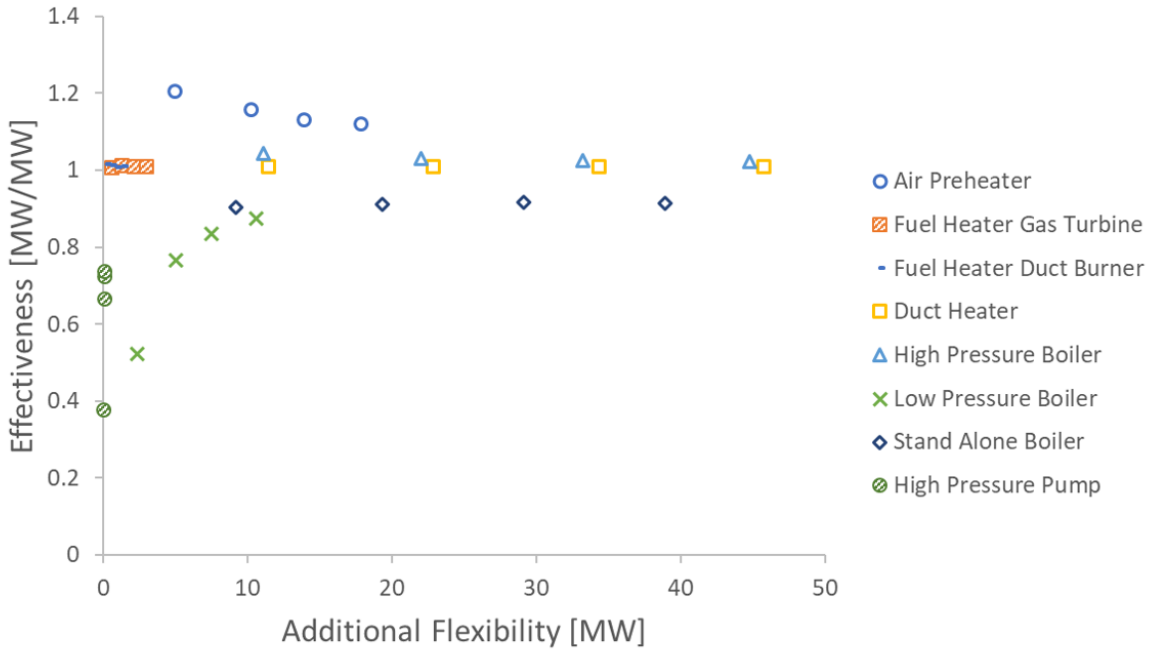

Figure 5.2: Effectiveness of the electric heaters at design process steam demand (120 t/h)

In figure 5.3 one can find the relative stack losses of the EHs. A RLS of 1 means that the losses are equal

to the losses of the system without deployment of an EH (operation mode 2 from table 5.2. A value of more than one implies that the losses have increased in reference to the losses at operation mode 2. This is the case with the operation of LPB and SB. The system becomes less efficient as the load of these EHs increase. The DH, HPB and AP show a more favourable result. Their increasing deployment results in smaller losses from the stack. The lower stack losses with operation of the AP can be explained by the smaller air flow through the HRSG. The specific enthalpy of the flow has increased.

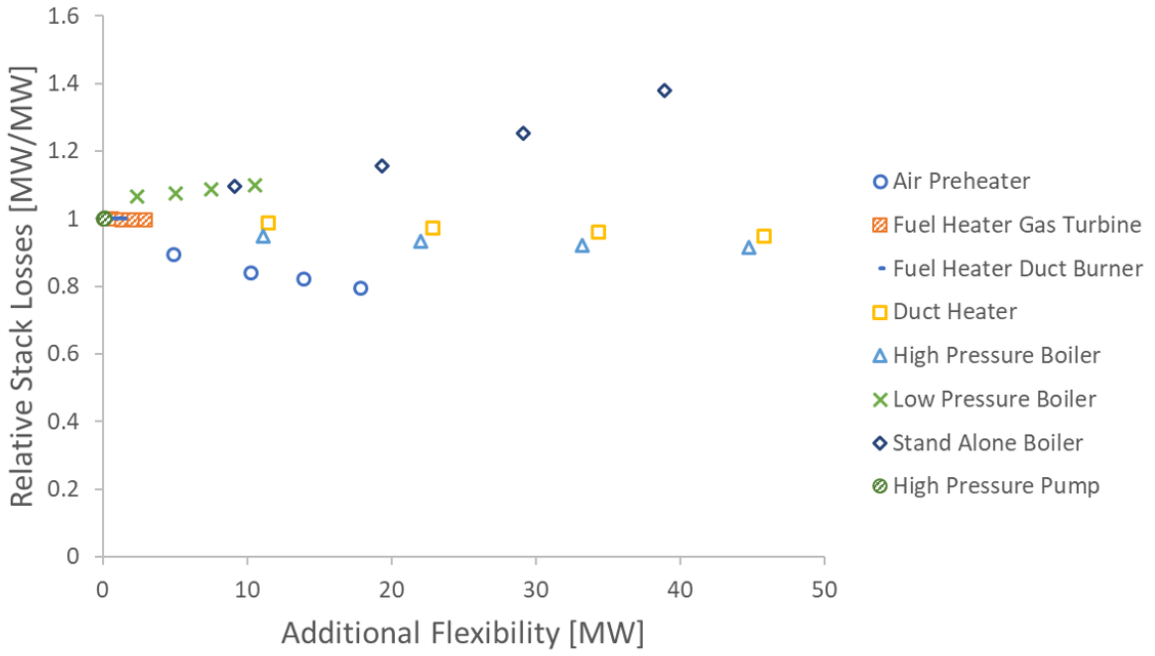

Figure 5.3: Relative stack losses of the electric heaters at design process steam demand (120 t/h)

5.4.2. 100 and 140 t/h

The EHs show similar results at the off-design steam demand of 100 t/h and 140 t/h. The set of graphs for both are contained in appendix A. The graph of the effectiveness at 140 t/h is emphasised in this section, figure 5.4.

There is no significant increase in Additional Flexibility (AF). In fact, in case of the SB the system encounters a decrease in maximum AF obtained of 5 MW. The trends of the curves remain unchanged. It is noticeable that there is a strong increase in effectiveness of the HPP, although it is inversely proportional to the power input. The effectiveness of the AP, DH, HPB and SB are now closer to one than for design process steam demand.

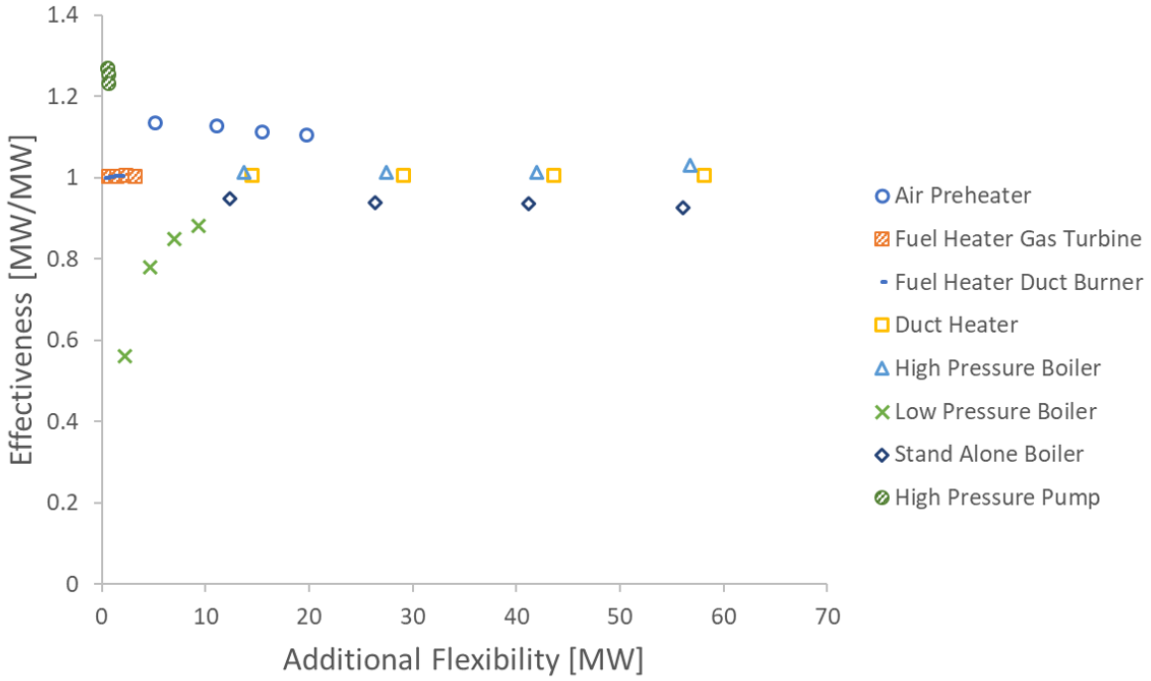

Figure 5.4: Effectiveness of the electric heaters at a process steam demand (140 t/h)

5.5. Combination of two Electric Heaters

As became apparent in section 5.4, the effectiveness of the AP terms of fuel savings is relatively high compared to its competing devices, but its range is limited. On the other hand, the DH, HPB and SB have a limited effectiveness, but do have a large AF. Therefore, the AP is deployed first and on top of that the DH, HPB or SB could be utilised. Would the combination of these systems lead to even more favourable results?

5.5.1. Limits

For each combination the logic holds that increasing the power input is useful up to the instance that zero fuel is consumed in the duct burner. Apart from the HPP at a process steam demand of 140 t/h, for which the process steam temperature is no longer the limiting factor, the operational load limits for the EHs do not change compared to operation without the AP, table 5.5.

Table 5.5: Overview of maximum Power input of Operation mode 3 for parallel operation of selected EHs

Overview				
Process steam demand	120	**100**	140	[t/h]
Air Preheater & Duct Heater (AP-DH)	33	**51**	65	[MW]
Air Preheater & High Pressure Boiler (AP-HPB)	32	**50**	58	[MW]
Air Preheater & Stand-alone Boiler (AP-SB)	9	**23**	37	[MW]

5.5.2. Results

The combinations of the AP-DH, AP-HPB, AP-SB result in a higher AF domain, figure 5.5. The increase for the AP-DH and AP-HPB are 25 MW and the increase for AP-SB is 9 MW. Compared to the case of stand-alone operation, the maximum RFS is higher. This is because the AP is able to save gas in the GT. In the previous analysis this was partly compensated with an increase in Duct Burner fuel consumption. In a combined configuration this can be compensated with an increase in DH, HPB or SB load.

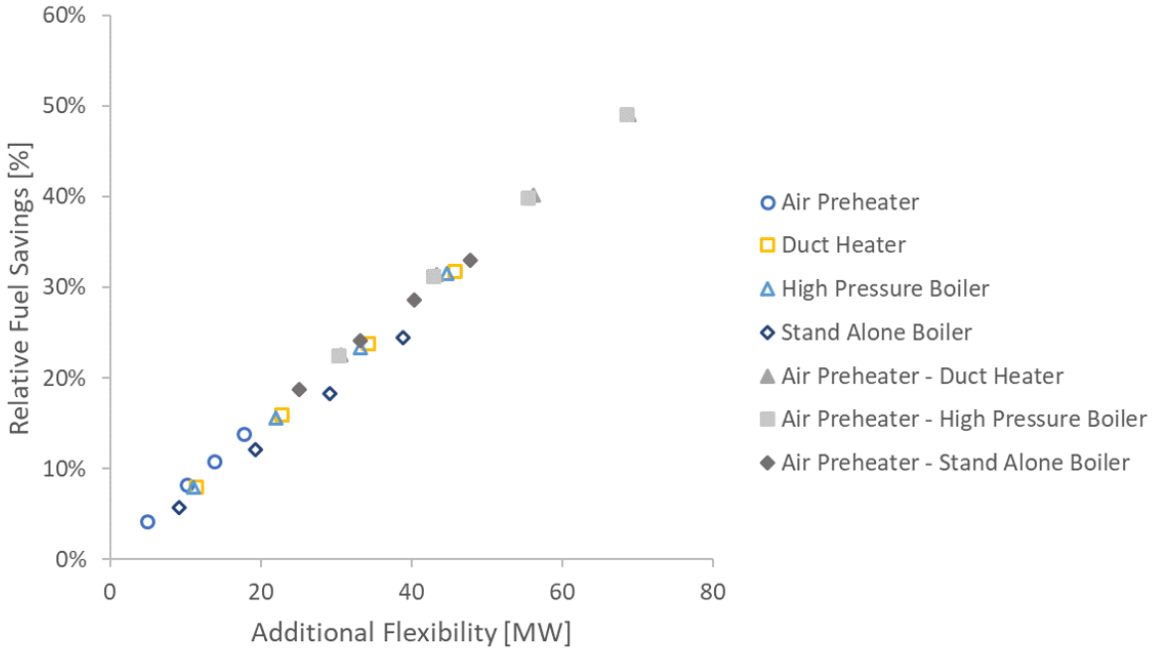

Figure 5.5: Relative fuel savings for the combinations of some of the electric heaters at design process steam demand (120 t/h)

In figure 5.6 a clear view on the effectiveness of the combinations is obtained. From the three combinations, the AP-SB performs worst, but still better than its stand-alone version. The AP-DH's and AP-HPB's effectiveness' are similar to each other.

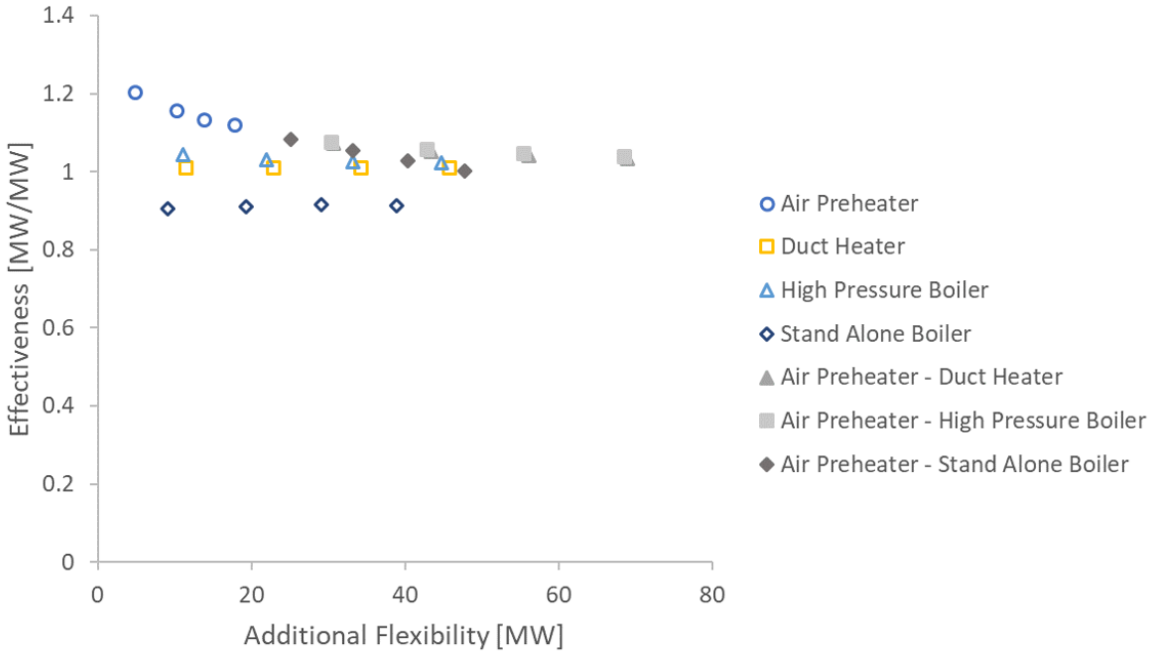

Figure 5.6: Effectiveness for the combinations of some of the electric heaters at design process steam demand (120 t/h)

The Relative Stack losses, figure 5.7, are for all combinations an improvement over their stand-alone version. The AP-DH and AP-HPB maintain the lower Stack Losses that were achieved with the sole AP. The AP-SB's stack losses increase, up to a point where they are higher than the losses of the reference plant, but

remain below the stack losses of the SB.

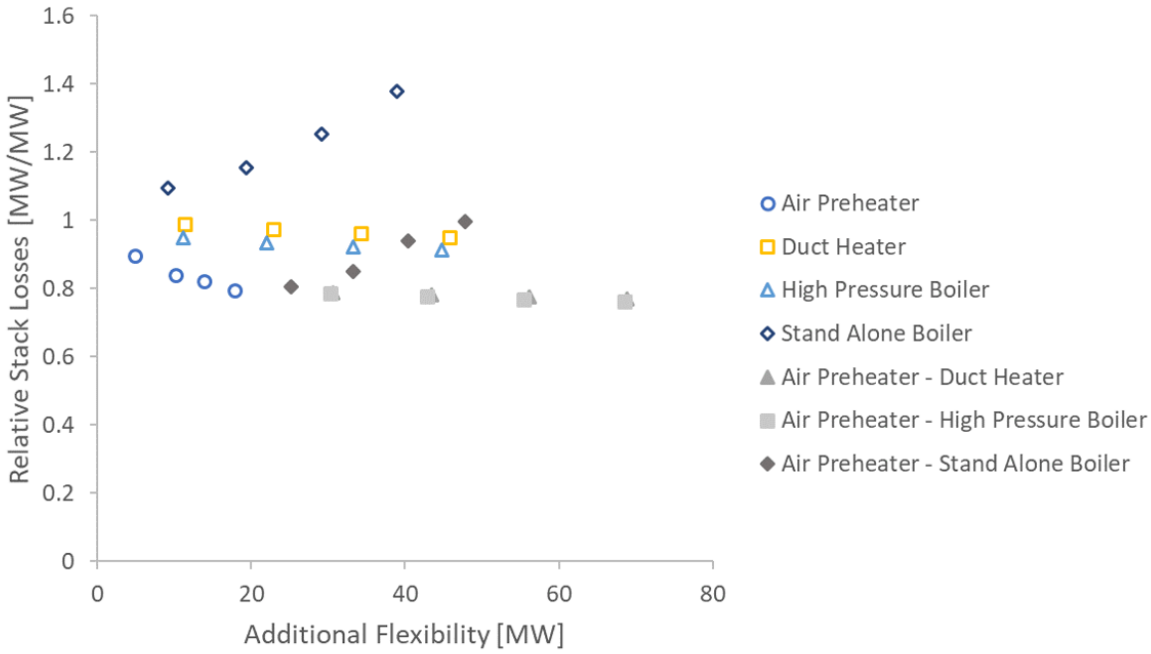

Figure 5.7: Relative stack losses for the combinations of some of the electric heaters at design process steam demand (120 t/h)

5.6. Conclusion

One could see that although the AP has a low operating range compared to DH, HPB and SB, its performance in terms of effectiveness is beneficial. Of the higher range devices the DH, HPB and the SB are interesting.

It was readily seen that the HPP did not stand a chance compared to the alternatives in terms of both AF and RFS. Its effectiveness varies a lot with a change in process steam demand. The effectiveness of the gas heaters was as good as the HPB and the SB, but the additional flexibility and the corresponding maximum RFS provided is poor. For LP holds the same, with in addition having higher stack losses.

The combination of the AP-DH, AP-HPB and AP-SB had been reviewed. These combinations all show improved performance in terms of RFS, AF and RSL.

The research will be continued with the unaccompanied operation of the AP, the DH, the HPB, and SB. Also the promising performance of the combinations of the AP-DH, AP-HPB and AP-SB will be further looked into. In the next chapter the dynamic behaviour of the critical part of the HRSG will be researched.

6

Dynamic model of the HRSG

One can imagine that the operation of the EH's induce some changes in the temperature profile over the HRSG. These changes in temperature induce the rise of additional mechanical stresses in both the flue gas duct and the water/steam path, leading to thermal fatigue. In this chapter a model is set-up that allows to study the dynamic behaviour of the HRSG in chapter 7.

To know where the critical locations of the HRSG exist, the spots where a lot of changes are to be expected are of interest. Therefore the system to be modelled will be demarcated first in section 6.1 with the use of the steady state model of chapter 5. A general model will be set up, which will describe the part of the HRSG that is within the system boundaries. The assumptions and conservation equations for each component are set up in section 6.3. An overview of the complete set of ordinary differential equations is given in section 6.4. The development of the model is elaborated on in section 6.5.

No electric device will interfere with this model yet, thus the solution of the model should tend to a steady state that is similar to the steady state obtained in the THERMOFLEX model, section 6.6. The dynamic model is modified to simulate the effect of the electric heater (EH), section 6.7.

6.1. The System Boundaries

The system boundaries can be defined using the THERMOFLEX model made for the analysis in chapter 5. Although THERMOFLEX only gives steady state solutions, it is able to provide a rough idea of the system's response to variations. By varying the loads of the gas turbine and the electric heater the locations where temperature fluctuations in the HRSG can be expected are identified. As can be seen from table 6.1 the temperature in the flue gases vary widely. Especially the DH has a large impact on the temperature. Another reason for large variations is whether or not duct firing is used. The temperature variations of the water/steam path, see table 6.2, are less compared to the flue gas path. However, due to thermal effects in the thick-walled headers it is not of less importance. Because it seems that most action takes place between the two HP superheaters, and because the heat transfer in the evaporator fixes the mass flow, the boundaries are taken as shown in figure 6.1. Outside these boundaries the stream conditions are assumed to be known and not that critical. Therefore, the gas turbine, the steam turbine system, the HP economisers and the entire LP cycle shall be disregarded.

Table 6.1: The absolute temperature for Mode 2 in column 2 and the relative changes compared to Mode 2 for maximum operation of AP, DH, HPB and SB for the flue gas path

Temperature of the flue gas path					
	T [K]	ΔT [K]			
Exit of	Mode 2	AP	DH	HPB	SB
Gas Turbine	837	35	0	-1	0
HP superheater II	766	-5	0	-30	-15
DH out	766	-5	343	-30	-15
DB out	1024	59	18	-298	-217
HP superheater I	880	27	10	-209	-135
HP evaporator	579	-1	0	-2	-2
HP Economiser II	437	-12	-2	-12	44
LP Superheater	436	-12	-2	-12	43
LP Evaporator	422	-2	0	-2	7
LP Economiser	420	-1	0	-1	5
HP economiser I	357	-5	-2	-5	28

Table 6.2: The absolute temperature for Mode 2 in column 2 and the relative changes compared to Mode 2 for maximum operation of AP, DH, HPB and SB for the water/steam path

Temperature of the water/steam path					
	T [K]	ΔT [K]			
Exit of	Mode 2	AP	DH	HPB	SB
HP Superheater II	778	0	0	-31	0
Desuperheater	674	-28	0	-54	-82
Injection water	354	-3	-2	-3	5
HP Superheater I	774	22	9	-154	-68
HPB	576	0	0	0	-1
HP Evaporator	576	0	0	0	-1
HP Economiser II	538	-11	-2	-14	33
HP Economiser I	412	-6	-1	-7	13
HP pump	354	-3	-2	-3	5
LP Superheater	428	-5	-1	-5	10
LP Evaporator	418	0	0	0	1
LP Economiser	414	4	1	4	-17
LP pump	353	-3	-2	-3	4

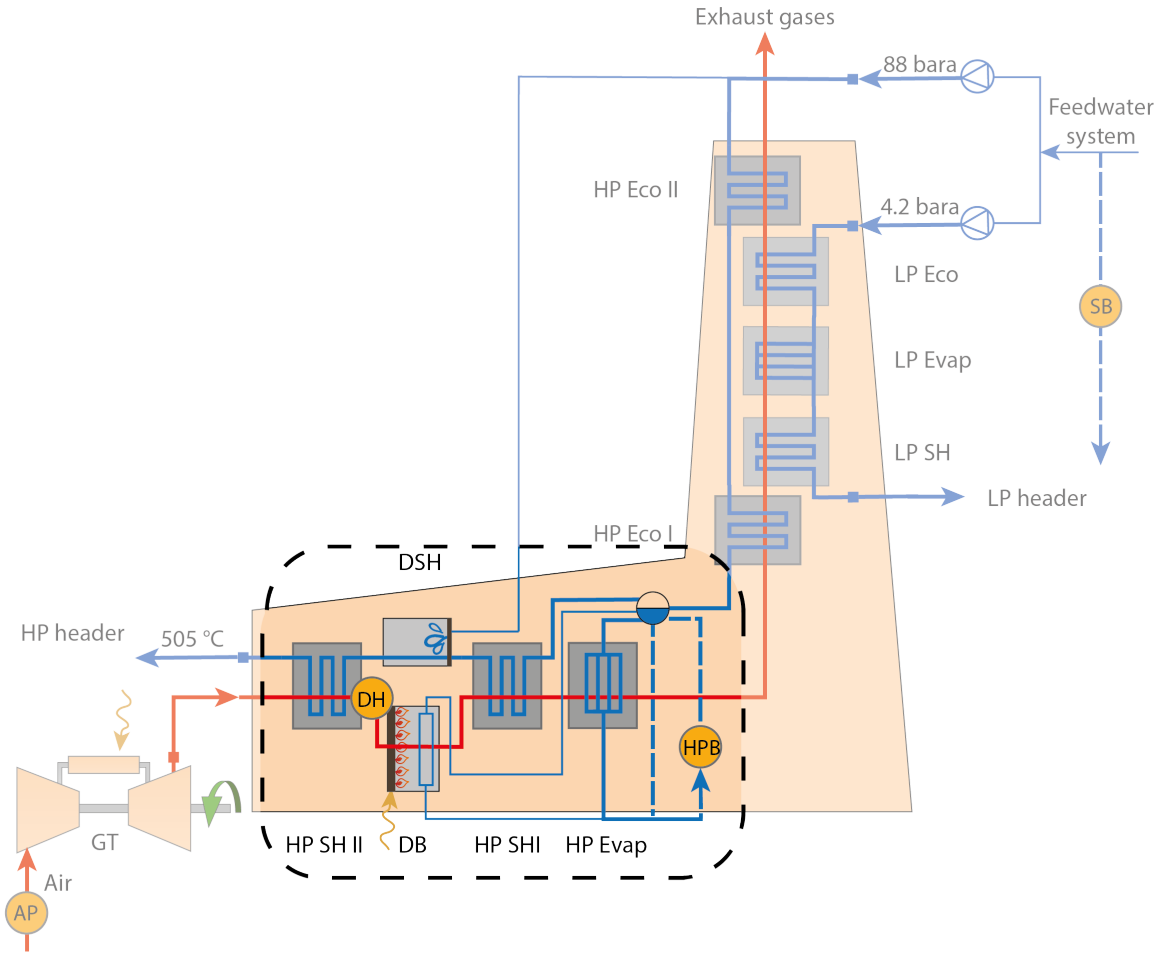

Figure 6.1: System boundaries for the dynamic model established using the steady state model from THERMOFLEX Thermoflow

6.2. Inputs of the system

In figure 6.2 the system bounaries are shown ones again. Inputs are indicated with an arrow towards the system, outputs pointing outwards. The temperature and mass flow of the flue gas entering the superheater II, known from the THERMOFLEX model, will be used as input of the dynamic model. The fuel consumption in the duct burner is an input. The mass flow of the water/steam path is fixed by the two evaporator systems and the injection water of the desuperheater. This injection water is a function of the outlet steam temperature of HP-SHII.

6.3. Conservation equations

The dynamic model will be based on two fundamental laws of physics. The conservation of mass and the conservation of energy. No mass or energy is created nor destroyed. The integral form of the conservation equations for control volumes is used. The formula for conversation of mass in a control volume is shown in equation 6.1 and the formula for the conservation of energy is shown in equation 6.2. The subscripts E and L stand for the 'Entering' and 'Leaving' flows of the system. Momentum is also conserved, but the effects of this conservation are not included in this analyses.

$$\frac{dm}{dt} = \sum_{E} \dot{m} - \sum_{L} \dot{m} \tag{6.1}$$

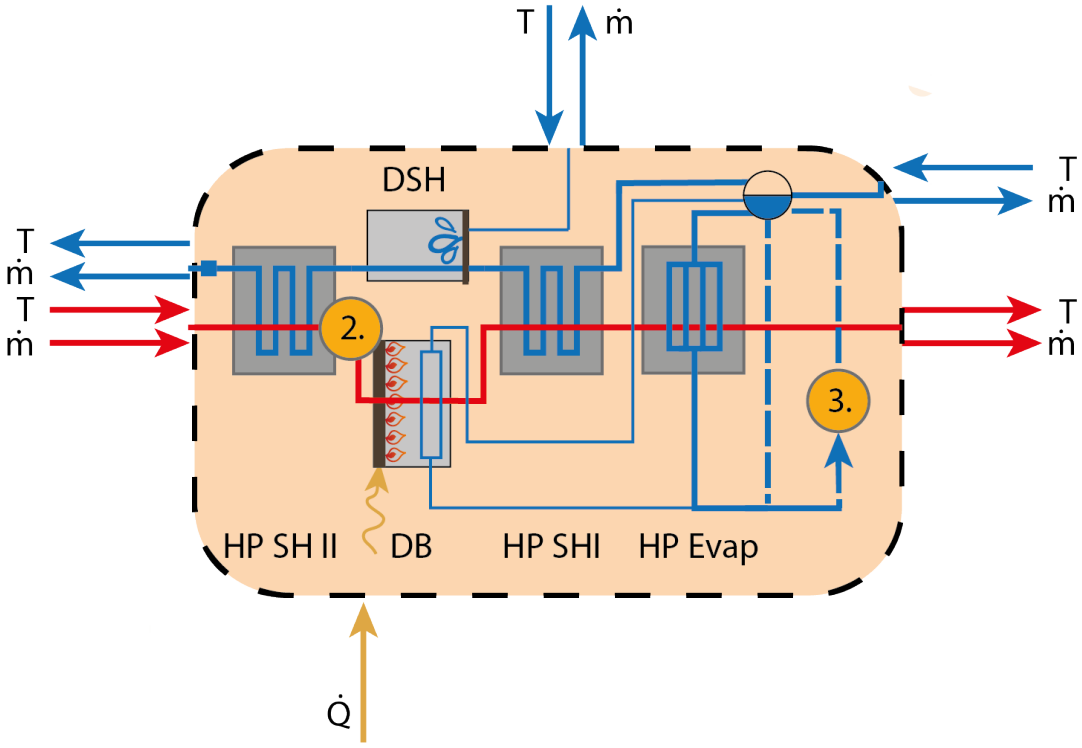

Figure 6.2: Knowns and unknowns at the system boundary.

$$\frac{dE}{dt} = \dot{Q} - \dot{W} + \sum_{E} \dot{m}(u + \frac{V}{2} + gz) - \sum_{E} \dot{m}(u + \frac{V}{2} + gz) \tag{6.2}$$

The total energy of a system E is the sum of the internal U, kinetic KE, and potential energy PE of the control volume (equation 6.3). Neglecting the kinetic and potential energy changes over time, and substituting equation 6.3 into equation 6.2 results in equation 6.4.

$$E = U + KE + PE \tag{6.3}$$

$$\frac{dU}{dt} = \dot{Q} - \dot{W}_{tot} + \sum_{E} \dot{m} \cdot u - \sum_{L} \dot{m} \cdot u \tag{6.4}$$

The work $\dot{W}$ done by the system could be separated into two components. One of which is the flow work, the work done on the boundaries due to the pressure of the flow, pv. The other contribution is work, on for example, shafts. The conservation of energy becomes:

$$\frac{dU}{dt} = \dot{Q} - \dot{W} + \sum_{E} \dot{m}(u + pv) - \sum_{L} \dot{m}(u + pv) \tag{6.5}$$

The sum of the internal energy and flow work $u+pv$ seen in equation 6.5 is well known as the specific enthalpy h. Substituting h will result in our final general conservation of energy equation, equation 6.6.

$$\frac{dU}{dt} = \dot{Q} - \dot{W} + \sum_{E} \dot{m}\, h - \sum_{L} \dot{m}\, h \tag{6.6}$$

The system consists of 3 domains; the water-steam path, the flue gas path and the tube material. The water/steam path is denoted with the subscript w and the flue gas path with the subscript fg. Formulating the conservation of mass and energy for each of the domains for each component will result in a system of differential equations. Solving this set of equations will give insight in the dynamic behaviour of the HRSG.

6.3.1. Conservation Equations of HP Heat exchangers

There are four heat exchangers within the system boundaries; HP Superheater II, HP Superheater I, the evaporation system in the duct burner and the HP evaporator. The evaporation system in the duct burner (DB evaporator) consist of the water walls and evaporation screen and is considered to be a single heat exchanger in this analysis.

Assumptions

Papers on the modeling of a HRSG [36] [37] [38] [39] are used as inspiration for suitable assumptions.

- The flue gas and water path are both assumed to be incompressible flows. This is a safe assumption, as the Mach number is far below 0.3.
- The thermal conductivity in the tube material is assumed to be infinite.
- Convective heat transfer is much larger than the heat transfer in longitudinal direction.

This means that the radial, longitudinal and circumferential temperature gradient in the material is zero. The temperature of the wall is uniform.

- The temperature of the flue gases is uniform over the cross section of the duct.
- The temperature of the water or steam is uniform over the cross section of the tubes.
- There is no work done in the heat exchangers: $\dot{W} = 0$.
- Blow down in the evaporator is ignored.
- The specific heat and the mass are taken as constants during the simulation.

Grid

The assumption is made that there exists one uniform temperature in the tube walls. This would not be physically possible as there does not exist a single wall temperature in the SHII or SHI that is higher than the highest temperature in the water/steam path and lower than the lowest temperature of the flue gas path. Temperature cross is the result, see the example in figure 6.3. In this case after the intersection both the water and the flue gas would be cooling the wall, and the wall temperature would decrease. If the wall temperature is lower than both the flue gas and water path, the wall is heated, and the temperature rises again. This mechanism in itself is not a problem, however the temperature ranges of the HE's do not allow this. To avoid temperature cross in the heat exchangers they are subdivided in a number of discretisation cells. Besides avoiding temperature cross there is another reason to subdivide the heat exchangers. The accuracy of the model will increase with an increase in the number of cells. The down side is that the computational time will increase with it.

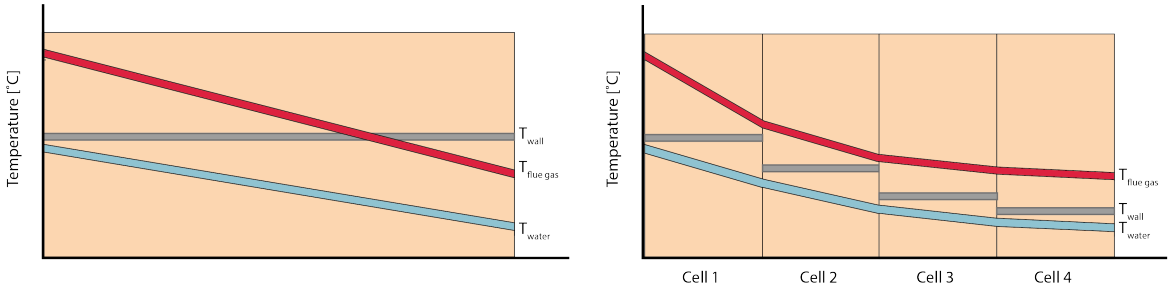

(a) Without subdivision: temperature cross occurs

(b) Coarse grid of four cells: no temperature cross occurs

Figure 6.3: Temperature profile for a heat exchanger

This subdivision will act as a very coarse grid of the system. In case of the SHII and SHI a decision on the grid is made based on the actual geometry of the heat exchangers. In figure 6.4 the configuration of SHII is shown and in figure 6.5 the configuration of SHI is shown. They have respectively 4 and 8 tube coils between the headers. For that reason the choice has been made to subdivide the superheater II into 4 cells and the superheater I into 8 cells. The HP evaporator will be divided into 4 cells (figure 6.6), in 7 it will be evident that this number is sufficient, and temperature cross is avoided.

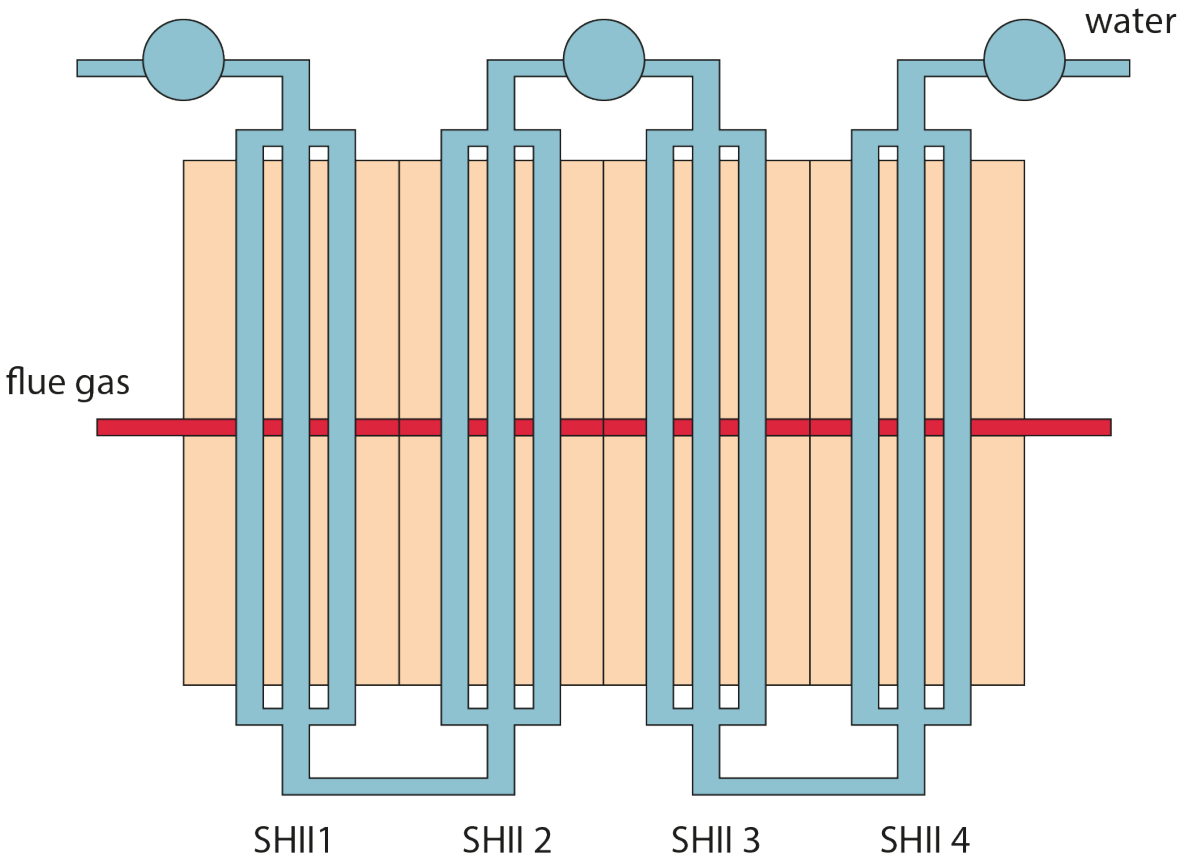

Figure 6.4: Schematic view on the configuration of the HP Superheater II. It consists of 4 coils connected by headers. Each coil has 3 staggered rows of finned tubes.

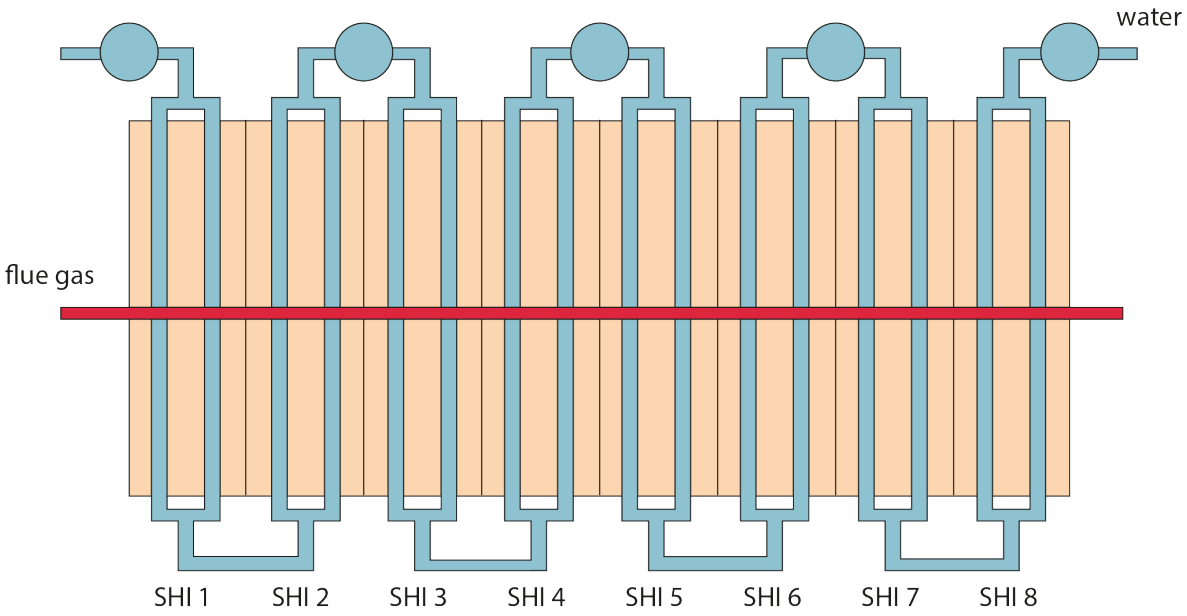

Figure 6.5: Schematic view on the configuration of the HP Superheater I. It consists of 8 coils connected by headers. Each coil has 2 in-line rows of bare tubes.

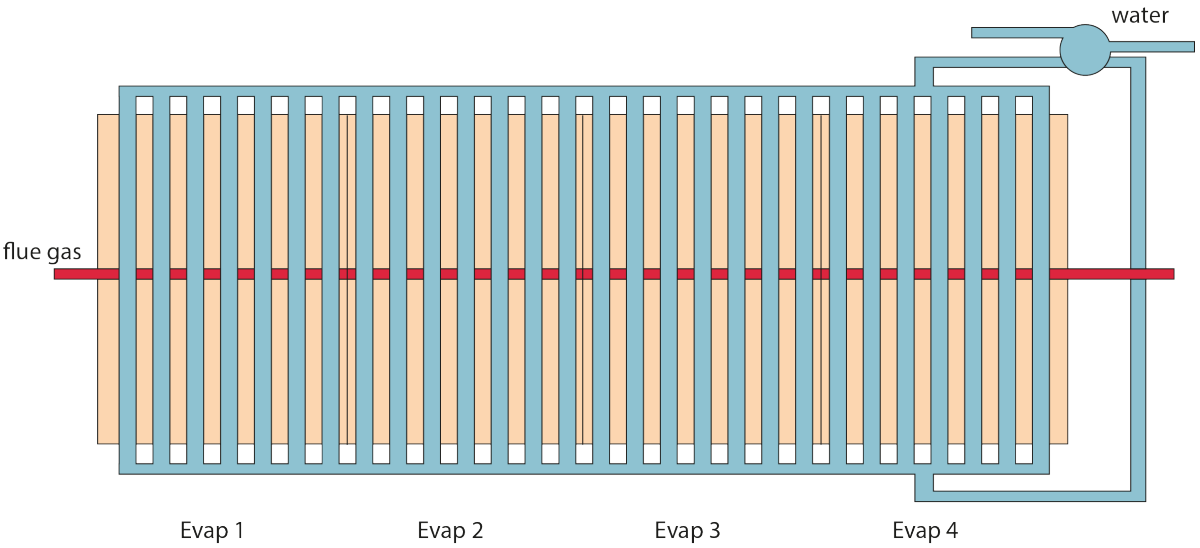

Figure 6.6: Schematic view on the configuration of the HP Evaporator. All the tube bundles are connected to the same header. The rows of finned tubes are configured in a staggered manner.

An example of a cell

In figure 6.7 the heat transfer from the flue gases to the water is shown for a single cell. The subscripts E and L denote respectively the entering and leaving stream.

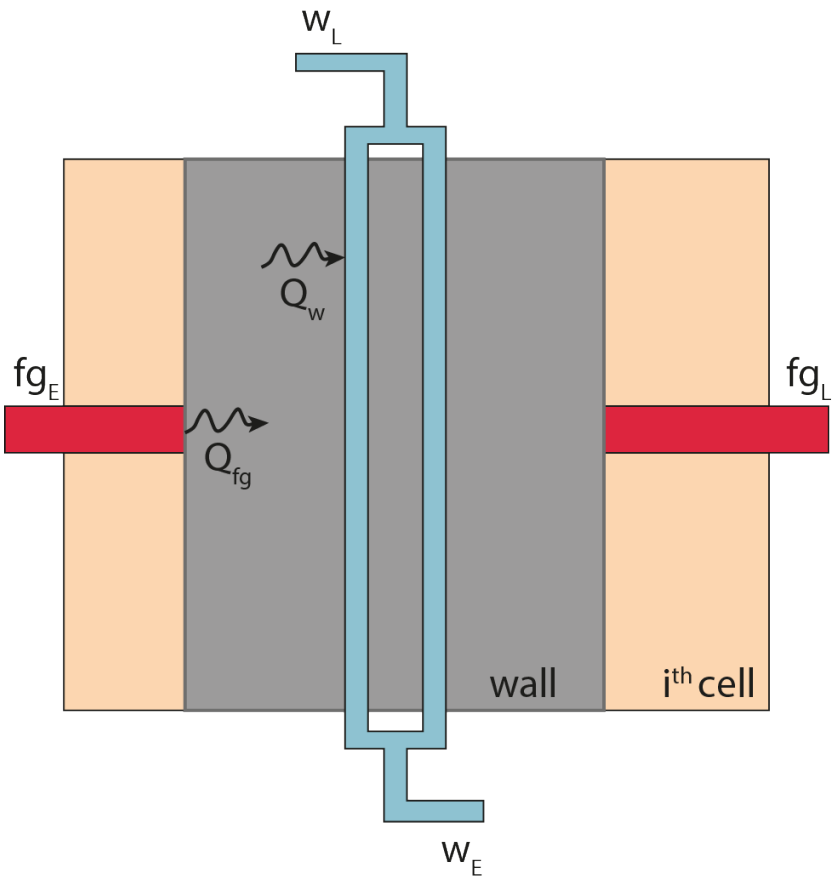

Figure 6.7: Heat transfer in a coil and the indication of the symbols

Mass conservation equations of a cell

Applying equation 6.1 to each domain of a cell of a heat exchanger, the mass conservation of that cell is known. The mass conservation of the water/steam path and the flue gas path of the heat exchangers are described in respectively equation 6.7 and 6.8. The flow of both domains is assumed to be incompressible, resulting the equations to be equal to zero. For all the heat exchangers the mass conservation equations are quite similar. As both equations equal zero, in both cases the entering flow is equal to the leaving flow, equation 6.9. *HE* can be substituted with the name of the heat exchanger of interest, *SHI*, *SHII* or *EVAP*. For the duct burner (*DB*) this is true only for the water/steam path. (For the mass conservation of the flue gas domain in the duct burner one is referred to equation 6.16 and equation 6.17.)

$$\frac{dM_{HE,w}}{dt} = -\dot{m}_{HE,w,i,E} + \dot{m}_{HE,w,i,E} = 0 \tag{6.7}$$

$$\frac{dM_{HE,fg}}{dt} = \dot{m}_{HE,fg,i,E} - \dot{m}_{HE,fg,i,L} = 0 \tag{6.8}$$

$$\dot{m}_{HE,w,i,E} = \dot{m}_{HE,w,i,L} \qquad \dot{m}_{HE,fg,i,E} = \dot{m}_{HE,fg,i,L} \tag{6.9}$$

From now on the mass flow in the heat exchanger cells will all be denoted with $\dot{m}_{HE,w}$ and $\dot{m}_{HE,fg}$ for water and flue gas respectively. Obviously, no mass is entering or leaving the control volume of the tube wall material. The mass conservation equation becomes trivial, see equation 6.10.

$$\dot{m}_{wall} = 0 \tag{6.10}$$

Conservation of energy equations of a cell

The internal energy U from equation 6.6 is equal to the mass of the fluid in cell $M_{HE,i}$ multiplied by the specific internal energy of that cell $u_{HE,i}$. As the mass does not change and no work is done in the cell, equation 6.6 can be rewritten for the water/steam path and the flue gas path, respectively equation 6.11 and 6.12.

$$M_{HE,w,i}\frac{du_{HE,w,i}}{dt} = \dot{Q}_{HE,w,i} + \dot{m}_{HE,w}\left(-h_{HE,w,i,E} + h_{HE,w,i,L}\right) \tag{6.11}$$

$$M_{HE,fg,i}\frac{du_{HE,fg,i}}{dt} = -\dot{Q}_{HE,fg,i} + \dot{m}_{HE,fg}\left(h_{HE,fg,i,E} - h_{HE,fg,i,L}\right) \tag{6.12}$$

The tube wall of the heat exchanger does not exert any work, thus $\dot{W} = 0$. As there is no mass flow, no energy is carried with this flow. The energy stored in the material can be rewritten as in equation 6.13, in which the heat capacity c_p is a function of temperature and pressure $c_p(p,T)$.

$$U = M_{HE,i} \cdot c_p \cdot T_{HE,i} \tag{6.13}$$

Substitution in equation 6.2 gives the conservation of energy for the tube material, shown in equation 6.14. The energy stored in the tube material is the difference between the incoming heat of the flue gases and the leaving heat to the water-steam cycle.

$$\frac{d}{dt}\left[Mc_pT\right]_{HE,i} = -(\dot{Q}_{HE,fg,i} + \dot{Q}_{HE,w,i}) \tag{6.14}$$

The negative sign in the RHS of the equation follows from the opposite perspective of the tube wall. The leaving heat from the flue gases will enter the material.

Heat transfer

The heat transfer Q from or to the domains water and flue gas is described with equation 6.15. It is dependent on the contact area A over which heat transfer occurs, the temperature difference ΔT between the domain and the heat transfer area, and a heat transfer coefficient. The heat transfer coefficient α depends on the several characteristics of the flow and geometry of the heat exchangers. A distinction is made between laminar, turbulent and transitional flows. For boiling other empirical relationships apply than for single phase heat transfer. The arrangement of the tubes, and whether or not they are finned is important to determine the heat transferred from the flue gas path. An overview of these relations can be found in appendix B. In figure 6.8 a close up of the wall is shown. Per coil there is a single wall temperature, but both the flue gas temperature and water/steam temperature vary over the coil

$$\dot{Q} = \alpha\, A \Delta T \tag{6.15}$$

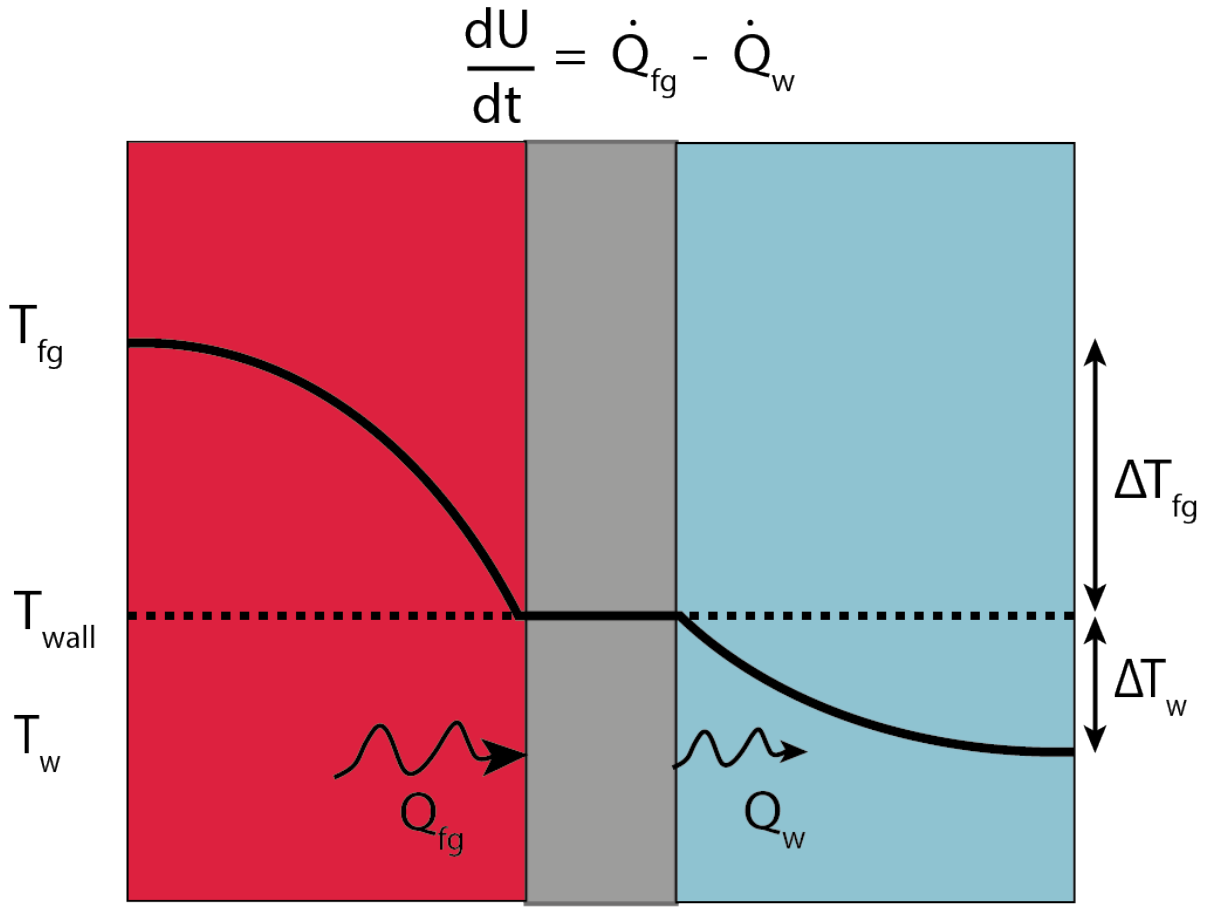

Figure 6.8: Heat transfer through a wall element

6.3.2. Duct Burner

In the duct burner the temperature of the flue gases is elevated by the combustion of gaseous fuel. Water walls and an evaporation screen are present to protect the HRSG from the resulting radiative heat. The duct burner is divided into two cells, see figure 6.9. In the first cell, the gaseous fuel combusted releases energy that is absorbed by the flue gases and causes the temperature to rise. In the second cell the hot flue gases transfer heat to the evaporation process by means of radiation and convection to the evaporation process in the water walls and the evaporation screen. The evaporation process is approached as one single system. This second cell is a heat exchanger as discussed earlier in section 6.3.1 and will not be discussed in this section.

Assumptions

- A combustion efficiency of 100% is assumed.
- Assuming no heat or mass accumulation in the duct burner, the time derivatives in equation 6.1 and equation 6.2 become zero.

Conservation of Mass

The mass conservation for cell 1 and cell 2 of the Duct Burner are described with respectively equation 6.16 and 6.17.

$$\frac{dM_{DB,fg,1}}{dt} = \dot{m}_{DB,fg,1,E} - \dot{m}_{DB,fg,1,L} + \dot{m}_{fuel} = 0 \tag{6.16}$$

$$\frac{dM_{DB,fg,2}}{dt} = \dot{m}_{DB,fg,2,E} - \dot{m}_{DB,fg,2,L} = 0 \tag{6.17}$$

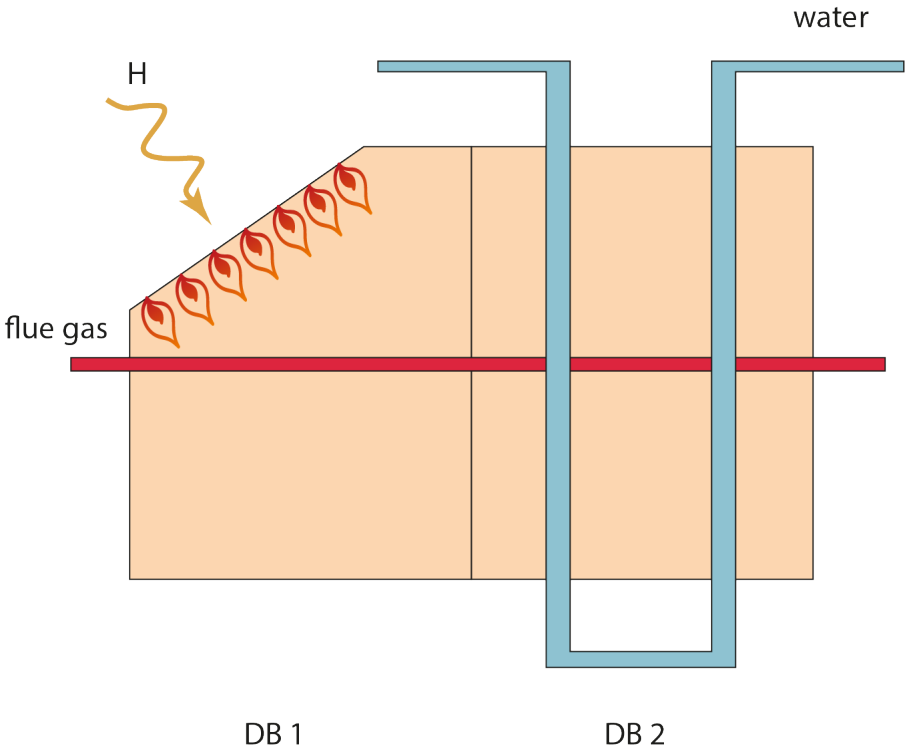

Figure 6.9: Schematic representation of the duct burner

Conservation of Energy

In the first cell combustion energy H is released by the combustion process, equation 6.18.

$$\frac{dU_{DB,fg,1}}{dt} = \dot{m}_{fuel} \cdot H + \dot{m}_{DB,fg,1,E}\, h_{DB,fg,1,E} - \dot{m}_{DB,fg,1,L}\, h_{DB,fg,1,L} = 0 \tag{6.18}$$

In the second cell the heat is transferred to the walls of the evaporator system.

$$\frac{dU_{DB,fg,2}}{dt} = \dot{Q}_{DB,fg} + \dot{m}_{DB,fg,2}\left(h_{DB,fg,2,E} - h_{DB,fg,2,L}\right) = 0 \tag{6.19}$$

6.3.3. Desuperheater

The desuperheater is essentially a mixer where one superheated stream flow is cooled or 'desuperheated' by adding subcooled water. In this model this injection water is a function of the superheated steam leaving the HP Superheater II and is controlled by a PI-controller (see Appendix D).

Assumptions

- No mass or heat accumulation: $dM/dt = 0$ and $dU/dt = 0$
- No pressure drop
- Adiabatic process (no heat is lost to the surroundings)
- Incompressible flow
- Ideal mixing of the injection water

Conservation of Mass

$$0 = \dot{m}_{DSH,w,E} + \dot{m}_{DSH,w,inj} - \dot{m}_{DSH,w,L} \tag{6.20}$$

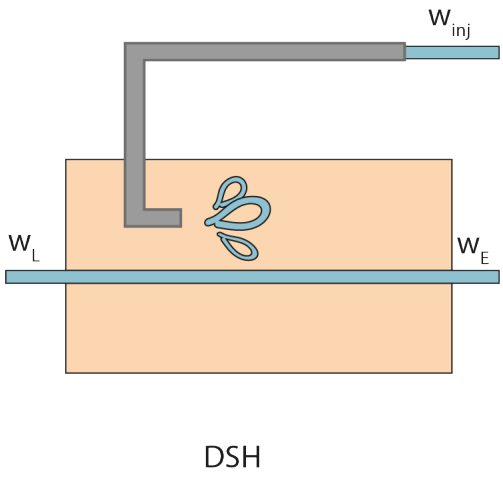

Figure 6.10: Schematic representation of the desuperheater

Conservation of Energy

$$\frac{dU_{DSH,w}}{dt} = \dot{m}_{DSH,w,E}\, h_{DSH,w,E} + \dot{m}_{DSH,w,inj}\, h_{DSH,w,inj} - \dot{m}_{DSH,w,L}\, h_{DSH,w,L} = 0 \tag{6.21}$$

6.4. Complete set of conservation equations

The equations established in the previous sections can be collected in matrices and form a set of ordinary differential equations (ODE). A solution of this set of equations can than be approximated by discretising the equations, see section 6.5. The equations for the conservation of mass for the entire system are collected separate from the equations for energy conservation, to simplify the discretisation process. The resulting matrices are contained in appendix C to improve the readability of this report.

6.5. Model development

A first order explicit numerical model, the Euler forward method, will be used to solve the differential equations that follow from the conservation equations in section 6.3.1. Using this method no knowledge of the parameters at future time steps is required. Therefore no iteration is required. That being said, the step size has to be sufficiently small to create a stable model [40]. It is common practise to start with implementing the forward Euler method, when this does not suffices, an implicit method could be used.

6.5.1. Discretisation

The mass conservation equations have the form of sets all have the form of $\mathbf{A}\cdot\vec{m} = \vec{0}$ and the energy conservation equations the form of $\mathbf{A}\cdot\vec{m} + \vec{\dot{Q}} = \frac{d\vec{U}}{dt}$. The system of equations is first discretised. The general equations of mass and energy conservation, from equations 6.1 and 6.6 could be rewritten as in equation 6.22 and 6.23.

$$M^{n+1} = M^n + \Delta t\left(\dot{m}_E^n - \dot{m}_L^n\right) \tag{6.22}$$

$$u^{n+1} = u^n + \dot{Q}^n - \dot{W}^n + \frac{\Delta t}{M^n}\left(\dot{m}_E^n\, h_E^n - \dot{m}_L^n\, h_L^n\right) \tag{6.23}$$

The flows that enter the system (with subscript E) are assumed to be known. By means of extrapolation of the temperature of the entering flow and the cell temperature at time step n, the temperature of the leaving flow can be calculated. This approach has the disadvantage that the diffusion in the model could turn out larger than the actual diffusion. Based on the temperature of the entering and leaving flows the enthalpy of these flows can be obtained.

6.5.2. Initial Values

The solution of the steady state model of THERMOFLEX is used to estimate the initial values of the dynamic model. This way, both the mass flow and temperatures of the flue gases path and water/steam path between

the components are set. The initial values of the parameters at the cell boundaries are estimated using linear interpolation.

Wall temperature

The inital coil wall temperatures are estimated a bit more careful. In figure 6.3 it can be seen that a wrong value can cause temperature crossing.

The heat transfer coefficient of superheated steam is lower than that of two-phase or subcooled water. Ranges of the heat transfer coefficients are shown in table 6.3. The superheated steam is water in the gas phase and has a smaller heat transfer coefficient than two-phase or subcooled water. This means that the temperature of the material of the evaporator and the economisers will stay close to the temperature of the passing water as the heat transfer with water is more effectively than the flue gas. The material's temperature in the superheaters will differ more to the temperature of the water, as the efficiency of the heat transfer to the steam is less effective. The cooling effect in the superheaters is less.

Table 6.3: Typical values of heat transfer coefficients for the different phases of a fluid [41]

Heat transfer coefficient [W/m^{2}K]			
25	-	250	For forced convection in gases
50	-	20,000	For forced convection in liquids
2,500	-	100,000	For boiling and condensing fluids

6.5.3. Convergence

If p is the solution of the system, the system converges if $\lim_{n\to\infty} p = p_n$ [40]. As the exact solution is initially unknown, a stopping criteria is used. When the relative absolute change of the solution from p_{n-1} to p_n is sufficiently small (with tolerance ε), it is said that the system has converged to a steady state solution, see equation 6.24. For each time step this criteria is executed.

$$\frac{|p_n - p_{n-1}|}{|p_n|} < \epsilon, \text{ if } p \neq 0 \tag{6.24}$$

The tolerance for the solution of both the mass flow and the temperature are $\epsilon = 10^{-5}$.

6.5.4. Stepsize

An appropriate step size Δt should be choosen. A step size that is too large could result in an instable system, where a too small step size significantly increases computational time. In the next sections the considerations regarding to step size are given. For the sake of computational time the step size is concluded to be $\Delta t = 0.01$ s, keeping in mind that the first 0.2 s after a change in the system probably unphysical results.

Maximum step size

The system of ODEs in section 6.4 is a non linear one. Not only does the enthalpy in the matrix **A** depend on the internal energy, so does the heat transfer $\dot{Q}$. The relationship between the internal energy and the heat transfer is non linear. Both the temperature difference ΔT and the heat transfer coefficient α from equation 6.15 depend on the internal energy. In most cases α even depends on a certain power of the Reynolds number (and thus internal energy). This means that the maximum step size allowed changes in time. It is possible to estimate this step size by linearising the system of equations for each step in time.

An appropriate step size can also be established by trial and error. Proving that a certain step size is suitable can be done by showing that doubling that particular step size results in a unstable system and that halving the chosen step size does not result in a significantly different solution.

A first guess for the step size is $\Delta t = 0.01$ s (figure 6.11a). From the graphs one can see that the results at this step size do not improve in terms of the global behaviour for a smaller step size $\Delta t = 0.005$ s (figure 6.11b). However, the initial response is different for both step sizes. The system with $\Delta t = 0.01$ s takes 13.4 s more to reach steady state. However, the computational time is lower (18 minutes for $\Delta t = 0.01$ s and 35 minutes for $\Delta t = 0.005$ s). The time step $\Delta t = 0.02$ s induces instability. Already after 5 time steps values or Reynolds numbers are reached for which the formula's from appendix B are invalid.

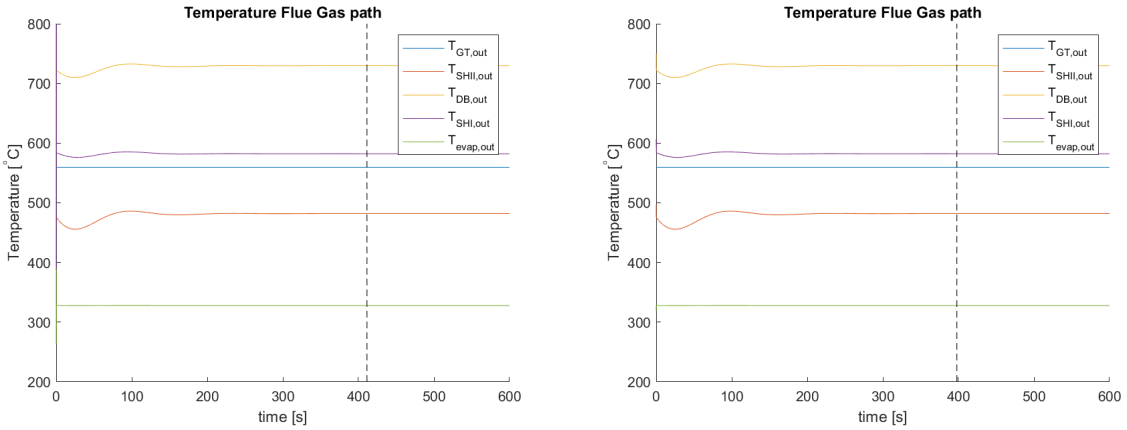

(a) $\Delta t = 0.01\,\mathrm{s}$ **(b)** $\Delta t = 0.005\,\mathrm{s}$

Figure 6.11: Convergence of the flue gas temperature to a steady state solution (dashed vertical line).

Characteristic time scale

It is essential that the time step used is not larger than the smallest characteristic time scale. If it would be larger, changes in temperature of a small particle would only be visible after the particle has already left the component it was in, being unable to transfer its energy. This would result in non physical solutions. The characteristic time scale is different for each component of the system. It is calculated by dividing the mass contained in a cell by the mass flow passing through, equation 6.25. The resulting time scales for each cell are shown in table 6.4. The mass flows are taken from the steady state model of THERMOFLEX. The mass content of each cell is estimated using the geometric data of the plant available.

$$\tilde{t} = \frac{M}{\dot{m}} \tag{6.25}$$

Table 6.4: Characteristic time scale for the domains and components that are subjected to heat transfer.

Domain	Component	Mass per cell [kg]	Mass Flow [kg/s]	Characteristic Time Scale [s]
Water/ Steam	Evaporator	1303.70	46.31*	28.15
	Duct Burner	108.98	5.82	18.71
	Superheater I	13.85	25.93	0.534
	Superheater II	13.71	25.93	0.529
Flue Gas	Evaporator	13.87	117.61	0.118
	Duct Burner	4.15	117.61	0.035
	Superheater I	2.83	117.61	0.024
	Superheater II	2.47	117.61	0.021

* The mass flow in the evaporator is based on a CR of 7 and 4 sections operating in parallel

The smallest characteristic time scale is the critical one, in case of this system it is the gas domain of the SH II with a $\tilde{t} = 0.021$ s.

System stiffness

When the solutions from figure 6.11 are studied for the initial response a strange phenomenon can be observed, see figure 6.12. The solution for each flow only alternates within a few degrees for the time step of $\Delta t = 0.005$s. The solution of the model with time step $\Delta t = 0.01$s has 500 °C difference between its maximum and minimum temperature at the outlet of SHI.

The problem is a so called "stiff" problem. The behaviour seen is characteristic for explicit solvers of these problems; small changes that lead to large deviations, that die out rapidly. It occurs in systems with a large variation in time scales. Due to the density difference in flue gas and water an order of magnitude 1000 exists

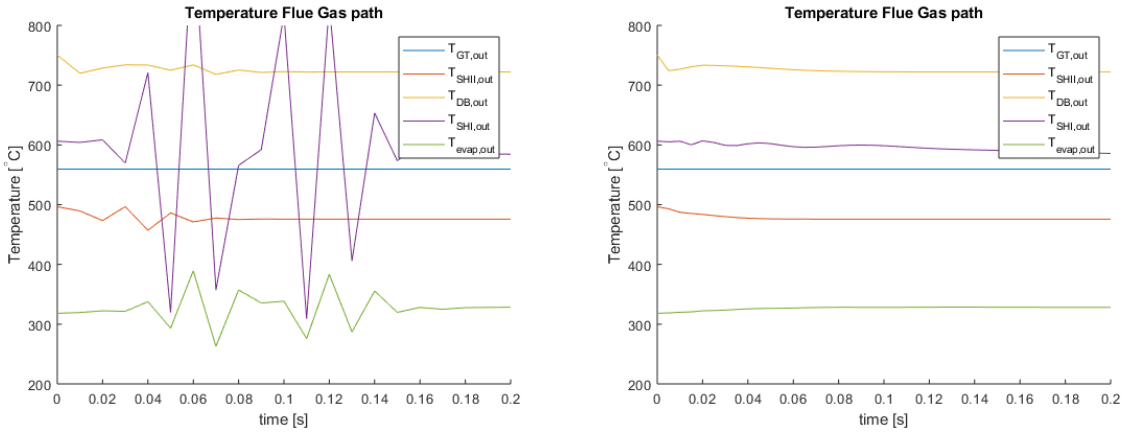

(a) A step size of $\Delta t = 0.01$ s is used

(b) A step size of $\Delta t = 0.005$ s is used

Figure 6.12: Close up of the models initial response

between the maximum and minimum characteristic time scale from table 6.4. It forces the time step to be small to avoid un-physically large variations in the solution. It would have been smart to revise the choice of the Euler Forward method, for less computation time.

As the purpose of the model is to study behaviour after a change has been applied, the step size that is appropriate for this system is $\Delta t = 0.005$ s.

6.6. Steady State solution of a dynamic model

In figure 6.11b the steady state solution is shown for the flue gas temperature between the components. In section 6.6.1 the solution is also shown for the temperature and mass flow of the water/steam path. To validate that the solution obtained from the dynamic model makes sense, the QT-diagram of the steady state solution of the THERMOFLEX model is compared to the steady state solution of the dynamic model, section 6.6.2.

6.6.1. Steady state solution

In figure 6.13a and 6.13b it is seen that the system converges towards a steady state value. The vertical dashed line indicates the instance steady state is true according to section 6.5.3. At this instance steady state is reached for all temperatures and mass flows in the system, including the wall temperature.

This is also the time it takes for the walls to adjust from the initial guessed temperature values, to temperatures that correspond to a zero change in internal energy of the system.

The time it takes to reach steady state is more or less dependent on the gains of the PI controller. A trade-off is made between the initial overshoot seen in the 3 graphs and the settling time.

6.6.2. Q-T diagram

To compare the steady state found by the dynamic model with the steady state solution from THERMOFLEX, both models are plotted in the same QT-diagram, 6.14.

The flue gas inside the SHII of the dynamic model transfers more than the THERMOFLEX model. The remaining part however transfers less heat in case of the dynamic model. The same adiabatic temperature in the duct burner is reached. The difference in slope of the two flue gas curves could be due to the pressure drop not being taken into account.

Naturally, the water/steam path show the same difference in heat transferred. The heat transferred inside the SHI of the dynamic model is not linear. This is the advantage of having multiple heat exchanger cells. In the dynamic model less heat is transferred inside the evaporator.

For the purpose of this research the model is decided to sufficiently represent the HRSG of interest.

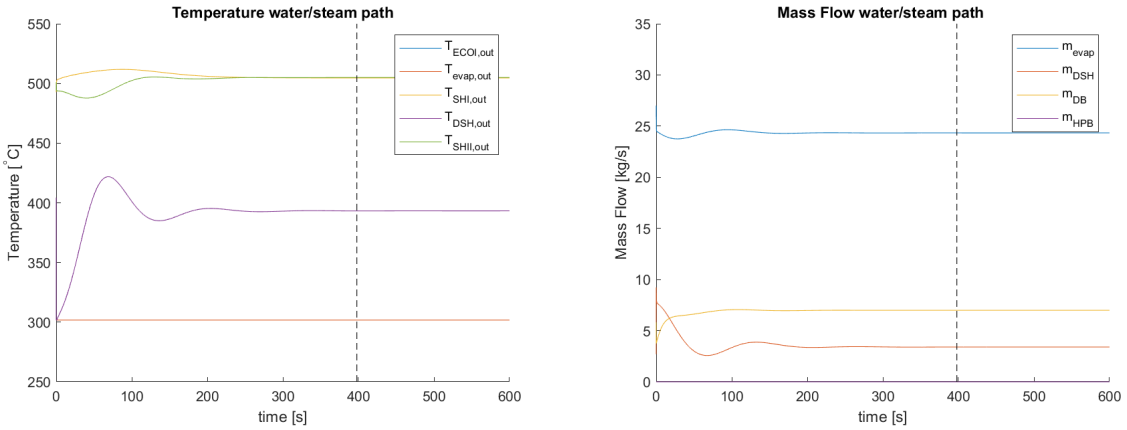

(a) Temperature

(b) Mass Flow

Figure 6.13: Converging to a steady state of the solution of the water/steam path in the HRSG ($\Delta t = 0.005\,\mathrm{s}$)

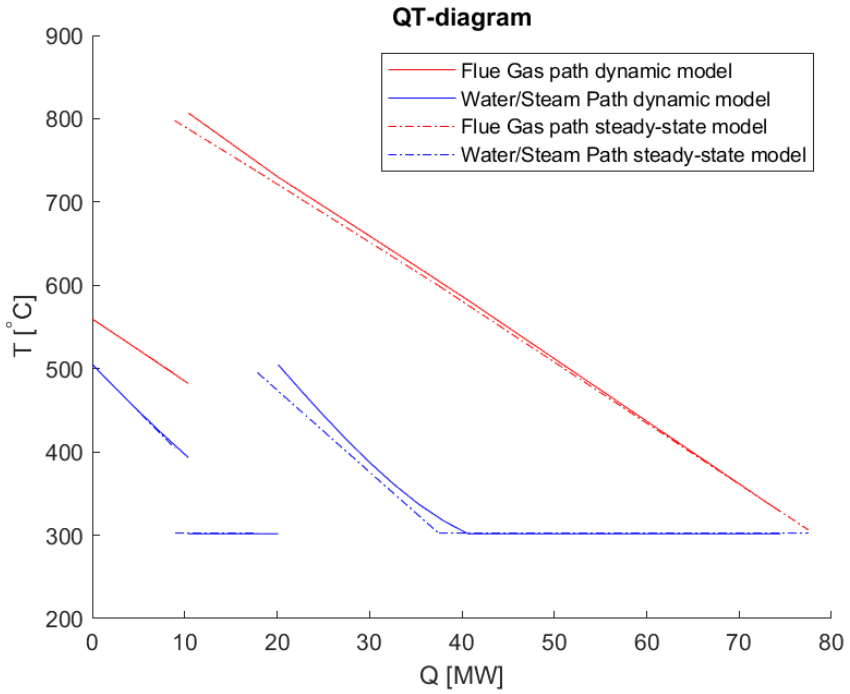

Figure 6.14: Comparison of the steady state temperature development inside the HRSG of the dynamic model and the THERMOFLEX model.

6.7. Simulation of the Electric Heaters

Now that the dynamic model is able to achieve a steady state solution which is similar to the steady state achieved by the THERMOFLEX model, electric heaters are implemented.

The input values will be changed from the input values for mode 2 to the ones for the EH of choice. In table 6.5 an overview of the input values is given. This change in input values will be enough for the AP, the SB and the AP-SB as their EH is not physically inside the system boundaries. For the remaining EH's an additional modification is required.

The heat added by the duct heater will solely result in a temperature increase. The change in properties of the flue gas under temperature variations are ignored. The temperature change is calculated using equation 6.26. Due to mass conservation, the mass flow through the DH is equal to the mass flow through the Superheater II. The ΔT that results from adding heat to the system is added to the temperature at the flue gas inlet

Table 6.5: Change in model input values to simulate the EH's

		Change in input values							
	Mode 2	AP	DH	HPB	SB	AP-DH	AP-HPB	AP-SB	
Fuel Consumption Duct Burner	1.0	0.1	-1.0	-1.0	-0.8	-1.0	-1.0	-0.5	[kg/s]
Gas Turbine Exhaust Temperature	837.4	35.2	-0.1	-0.6	-0.3	35.2	34.4	35.0	[K]
Gas Turbine Exhaust mass flow	112.7	-16.9	0.0	0.0	0.0	-16.9	-16.9	-16.9	[kg/s]
Inlet Temperature Evaporator	538.2	-11.0	-1.5	-14.4	32.7	-13.2	-35.3	19.6	[K]
Heat added EH	0.0	0.0	45.8	44.4	0.0	51.1	50.4	0.0	[MW]

of the Duct Burner.

$$\dot{Q}_{DH} = \dot{m}_{DH,fg} \cdot c_p \, \Delta T \tag{6.26}$$

The heat added by the high pressure boiler (HPB) will evaporate a certain mass flow of water. Setting up a energy conservation equation for a system without mass and energy accumulation, this mass flow can be established, equation 6.27. This mass flow is added at the evaporator exit.

$$0 = \dot{Q}_{HPB} + \dot{m}_{HPB} \cdot \Delta h \tag{6.27}$$

7

Results on the dynamic behaviour

The model prepared in chapter 6 is used to research the dynamic response of the Heat Recovery Steam Generator (HRSG) to changes on account of an electric heater. The central question *What is the dynamic behaviour of each of the 'high potential' design cases?* In section 7.1 the issues that go with HRSG cycling are briefly discussed. Taking these issues into account relevant parameters can be set up to determine the sensitivity of the HRSG.

In section 7.2.1 the minimum ramp time required by the different EHs is discussed. The change in coil-to-coil temperature difference is discussed in 7.2.3. In section 7.2.2 an overview of the absolute temperature change in the walls of the SHII, SHI and DB is given. In section 7.3 a small discussion on the options is given.

Initially a step response deployment of the EHs is used. The largest temperature gradients will occur. If the system responds within the 25 °C/min constraint, no issues have to be expected. However, if necessary from a thermal stresses perspective a ramp function is used to allow the system to adapt to the new conditions within the set limitations. Ramp times 5, 10 and 15 are checked to obtain a view on the response time of the system. The system should be able to adapt without exceeding the set limits within 15 minutes, to be able for it to act on the imbalance market.

7.1. Cycling

During the start-up and shut-down of the CHP installation certain temperature and pressure differentials are present. The temperature and pressure during these events do not only vary in space, but also in time. Due to differences in thermal expansion upon heating mechanical stresses arise. The plants are designed to withstand a certain amount of start-up and shut-down events. Special care is taken to minimise the effects as this would decrease the life time of the equipment.

Due to a change in the trends on the energy market a change in the characteristic HRSG operation is seen. Whereas it was common practice to operate a CHP in Base Load, it is now more desirable to operate in a flexible manner. The integration of an EH in the HRSG implies that besides the conventional start-up and shut-down procedures an additional procedure will frequently take place: the start-up and shut-down of the EH. In this additional procedure the high pressure is already present, so the pressure differentials can be assumed small compared to the pressure differentials during the start-up and shut-down procedures. The temperature differentials induced by the deployment of an EH probably differ from the ones at conventional start-up and shut-down. This calls for a more elaborate analysis than the steady state analysis given in chapter 5.

Solid materials expand under influence of temperature changes. The strain in one direction of a material element is determined with equation 7.1 [42].

$$\epsilon = \text{TEC} \cdot [T - T(t=0)] \tag{7.1}$$

This relationship depends on the temperature change over time and the material property 'thermal expansion coefficient' (TEC [K^{-1}]). Often TEC > 0, such that a material expands upon heating, and contracts upon cooling. If the material is isotropic, it will only change in volume, and not in shape. As long as the ma-

terial is free to deform, no mechanical stresses result from the temperature change. However, if the material is constrained on both ends stresses will develop.

In section 7.1.2 and section 7.1.1 two issues induced by changes in absolute thermal expansion inside the HRSG are discussed.

Two different types of temperature gradients must be considered. First, the temperature gradients over the thickness of the materials. Second, the row-to-row temperature difference, where the temperature of the material upstream of the gas path is higher than the temperature down stream. These phenomena will be described in respectively section 7.1.2 and section 7.1.1. For more information the book [43] can be consulted.

7.1.1. Maximum time derivative of the temperature in the headers

The temperature gradients inside the material itself are important. When, for example, the fluid flowing into the headers of a heat exchanger is subjected to an increase in temperature, the material in direct contact with the fluid will expand. However, the material more distant from the contact area lacks in temperature increase and is not yet expanding. The inner material will press against the outer material and mechanical stresses will form. This phenomenon is a function of the temperature difference over the cross section of the header.

The maximum temperature difference that exists over the thickness of the header wall depends on the rate at which this temperature change at the inner diameter takes place. The response of the temperature at the outer diameter for a step change in temperature at the inner diameter is shown in figure 7.1a. The temperature difference over the thickness is immediately at its maximum. If however, the temperature change at the inner diameter is a ramp function, the maximum temperature difference over the thickness will be smaller and will occur at a later instance (7.1b).

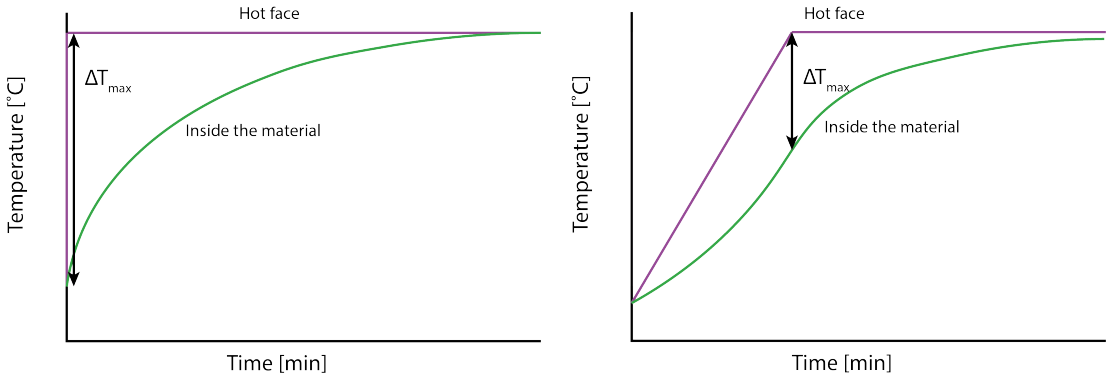

(a) Step response

(b) Ramp time of 10 minutes.

Figure 7.1: Response of two faces of a material subjected to a temperature change at one side [43].

Another issue that arises with a change in temperature in the headers is the difference in expansion of the thin-walled tubes and the thick-walled headers. The welded joints will have to endure additional stresses caused by this difference in thermal expansion rate. In the HRSG of the Delesto system, a maximum change in temperature of 25 °C/min is considered to be acceptable ($\frac{dT}{dt} = 0.42$ °C/s).

7.1.2. Row-to-row temperature difference

One can imagine that a temperature gradient exists over the heat exchangers of a HRSG. The temperature of the material close to the gas turbine outlet is higher than the material closer to the stack.

A row-to-row temperature gradient will result in differences in thermal expansion of the rows. Especially during start-up and shut-down the effects are severe. These differences in expansion rates are already taken into account at the design of the HRSG. If the entire heat exchanger was fixed in space, mechanical stresses would develop due to thermal effects, but smart construction of the coils enables the heat exchanger to expand. However, the tube rows that are parallel inside a coil are fixed to each other. Stresses due to thermal effects will arise. The model constructed in chapter 6 only solves one wall temperature per cell. These cells correspond (at least for the HP superheater II and superheater I) to the coils. This is considered to be sufficient information for a qualitative analysis. If one assumes a linear temperature profile inside the coils (figure 7.2), the row-to-row temperature difference is determined by dividing the coil-to-coil difference by the number of rows in a coil.

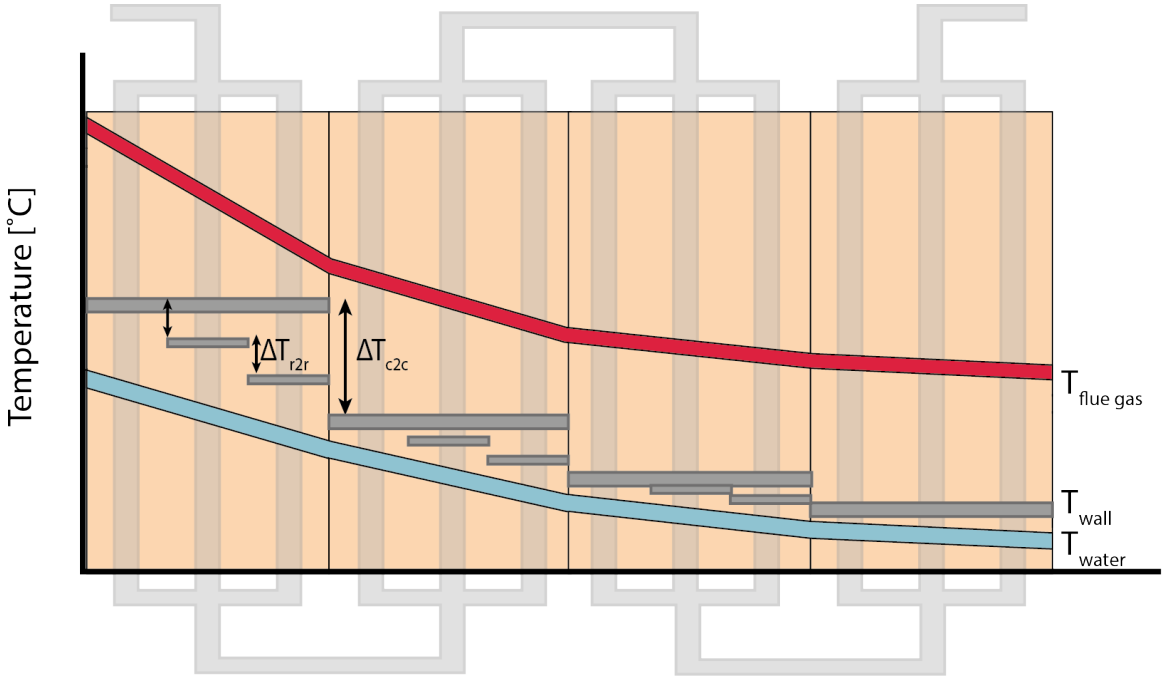

Figure 7.2: Relation between the coil-to-coil (c2c) and the row-to-row (r2r) temperature difference in a heat exchanger.

7.2. Results of the dynamic model

In this section the results on the time derivative of the header temperature and the row-to-row temperature difference are discussed, respectively in section 7.2.1 and 7.2.3. One is referred to appendix E for the graphs not used in the discussion in this section.

7.2.1. Time derivative of the header temperature

In table 7.1 the time in which the numerous EHs are able to ramp to maximum load, without exceeding the constraint of the HRSG of the maximum time derivative of 0.4 °C/s, is summarised. Only the durations of 5, 10 and 15 minutes are checked. It can be seen that all of the EHs are able to ramp up to maximum load within the set limit of 15 min. The AP-DH and AP-SB are just not able to ramp within the 10 minutes. The AP is the quickest of the EHs, this can be understood by seeing that the maximum operation of the AP induce smaller changes than the maximum operation of the remaining EHs. The critical heat exchanger is in most cases the SHII. Only in case of the deployment of the HPB, SHI determines the minimum ramp time.

Table 7.1: Minimum ramp time of the EHs corresponding to a maximum time derivative of 0.4 °C/s

	Minimum ramp time within [min]	Largest temperature derivative in Superheater
Air Preheater	5	II
Duct Heater	10	II
High Pressure Boiler	10	I
Stand-alone Boiler	10	II
Air Preheater - Duct Heater	10	II
Air Preheater - High Pressure Boiler	10	I
Air Preheater - Stand-alone Boiler	10	II

In figure 7.3 the temperature in the headers of SHII and SHI are shown for the AP with a ramp time of 5 minutes. Just like for all the other EHs the curves look smooth and no sudden changes appear. If one would look to the derivative of these curves, the changes in trend are seen more clearly. Also it can be readily seen whether or not the maximum time derivative of 25 °C is exceeded.

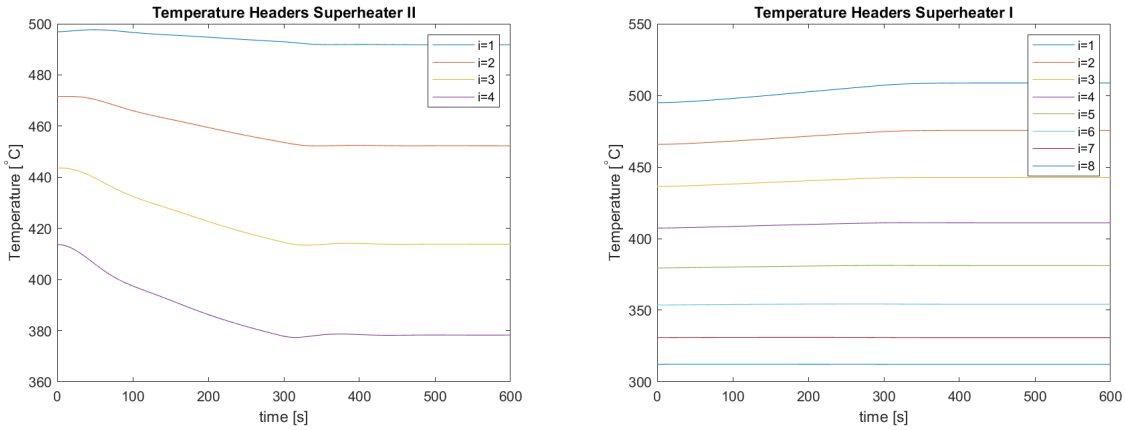

(a) Superheater II **(b)** Superheater I

Figure 7.3: Temperature of the steam in the headers of superheater II and superheater I at a ramp up time of the AP of 5 minutes

In figure 7.4 one can see the time derivatives of the temperature in the headers for the AP with a ramp time of 5 minutes. It is seen that the AP already stays well within the limits with respect to the maximum change in temperature over time. Different phenomena can be distinguished. The oscillations in the derivative of the temperature are due to the fact that the control of the desuperheater is 'searching' for a new appropriate amount of injection mass flow. This translates in temperature fluctuations in the headers of SHII. At 300 s the maximum load of te AP is reached, and a new steady state is achieved.

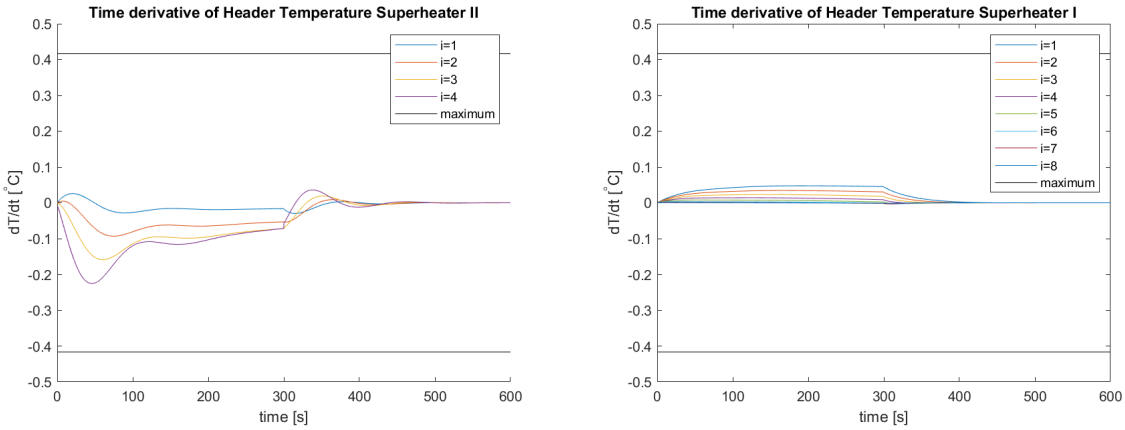

(a) Superheater II **(b)** Superheater I

Figure 7.4: Time derivative of the temperature of the steam in the headers of superheater II and superheater I at a ramp up time of the AP of 5 minutes

In figure 7.5 the time derivative of the temperature in the headers of the SHII and SHI are shown for the operation of the HPB with a ramp time of 10 minutes. The HPB is the only heater for which the largest time derivative occurs in the SHI (table 7.1). The in-continuity in $\Delta T/\Delta t$ around 580 s for both heat exchangers can be explained by looking into the decreased amount of mass flow through the DB evaporator. For a Re < 2300 the model changes from calculation scheme. The heat transfer coefficient of laminar flow is considerably lower than of transitional or turbulent flow, which results in a sudden drop in mass flow through the DB evaporator. The effects are not visible in the header temperature of both the SHI and SHII. However, because of the nature of the change the effects are very clear in the numerical time derivatives of the temperature.

The rapid decrease in $\Delta T/\Delta t$ around 550 s is explained with the fact that the amount of injection water becomes zero at this point. This effect is most strongly seen in the header close to the desuperheater (header 4). The temperature at the outlet of the SHII will continue to decrease. At 600 s the EH reached its maximum

load and the temperature in the headers will stop decreasing. It is clear that the SHII is only really affected when the temperature at its outlet is out of range of the control in the DSH.

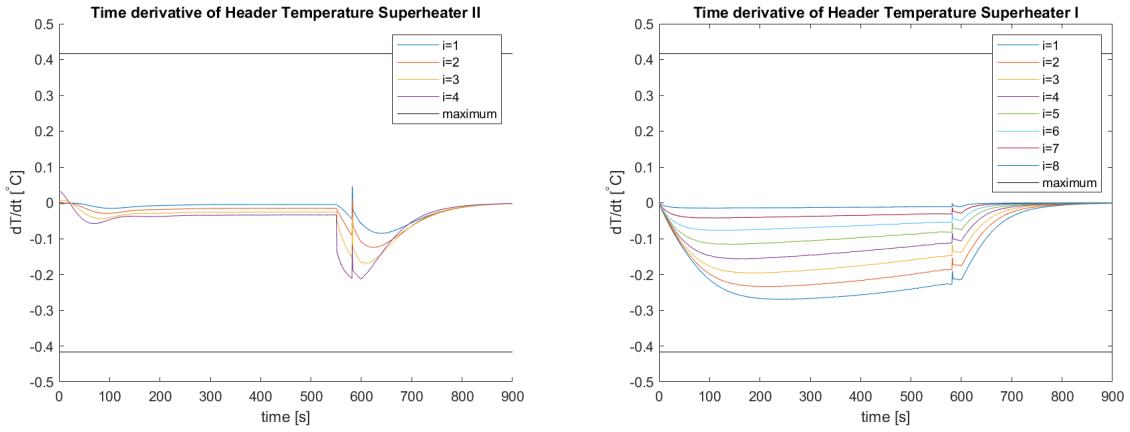

(a) Superheater II

(b) Superheater I

Figure 7.5: Time derivative of the temperature of the steam in the headers of superheater II and superheater I at a ramp up time of the HPB of 10 minutes

7.2.2. Wall temperature

Before the row-to-row temperature difference is looked into, the change in wall temperature over time is studied. In table 7.2 the maximum change in wall temperature of the heat exchangers induced by the EHs is shown. The evaporator wall temperature is not in the list, as it is assumed to be constant.

In most heat exchangers the sign of the temperature is equal for each cell in the heat exchanger. However, during he operation of the AP, the superheater II will encounter a temperature increase for a cell close to the gas turbine and a drop for the cell more distant from the gas turbine. The AP induce smallest change of all the heat exchangers. The rise in wall temperature for the SHI and the DB can be explained with the increased fuel consumption in the duct burner.

For all EHs but the AP, the biggest wall temperature change is seen in the SHI, which is due to the decrease in fuel consumption in the DB. The DH, HPB and SB have similar results for wall temperature decrease as their combinations with the AP. The maximum decrease in wall temperature of the DB is $-40\,^{\circ}\mathrm{C}$. This corresponds to the event in which the mass flow inside the DB evaporator has shifted from a transitional to a laminar flow, discussed in section 7.2.1.

Table 7.2 is to a great extent comparable with the information seen in table 6.1 and table 6.2: it shows information on the change in steady state temperature induced by the EH. However, table 6.1 and table 6.2 did not give any information on the wall temperature itself.

Table 7.2: Maximum change in wall temperature during simulation time

Wall temperature							
	Superheater II		Superheater I		Duct Burner		
	$T(t=0)$	max ΔT	$T(t=0)$	max ΔT	$T(t=0)$	max ΔT	
Air Preheater		-33		+16		+12	[°C]
Duct Heater		-64		-84		-40	[°C]
High Pressure Boiler		-40		-162		-40	[°C]
Stand-alone Boiler	431	-65	510	-83	395	-40	[°C]
Air Preheater - Duct Heater		-69		-79		-40	[°C]
Air Preheater - High Pressure Boiler		-47		-168		-40	[°C]
Air Preheater - Stand-alone Boiler		-68		-79		-40	[°C]

The wall temperature of the SHII and SHI at deployment of the HPB with a ramp time of 10 minutes is shown in respectively figure 7.6a and figure 7.6b. The sudden temperature drop in the SHII near $t = 500\,\mathrm{s}$ can

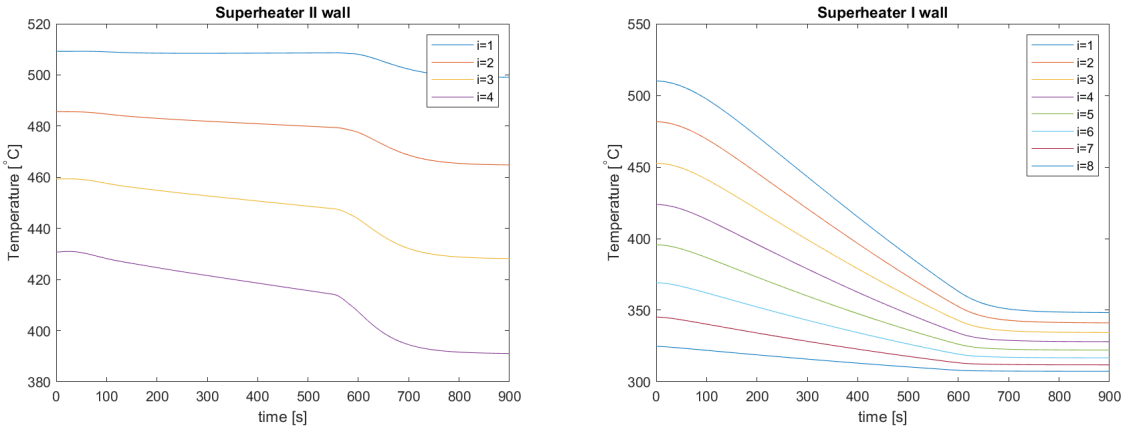

(a) Superheater II

(b) Superheater I

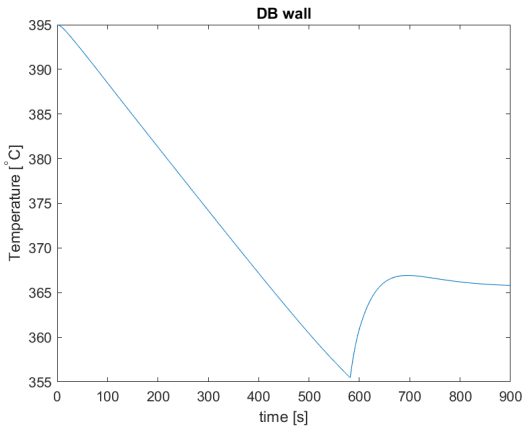

(c) DB evaporator

Figure 7.6: Wall temperature of the coils in superheater II and superheater I and duct burner evaporator at a ramp up time of the HPB of 10 minutes.

be explained with that the injected mass flow reached zero and the inlet temperature of the SHII is equal to the outlet temperature of SHI.

The large wall temperature drop of the SHI for the HPB (and AP-HPB) is explained with the temperature drop in both the flue gases and steam passing through the heat exchanger. The temperature drop in the steam path is due to an increased mass flow caused by the HPB.

The wall temperature over time of the DB evaporator is shown in figure 7.6c. The wall temperature decreases 40 °C with the decrease of duct firing. After a shift in flow characteristics, the temperature settles around 363 °C.

From figure 7.6 one can already see that the difference in wall temperature becomes larger over time for the SHII and smaller over time for the SHI. This difference in wall temperature is referred to as the coil-to-coil temperature difference and is further discussed in section 7.2.3.

7.2.3. Time derivative of the temperature difference between the coils

In section 7.2.2 it became apparent that the difference in temperature between the coils (ΔT_{c2c}) is not constant over time. Dependent on the EH deployed the temperature difference between the coils increase or decrease. In table 7.3 the maximum change in coil to coil Δ_{c2c} temperature difference over time according to the dynamic model are summarised. The coils between which the maximum occurs might be different for each instance. The row-to-row temperature difference is the coil-to-coil temperature difference divided by the number of rows inside a coil, for the SHII the number is three and for the SHI the number is two. The change in row-to-row temperature difference Δ_{r2r} over time is also stated in 7.3.

The difference between the rows does not seem very big. The temperature differences inside the SHII

increase independent on the type of EH used. Due to the increased amount of water injected in the desuperheater, the largest increase can be expected during the deployment of the DH and SB. The temperature difference between the rows of the Superheater I becomes smaller for all EHs but the AP. The drop in temperature difference can be explained with the lack of firing in the duct burner, which is not present at the AP deployment.

Table 7.3: Maximum change in coil-to-coil temperature difference.

Row-to-row temperature difference [°C]

	Superheater II			Superheater I		
	ΔT^0_{c2c}	max Δ_{c2c}	max Δ_{r2r}	ΔT^0_{c2c}	max Δ_{c2c}	max Δ_{r2r}
Air Preheater	24	+16	+5	28	+4	+2
Duct Heater	29	+27	+9	29	-19	-10
High Pressure Boiler	24	+11	+4	29	-22	-11
Stand-alone Boiler	29	+27	+9	29	-18	-9
Air Preheater - Duct Heater	26	+30	+10	28	-19	-10
Air Preheater - High Pressure Boiler	24	+18	+6	29	-23	-12
Air Preheater - Stand-alone Boiler	26	+30	+10	28	-19	-10

In figure 7.7a one could see the temperature difference between the coils of SHII over time when the SB has a ramp time of 10 minutes. After 400 s the graph shows a sharp change in trend. At this instance, the desuperheater injects so much water that water with saturation temperature enters the SHII. The further increase of injection water does not result in further temperature decrease for the coil closest to the desuperheater, therefore the coil-to-coil temperature difference at this location settles around 40 °C until the ramp time is reached.

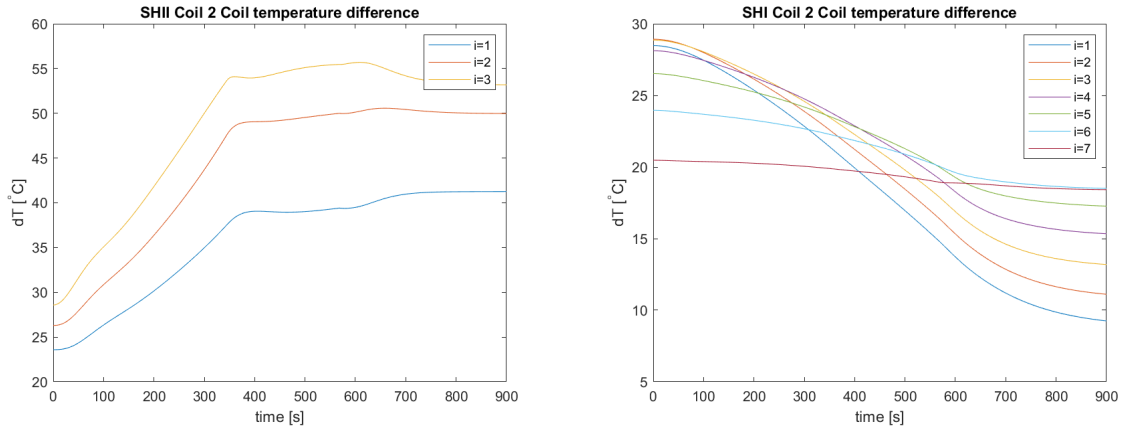

(a) Superheater II

(b) Superheater I

Figure 7.7: Coil-to-coil temperature difference over time of the superheater II and superheater I at a ramp up time of the SB of 10 minutes

In figure 7.7b the coil-to-coil temperature difference in the SHI is shown. It is seen that between all the coils the temperature difference decreases over time. The difference between the first coils of the superheater (from the flue gas perspective) decreases more than the difference at last coils, resulting in a spacial shift of greatest stresses.

The coil-to-coil temperature difference in SHII and SHI induced by APSB is shown in figure in 7.8. The results are comparable with the result seen from the SB (7.7). However, the temperature profile across the coils in SHII is more linear.

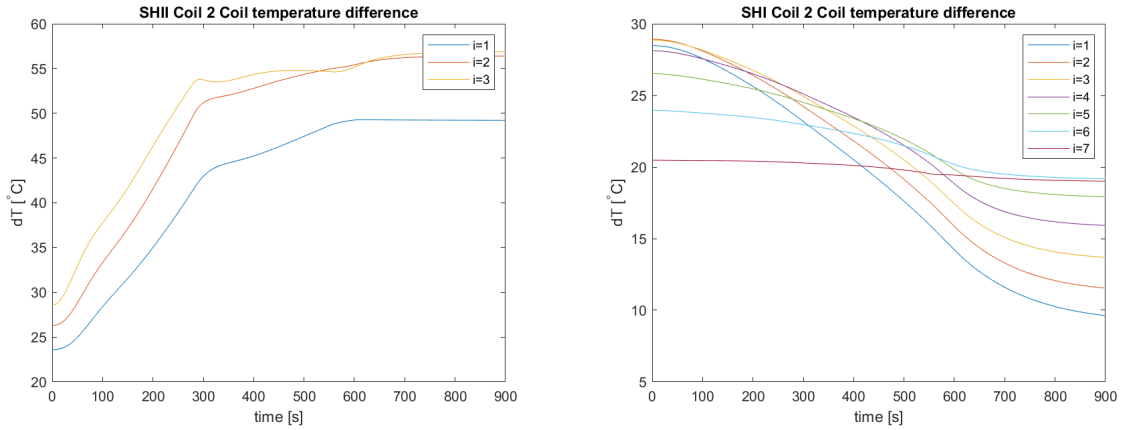

(a) Superheater II

(b) Superheater I

Figure 7.8: Coil-to-coil temperature difference over time of the superheater II and superheater I at a ramp up time of the APSB of 10 minutes

7.3. Conclusion

The analysis on the time derivative shows that all EHs are capable to ramp to maximum load in 10 minutes. That is within the grid requirement of the Dutch grid operator to operate on the imbalance market.

The desuperheater could cause sudden changes in the time derivatives in the desuperheater. Zero injected mass flow causes a sudden negative time derivative, whereas a saturated outlet of the desuperheater a sudden positive time derivative in the SHII. One can understand that the behaviour of the HRSG is sensitive to the control of the desuperheater.

The mass flow in the DB evaporator greatly affects the time derivative of the steam temperature in the headers of both superheaters, but only for a short duration. It is caused by a sudden change in calculation method inside the programme. The decrease in the DB evaporator mass flow is not expected to cause such an abrupt change in the real system.

The findings of the wall temperature evaluation implicate that especially during the operation of the HPB the SHI undergoes a large decrease in temperature.

The review on the change in row-to-row temperature difference showed that the largest changes are expected to happen for the deployment of the APDH and the APSB.

Overall, the AP brings about the smallest changes in the HRSG, therefore it is in terms of dynamic behaviour particularly well suited for the flexible operation of the CHP. The DH and the SB cause moderate changes in the plant, while the HPB cause extreme changes. Those extreme changes increase the risk of failure. For that reason the HPB is not considered to be a technical feasible option.

In the next chapter the financial performance of the AP, the DH, the SB, the APDH and the APSB will be studied.

8

Financial Performance

A simple business case is set up for the electric heaters (EHs) that showed positive results in the steady state and the dynamic analysis. To decide if any of the EHs is financial feasible, different aspects of the financial performance will be looked into. The profits from acting on the energy market, the costs that will come with installing, operation and maintenance will be looked into. This way an answer to the central question: *What is the expected financial performance of the remaining electric heater concepts?* is given.

In chapter 1 some of the phenomena on the electricity market are already explained. In this chapter the prospects of the energy market are investigated. Data from 2015 to 2018 is used to get an idea about the business case of the EHs.

8.1. Prospect on the spot market

Producing less net electricity with the deployment of an EH, would cut the profits from electricity. It would also save on the natural gas used and the costs for emitting CO_2 that comes with combustion. Looking into the expected price developments of these three components (Electricity, Natural gas, and CO_2), will provide insight into the feasibility of acting on the spot market in 2019.

Electricity prices

As already mentioned in chapter 1, electricity prices are expected to rise and become more volatile in the near future, see figure 1.4.

Natural gas prices

The natural gas price is expected to increase. In figure 8.1 the future gas prices in $/MWh according the world bank can be found.

Carbon Dioxide Allowances

The European Union Emission Trading System (EU ETS) is created to stimulate the decrease in carbon dioxide emissions. When initiated in 2005 it was expected that the price would stabilise around 30 €/t CO_2. This was not the case. A large surplus of the emission allowances and a decrease in electricity demand due to the financial crisis caused the price to settle around 5 €/t CO_2 [45], see figure 8.2. This low price prevents fair competition between coal power plants and renewable energy production. There is also a lack of financial incentive to decrease greenhouse gas emissions. Reformations were needed. The amount of allowances in the Market Stability Reserve is doubled, which means that there are fewer on the free market. One can already notice the effect on the market value in figure 8.2. From 2023 on, a percentage of the allowances will be taken from the market annually [46] [47]. When this happens, it is expected that the trade will tighten up even more. According to a report from CarbonTracker [48] from April 2018, the prices of carbon dioxide would exceed 15 €/t CO_2 in 2018 and 20 €/t in 2019, but from the picture it is clear that both milestones have already been reached. Furthermore, CarbonTracker predicts that the prices will be between 20 €/t and 25 €/t around 2020.

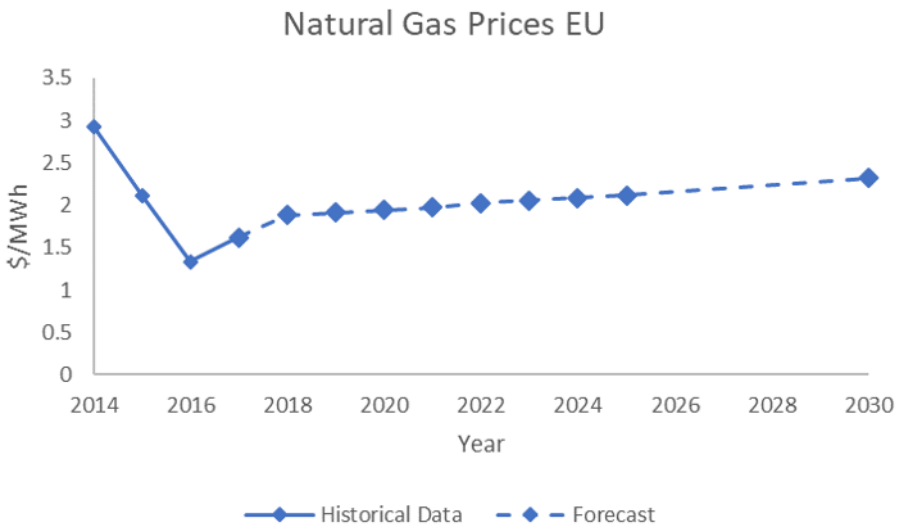

Figure 8.1: Development of the gas price according to the World Bank [44]

Figure 8.2: CO_2 european emission allowances market value in €/t [49]

8.2. Acting on the spot market

Available data on power, gas and emission prices in the period from 2015 to 2018 is used to estimate the profits that could have been made in this period with the deployment of the EHs. Obviously, the data from 2018 is not complete at the time of writing, so this data is extrapolated. On the spot market hourly prices are available. The net saved money induced by the deployment of the EH with respect to the operation in Mode 2 is researched. In 8.2.1 the method for calculating these savings is shown. In 8.2.2 the results are discussed for the year 2017 and in 8.2.3 the development of these savings over the years 2015 to 2018 is reviewed.

8.2.1. Calculation of the profits

The loss in revenue from the decrease in generated electricity is calculated by multiplying the APX price per MWh with the decrease in MWh.

$$\Delta C_{power} = \Delta\text{Power} \cdot p_{Power} \tag{8.1}$$

The costs saved corresponding to the saved gas is calculated with

$$\Delta C_{gas} = \Delta\text{Gas} \cdot \frac{35.16}{31.56} \cdot p_{gas} \tag{8.2}$$

Where the factor 35.16/31.65 is a conversion factor from the Higher Heating Value to the Lower Heating Value of gas.

The costs saved with the savings in CO_2 emissions are calculated with

$$\Delta C_{CO_2} = \Delta \text{Gas} \cdot 0.0561 \cdot 3.6 \cdot p_{CO_2} \tag{8.3}$$

The factor 0.0561 is the amount of CO_2 in kg emitted when 1 MJ of gas is combusted.

Combining these three components per hour, results in the total savings for that hour, see equation 8.4. If the saved amount of money is negative, the EH is not deployed in that hour. Summing the hourly savings, one gets an insight into the possible savings in a year. In section 8.2.2 the result is shown for the year 2017.

$$\Delta C = -\Delta C_{power} + \Delta C_{gas} + \Delta C_{CO_2} \tag{8.4}$$

8.2.2. Savings by acting on the spot market in 2017

The result of the method described in section 8.2.1 is shown for 2017 in figure 8.3. The AP-DH is the most rewarding electric heater. It makes sense that the AP-SB and the DH are approximately equally profitable. Both EHs reduce their fuel consumption and power generation about the same amount. The AP has the highest number of occasions for which it can be utilised, but due to its relative small effect, the saved amount of money remains small. Despite the large capacity of the SB compared to the AP, the SB barely exceeds the savings of the AP. The SB consumes 27 MW less fuel to generate 24 MW less power. This shows that the profit on the spot market is mainly determined by the effectiveness of the EH.

Combining the AP with the DH and the SB further increases the savings with respectively 17 k€ and 11 k€. The AP-DH profits increase more than the profits of a single AP. The AP-SB profits increase less, which can be explained by the smaller increase in capacity compared to AP-DH.

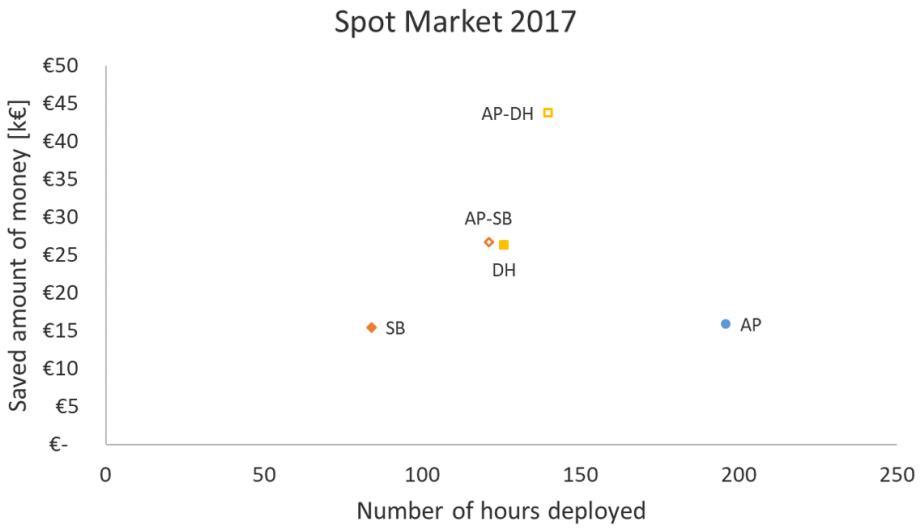

Figure 8.3: Profits that could have been made from the utilisation of an electric heater versus the number of times it could have been deployed for the year 2017.

8.2.3. Evolution of the profits on the spot market

The profits that could have been made by the EHs on the spot market from 2015 to 2018 are shown in 8.4. It becomes apparent that the acting of the EHs on the spot market is motivated by maintaining the power output, while gas savings are pursued. The reduction of net power output is perceived as undesired. This is seen from the relatively low SB and AP-SB profits compared to the configurations with the DH. For the same amount of gas saved, the profits of the SB are significantly lower. This effect is true for all the shown years,but the degree of this effect differs per year. In the year 2015 the SB profits are even low enough to drop below the profits of the AP, while the gas savings of the SB are significantly higher.

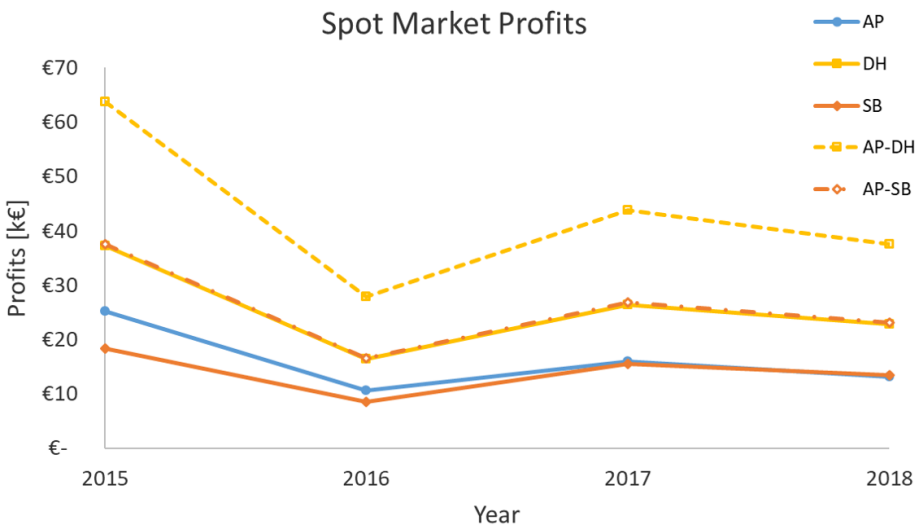

Figure 8.4: Profits obtained by the deployment of an electric heater per year. The profits of 2018 are extrapolated from the data that was available.

8.3. Acting on the imbalance market

Imbalance price data from TenneT from 2015 to 2018 is used to see the number of Program Time Units (PTUs) the EH can be used and the amount of money saved this way. (1 PTU = 15 minutes).

The capacity on the imbalance market is not that large, and the deployment of the EHs will have an effect on the price establishment of the grid operator. This effect is not taken into account.

8.3.1. Calculation of the profits

The data of the imbalance market is available per PTU. So, the same equations as for the spot market can be used (equation 8.1, 8.2 and 8.3), but now they have to be divided by a factor 4 as there are four PTUs in an hour. Equation 8.4 can be used to calculate the total savings per PTU of an EH in the imbalance market. Only if the savings are higher than zero, the EH is worth deploying. The results for the year 2017 are shortly described in section 8.3.2.

In case the results at a certain PTU are better for the AP than for the combination of the AP with DH or SB, only the AP is deployed.

8.3.2. Savings in the imbalance market in 2017

In figure 8.5 the results for the calculation of the profits on the imbalance market are shown for 2017. The profits on the imbalance market are two orders of magnitude higher than the profits on the spot market. It becomes clear that on the imbalance market additional flexibility is rewarded more than the savings of gas. The configurations with the SB are slightly less efficient than the ones with the HPB and DH, and offer therefore more flexibility. In contrast to the operation on the spot market, the SB is the most profitable option. On the imbalance market additional flexibility offered by the EH is the most valuable parameter to make profit.

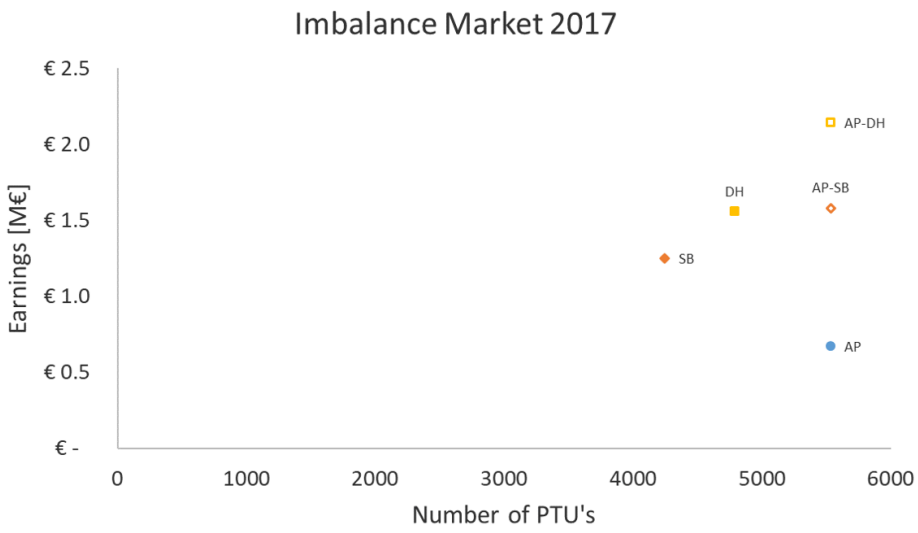

Figure 8.5: Potential profits on the imbalance market in 2017 versus the number of PTUs the electric heater could have been deployed.

8.3.3. Evolution of the profits on the imbalance market

The profits that could have been made by the EHs on the imbalance market from 2015 to 2018 are shown in 8.6. The differences between the profit of the EHs are smallest in 2017. Which means that this year the gas savings trade is a little more dominant than in other years. However, over the years, only small differences in the third group are seen. The EHs all have approximately the same relative profits development over the years.

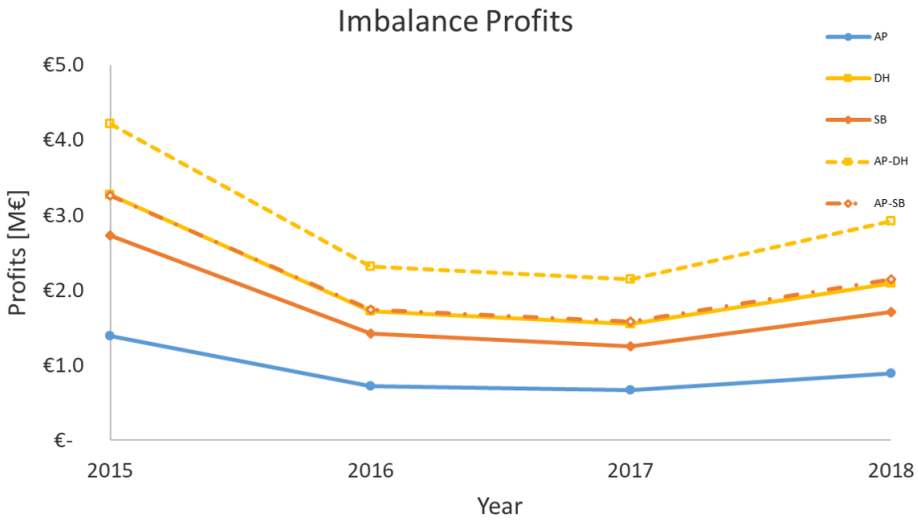

Figure 8.6: Evolution of the profits made with the utilisation of an electric heater at the imbalance market over several years. The profits of 2018 are extrapolated from the data that was available.

If one compares the 2017's evolution of the profits from the imbalance market (figure 8.6) with the profits from the spot market (figure 8.4), one can see that a successful year in terms of the spot market does not necessarily mean a successful year in terms of the imbalance market. And comparing the year 2015 for the two markets shows that success can be true for both markets in the same year.

8.4. Transportation costs

A fee has to be paid to be connected to the grid [50]. This fee consists of connection and transmission service tariffs, which are summarised for Delesto in table 8.1. As Delesto already has access to a grid connection, the initial connection tariff is excluded from this table. The periodic connection tariff is in place to account for the maintenance of only that particular connection. The non-transmission-related consumer tariff is to account for administration costs. The transmission-related consumer tariff covers the transmission of the power itself. The tariffs are revised yearly.

Table 8.1: Transmission tariffs for the years 2015 to 2018 [50]

			2015	2016	2017	2018
Periodic connection tariff	per year	€	12478.96	12478.96	12478.96	12478.96
Non-transmission-related consumer tariff	kW_e contracted per year	€	7.85	6.75	5.64	6.87
Transmission-related consumer tariff	kW_e consumed per month	€	0.91	0.81	0.65	0.7

Policies state that the consumer of electricity pays for the transportation of the electricity, even though the consumption itself helps balancing the system.

8.5. Capital and operational expenditure

The capital expenditure (CAPEX) of both electrode boilers is said to be around 120 €/kW_e of which the installation itself is the greatest share of expenses. Additional costs for higher pressure equipment are marginal. The costs of operations and maintenance, the operational expenditure (OPEX) are set to 2% of the CAPEX. In table 8.2 the CAPEX and OPEX are summarised for the AP, the DH and the SB and their combinations.

Table 8.2: Overview of the CAPEX and OPEX of the electric heater concepts of interest

	Capacity [MW]	CAPEX [once]	OPEX [per year]
AP	7.2	€900,000	€18,000
DH	45.8	€5,500,000	€110,000
SB	37.1	€4,500,000	€90,000
AP-DH	51.1	€7,000,000	€140,000
AP-SB	41.0	€5,800,000	€116,000

Considerations regarding the CAPEX of the duct heater

The heating of air is not a very efficient process. In case of the DH, to transfer 46 MW heat to 115kg/s flue gas with elements with a typical surface load of 2.5 W/cm^2 one would need a contact area of 1840 m^2 [51]. With a cross sectional area in the duct of approximately 20 m^2, 92 rows of heating elements would be needed. Each row being 0.6 m deep, one needs approximately 55 m of length inside the duct between the SHII and the DB. The DH alone weighs 189 t, if one assumes a power-to-weight ratio of 4 kW/kg [52]. For comparison, the weight of an HRSG can be 7000 t [43]. Not even including the additional duct material already adds 3% to the total weight. Besides the significant pressure drop over the DH elements, one can readily understand that this does not fit inside the existing duct of Delesto. It is not realistic to modify the CHP in such a way that it would fit, as one would probably even have to reinforce the foundation due to an increase in weight in the duct.

For the AP, the amount of space is less of an issue. The AP has to be located upstream of the gas turbine, where the amount of space is not as critical as inside the HRSG. For a capacity of 7.2 MW the installation would 'only' weigh 30 t.

8.6. Business case

The collection of the aforementioned costs and profits will result in a business case. The net profits are calculated for each year from 2015 to 2018. The life cycle is assumed to be 15 years and the depreciation is done linearly. For the OPEX an average value per year is taken. In figure 8.7 the summary for the separate boiler

is shown, in appendix F one can find the summary for the AP, DH, APDH and APSB. The net profit is the difference between the sum of the expenses (the left column) and the sum of the income (the right column).

The OPEX and CAPEX are constant per year. The transportation costs differ per year, due to the changing transmission service tariffs. The transportation costs comprise half of the total expenses.

It is readily seen that the income generated by the operation on the spot market is almost negligible compared to the income generated by acting on the imbalance market. The business case is almost entirely dependent on the income from the imbalance market. The profit the EH would have made on this market varies widely per year. Although the overall picture looks promising, the uncertainty of the incomes from the imbalance market should not be ignored.

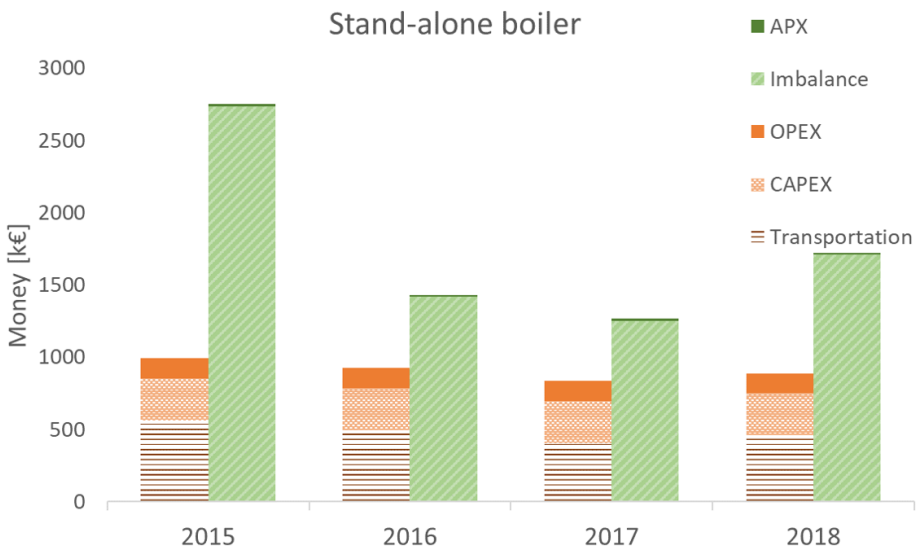

Figure 8.7: Approximated income and expenses for the stand-alone boiler from 2015 to 2018

8.6.1. Estimated payback period

The payback period is the number of years it would take before the investment has paid itself back. This quantifies the risk of the investment. The lower the number of years, the lower the risk.

The analysis done in figure 8.7 is done for each EH, after which the net profits are averaged over the four years. By dividing the CAPEX by the average profit per year, the payback period is obtained. In table 8.3 the results are collected for each EH.

Table 8.3: Number of years it takes to have a return on investment for the EHs.

	Capacity [MW]	Payback period [year]
AP	7.2	1.5
DH	45.8	8.1
SB	29.2	4.7
AP-DH	58.3	7.1
AP-SB	29.9	2.7

The payback period for the AP is only 1.5 years. So, if the life cycle is indeed 15 years, the AP is profitable for 13.5 years. It shows that a large EH capacity is not beneficial for the payback period. The DH and the AP-DH have the largest payback period, which is explained by the larger capacity. In this analysis the considerations described in section 8.5 are not yet taken into account, which would only further increase the payback period. The payback period of the SB stays within the 5 years, and would also decrease with the addition of the AP. From these results it can be concluded that the increase of profits attributed by the combination with the AP outweighs the increase of additional costs of capacity.

8.7. Conclusion

Some of the theoretical incomes and expenses of the EH concepts for the years between 2015 and 2018 are looked into in this chapter. Although the analysis performed was a simplified view on the real participation on the market, it gives insights into the relative financial performance of an EH with respect to its competitors. On the spot market the effectiveness is the most relevant parameter to be profitable, while on the imbalance market additional flexibility is of the greatest value. Given these conditions, it can be concluded from the results of the analysis that the AP has the best financial performance.

9

Conclusions and recommendations

In this thesis the technical and financial feasibility of the implementation of a power to heat application in an existing combined heat and power plant is studied. Research has been done on the steady state and dynamic behaviour of the system including the electric heater concepts in terms of thermodynamics. The electric heaters with the most promising results were subjected to a financial evaluation. In section 9.1 the most important conclusions are summarised. In section 9.2, recommendations for further steps are made.

9.1. Conclusions

Altogether the air preheater shows the best results in terms of technical and financial feasibility. Additionally, its presence would reduce the risk of the duct heater and the stand-alone boiler.

Answers on the central questions constructed in chapter 1 are given in this section.

9.1.1. Design requirements

- What are the possibilities to adjust the HRSG of a CHP in such a way that it can respond to the excess electricity on the grid?

The Delesto system is required to be able to fulfil a steam production of 120 t/h at a pressure of 4.2 bar. The capability to produce steam at a pressure of 30.5 bar has to be maintained. The gas turbine has a practical operational range of 80 % part load to full load. Auxiliary firing enables the fulfilment of the process steam demand regardless of the operational load of the gas turbine. In this research, the steam turbine will be kept operational at full load.

Electricity could be used to produce (part of) the process steam demand. This induces a decrease in the fuel consumption of the Combined Heat and Power installation. The electrode boiler and the immersion boiler are considered for this application of power to heat. Other power-to-heat devices might be suitable, but are not discussed in this study.

9.1.2. Steady state performance

- What is the steady state behaviour of the numerous electric heater concepts?

Eight electric heater concepts are proposed, among them: an air preheater located upstream of the gas turbine; a duct heater located in the HRSG upstream of the duct burner; a high pressure boiler located parallel to the high pressure evaporator of the HRSG; and a stand-alone boiler external from the HRSG.

Among the electric heater concepts that were studied: the duct heater, the high pressure boiler and the stand-alone boiler show the best steady state performance in terms of "Additional Flexibility" offered. The air preheater shows good steady state performance in terms of "Effectiveness". Additionally, the air preheater is capable of improving the performance of the duct heater, the high pressure boiler and the stand-alone boiler in terms of "Additional Flexibility", "Effectiveness" and the "Relative Stack Losses".

9.1.3. Study on the dynamic behaviour

- What is the dynamic behaviour of each of the 'high potential' design cases?

It is concluded that a model including the two high pressure superheaters, the high pressure evaporator and the desuperheater and duct burner, is sufficient to simulate the critical changes in the HRSG. Temperature changes in the headers of the first superheater are expected in response to changes in the fuel consumption of the duct burner. Temperature changes in the headers of the second superheater are expected in response to changes in the amount of water injected in the desuperheater.

According to the dynamic model constructed, the studied electric heater concepts are all able to ramp to maximum load within 15 minutes without exceeding the maximum rate of 25 °C/min in the superheater headers. This implies that the electric heaters are suitable to deploy as demand response on the imbalance market. On account of the high pressure boiler, the coil material of the first superheater experiences a temperature change that is considered to be too severe. This study has shown that the difference in expansion rate inside the coils due to thermal effects are not expected to cause failure.

9.1.4. Financial performance

- What is the expected financial performance of the remaining electric heater concepts?

The profits on the spot and imbalance market are estimated based on historical price data on power, gas and CO_2 emissions. This study indicates that the spot market rewards the high effectiveness, and that the imbalance market rewards the additional flexibility provided by an electric heater concept. The potential profits on the imbalance market are two orders of magnitude higher than the potential profits on the spot market. Half of the total expenses comprise of the transportation costs of the power. The evaluation of the payback time of the electric heaters indicates that the air preheater is the electric heater with the lowest financial risk. Another finding that came as a result of the payback time evaluation is that a low capacity might be beneficial over a high capacity of the electric heater.

9.2. Recommendations

The research has given insights on the technical and financial feasibility of the implementation of power-to-heat in a Combined Heat and Power installation. In light of this research, a strong case can be made for the implementation of an electric heater, but further work is required.

This research indicates that the air preheater is the most effective in saving gas, with a low ramp time and a low financial risk. The technical feasibility of this electric heater should be further researched. The further development of plans to implement the air preheater (with or without the addition of the stand-alone boiler) is strongly recommended.

It is unfortunate that the study did not include the interaction between the electric heater and the imbalance market. The presence of the electric heater and electrification in general will have a dampening effect on the price bids from TenneT-NL. The profits on the imbalance market will be smaller than indicated in this thesis. Power-to-heat applications will harm their own business case, and this phenomenon should be well understood.

As one could have seen from the business case that was setup, a great share of the expenses was on account of the power transportation. The reformation of regulations regarding these transportation costs might help to motivate power market participants to provide downward flexibility.

If the dynamic model is used for further research some improvements are advised. The "stiff" nature of the Heat Recovery Steam Generator problem requires an implicit instead of an explicit ordinary differential equation solver. The model should be modified, to avoid instability and inconvenient small step sizes. Furthermore, the response of the desuperheater is essential to the behaviour of the HRSG. A greater focus on the control of the model could translate in smaller ramp times. Besides that integral wind-up of the controller should be avoided.

After the steady state analysis, the electric heaters with a small additional flexibility were disregarded. The assumption was made that lower additional flexibility would result in low profits. However, small additional

flexibility was often caused by a small maximum capacity of the electric heater. The decrease in capital expenditure for smaller capacity EHs might outweigh the decrease in profits. On account of the financial study, the exclusion of the low pressure boiler and both heaters could be interesting to revise.

Bibliography

[1] Overall progress towards the European Union's '20-20-20' climate and energy targets. Technical report, European Environment Agency, jun 2017.

[2] Rutte iii legt lat aanpak co2 hoger dan eu. https://www.europa-nu.nl/id/vkichk74ocz6/nieuws/rutte_iii_legt_lat_aanpak_co2_hoger_dan, 2017. (Accessed on 09/12/2017).

[3] Ministerie van Economische Zaken. Energierapport: transitie naar duurzaam. *Den Haag*, 2016.

[4] SER. Energieakkoord. https://www.energieakkoordser.nl/, 2013.

[5] Joost Gerdes, Sjoerd Marbus, and Martijn Boelhoewer. Energietrends. www.energietrends.info, 2016.

[6] Share of renewable energy at 5.9% in 2016. https://www.cbs.nl/en-gb/news/2017/22/share-of-renewable-energy-at-5-9-in-2016, May 2017. (Accessed on 05/09/2017).

[7] Frans Rooijers Sebastiaan Hers, Maarten Afman, Sofia Cherif. Potential for Power-to-Heat in the Netherlands, 2015.

[8] Marit Van Hout, Paul Koutstaal, Ozge Ozdemir, and Ad Seebregts. Quantifying flexibility markets, 2014.

[9] TenneT. Activities TenneT. https://www.tennet.eu/.

[10] Hans Ziesing. Energieverbrauch in Deutschland im Jahr 2017. Technical report, Arbeitsgemeinschaft Energie bilanzen e. V, Berlin, 2018.

[11] Fabio Genoese ; Massimo Genoese ; Martin Wietschel. Occurrence of negative prices on the German spot market for electricity and their influence on balancing power markets. *2010 7th International Conference on the European Energy Market*, 2010.

[12] EPEXSPOT. German market, Day-ahead (2017-12-26). http://www.epexspot.com/en/market-data/dayaheadauction/chart/auction-chart/2017-12-26/DE, 2017.

[13] Erik van der Walle. Wie de balans verstoort, moet dokken. https://www.nrc.nl/nieuws/2018/05/04/wie-de-balans-verstoort-moet-dokken-a1601958, 2018. (Accessed on 30/05/2018).

[14] National Energy Outlook 2016, 2016.

[15] Aardgas en elektriciteit, gemiddelde prijzen van eindverbruikers. {http://statline.cbs.nl/StatWeb/publication/?VW=T{&}DM=SLNL{&}PA=81309NED{&}D1=0-1,3,5,7-8,11,15{&}D2=0{&}D3=a{&}D4=a{&}HD=121114-1344{&}HDR=G1,G2,T{&}STB=G3}, note = (Accessed on 28/09/2018) year = 2018.

[16] B.L. Schepers and S.J. Aarnink. Kansen voor warmte. Technical report, CE Delft, 2014.

[17] Morten B. Blarke. Towards an intermittency-friendly energy system: Comparing electric boilers and heat pumps in distributed cogeneration. *Applied Energy*, 2012.

[18] Example of an aggregated curve. http://www.epexspot.com/en/market-data/dayaheadauction/curve/auction-aggregated-curve/2016-05-02/DE.

[19] AkzoNobel. Year Report. http://report.akzonobel.com/2017/ar/{%}7D. (Accessed on 25/05/2018).

[20] Herbert IH Saravanamuttoo, Gordon Frederick Crichton Rogers, and Henry Cohen. *Gas turbine theory*. Pearson Education, 2001.

[21] Bedrijfsvoorschriften "Breda" Bijgestookte Afgassenketel achter een Thomassen gas turbine. Technical report, B.V. Machinefabriek "Breda".

[22] R Bahrampoury, A Behbahaninia, A Shadaram, and E Taghdiri. Comparison between in-line and staggered arrangements in heat recovery steam generators. *IEEES-4. United Emirate*, 2009.

[23] V Ganapathy. Engineering Practice Understanding Boiler Circulation Proper arrangement of drum baffling, sizing and location of dowcomers and risers will ensure a good natural-circulation system.

[24] Peter Meibom, Juha Kiviluoma, Rüdiger Barth, Heike Brand, Christoph Weber, and Helge V. Larsen. Value of electric heat boilers and heat pumps for wind power integration. *Wind Energy*, 2007.

[25] Maria Grønnegaard Nielsen, Juan Miguel Morales, Marco Zugno, Thomas Engberg Pedersen, and Henrik Madsen. Economic valuation of heat pumps and electric boilers in the Danish energy system. *Applied Energy*, 2016.

[26] Jon Gustav Kirkerud, Torjus Folsland Bolkesjø, and Erik Trømborg. Power-to-heat as a flexibility measure for integration of renewable energy. *Energy*, 128:776–784, 2017.

[27] Parat high voltage electrode boiler - parat halvorsen. https://www.parat.no/en/products/industry/parat-ieh-high-voltage-electrode-boiler/. (Accessed on 09/03/2018).

[28] Bert den Ouden, Maarten Afman, Egbert Klop, Grift.Jan, and Niki Lintmeijer. Electrification in the Dutch process industry. Technical report, Berenschot, 2017.

[29] Anoop Kumar Shukla and Onkar Singh. Effect of Compressor Inlet Temperature & Relative Humidity on Gas Turbine Cycle Performance. *International Journal of Scientific & Engineering Research*, 5(5), 2014.

[30] R Broad and D Shiferaw. The compact future of fuel gas performance heating. *Energy-Tech Magazine*, 2015.

[31] Fuels and chemicals - auto ignition temperatures. https://www.engineeringtoolbox.com/fuels-ignition-temperatures-d_171.html.

[32] Natural gas. http://www.newworldencyclopedia.org/entry/Natural_gas.

[33] DM Erickson, SA Day, and R Doyle. Design considerations for heated gas fuel. *GE Power Systems GER-4189b*, 2003.

[34] THERMOFLEX®. https://www.thermoflow.com/, 2018.

[35] Ivar S Ertesvåg. Exergetic comparison of efficiency indicators for combined heat and power (chp). *Energy*, 32(11):2038–2050, 2007.

[36] Stefano Bracco, Ilka Faccioli, and Michele Troilo. A Numerical Discretization Method for the Dynamic Simulation of a Double-Pipe Heat Exchanger. *International Journal of Energy*, 1(3):47–58, 2007.

[37] A. Ong'iro, V .I. Ugursal, A.M.Al Taweel, and J. D. Walker. Modeling of Heat Recovery Steam Generator Preformance. *Applied Thermal Engineering*, 17(5):427–446, 1997.

[38] M. R. Ansari and V. Mortazavi. Simulation of dynamical response of a countercurrent heat exchanger to inlet temperature or mass flow rate change. *Applied Thermal Engineering*, 2006.

[39] Joel H Ferziger and Milovan Peric. *Computational methods for fluid dynamics*. Springer Science & Business Media, 2012.

[40] Cornelis Vuik, P Van Beek, F Vermolen, and J Van Kan. *Numerical Methods for Ordinary differential equations*. VSSD, 2007.

[41] VDI-Gesellschaft Verfahrenstechnik und Chemieingenieurwesen. *VDI Heat Atlas*.

[42] Reza Eslami, Richard B. Hetnarski, Jozef Ignaczak, Naotake Noda, Naobumi Sumi, and Yoshinobu Tanigawa. *Fundamentals of Linear Elasticity*, pages 35–64. Springer Netherlands, Dordrecht, 2013.

[43] Vernon L Eriksen. *Heat Recovery Steam Generator Technology*. Woodhead Publishing, 2017.

[44] World Bank. Cmo-april-2018-forecasts.pdf. http://pubdocs.worldbank.org/en/458391524495555669/CMO-April-2018-Forecasts.pdf, April 2018. (Accessed on 09/03/2018).

[45] Scenarios for the Dutch electricity supply system. Technical report, Frontier Economics Ltd, London, 2015.

[46] European Council Council of the European Union. Reform of the eu emissions trading scheme - consilium. http://www.consilium.europa.eu/en/policies/climate-change/reform-eu-ets/, November 2017. (Accessed on 09/03/2018).

[47] European Council Council of the European Union. Reform of the eu emissions trading system – council endorses deal with european parliament - consilium. http://www.consilium.europa.eu/en/press/press-releases/2017/11/22/reform-of-the-eu-emissions-trading-system-council-endorses-deal-with-european-parliament/, November 2017. (Accessed on 09/03/2018).

[48] CarbonTracker. Carbon clampdown: Closing the gap to a paris-compliant eu-ets - carbon tracker initiative. https://www.carbontracker.org/reports/carbon-clampdown/, April 2018. (Accessed on 09/30/2018).

[49] BusinessInsider. Co2 european emission allowances price in euro | markets insider. https://markets.businessinsider.com/commodities/co2-emissionsrechte/euro. (Accessed on 09/03/2018).

[50] Tariffs - tennet. https://www.tennet.eu/electricity-market/dutch-market/tariffs/. (Accessed on 10/09/2018).

[51] SinusJevi. Duct heaters type effk - sinusjevi. http://www.sinusjevi.com/products/duct-heaters-type-effk/. (Accessed on 10/6/2018).

[52] Duct heaters - wattco. https://www.wattco.com/product_category/duct-heaters/. (Accessed on 9/09/2018).

[53] Michael F Modest. *Radiative heat transfer*. Academic press, 2013.

A

Results for 100 and 140 t/h

A.1. 100 t/h

Relative fuel savings

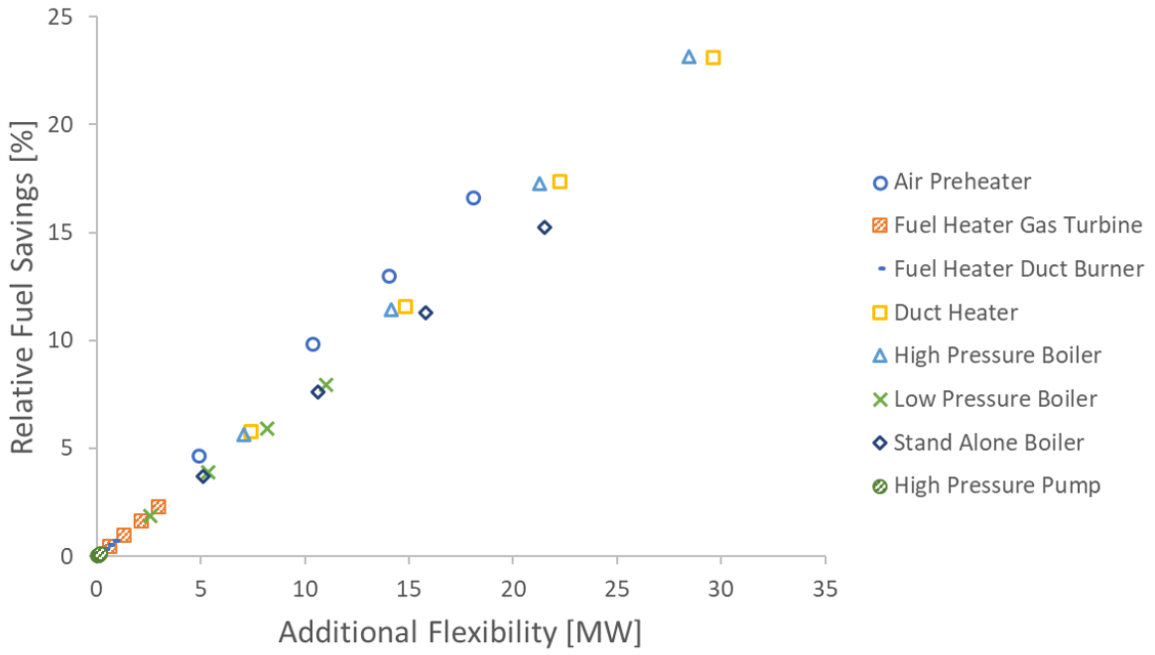

Figure A.1: Relative fuel savings of the electric heaters at process steam demand (120 t/h)

Effectiveness

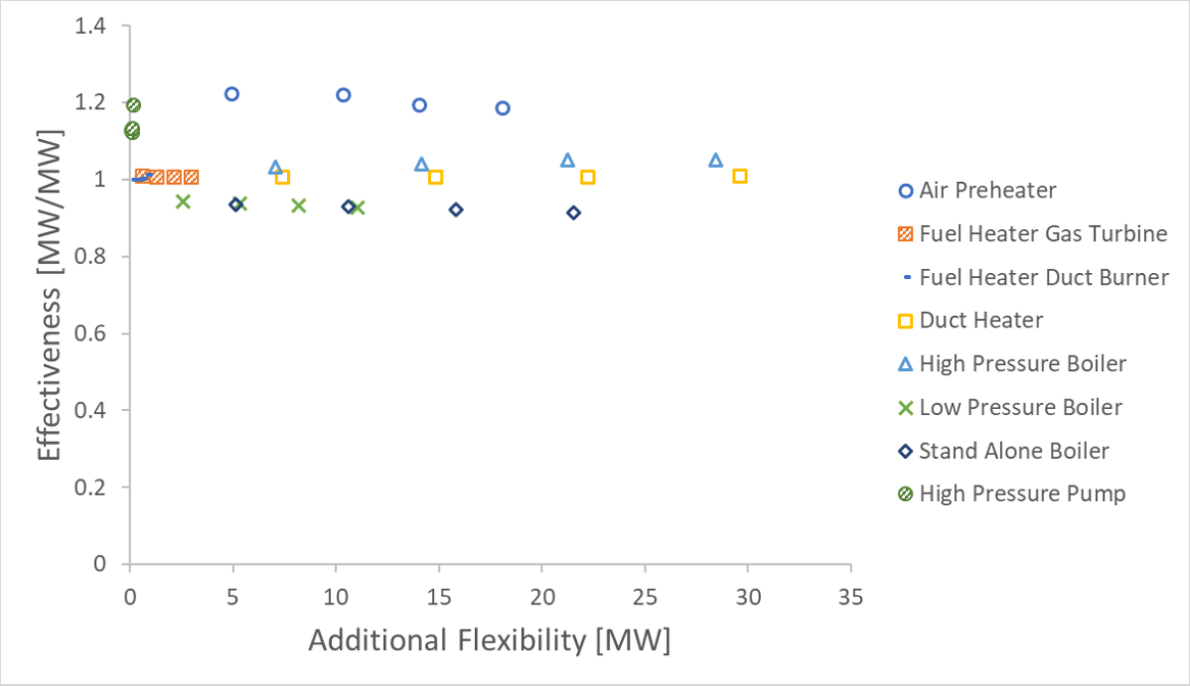

Figure A.2: Effectiveness of the electric heaters at process steam demand (100 t/h)

Relative stack losses

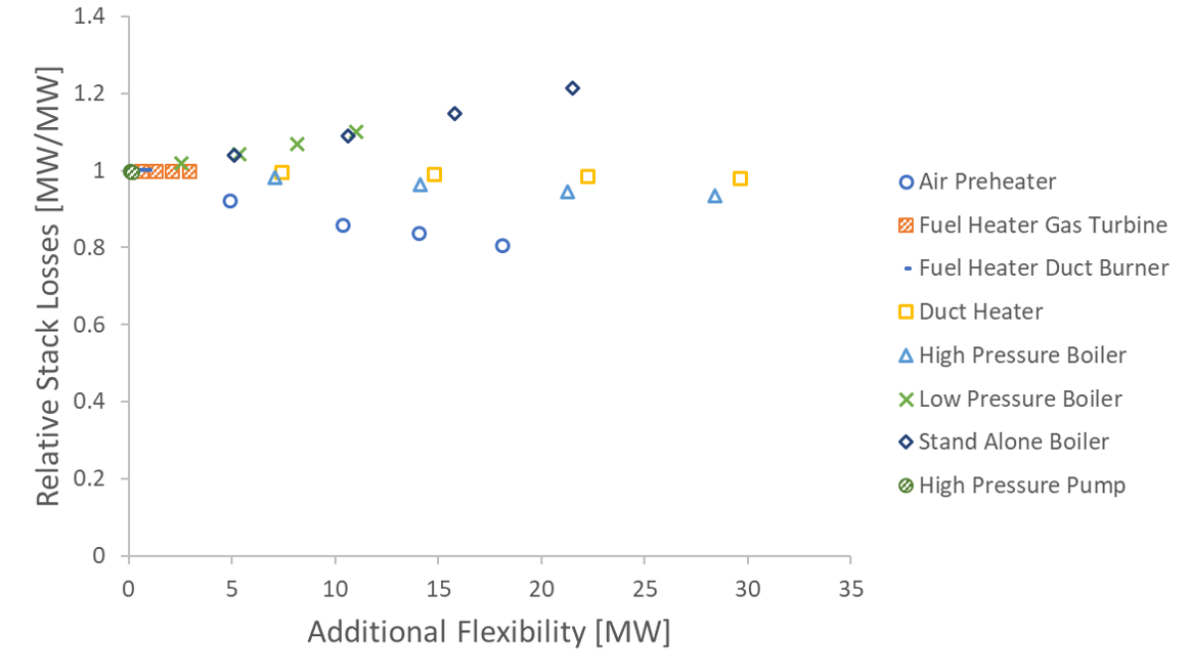

Figure A.3: Relative stack losses of the electric heaters at process steam demand (100 t/h)

A.2. 140 t/h

Relative fuel savings

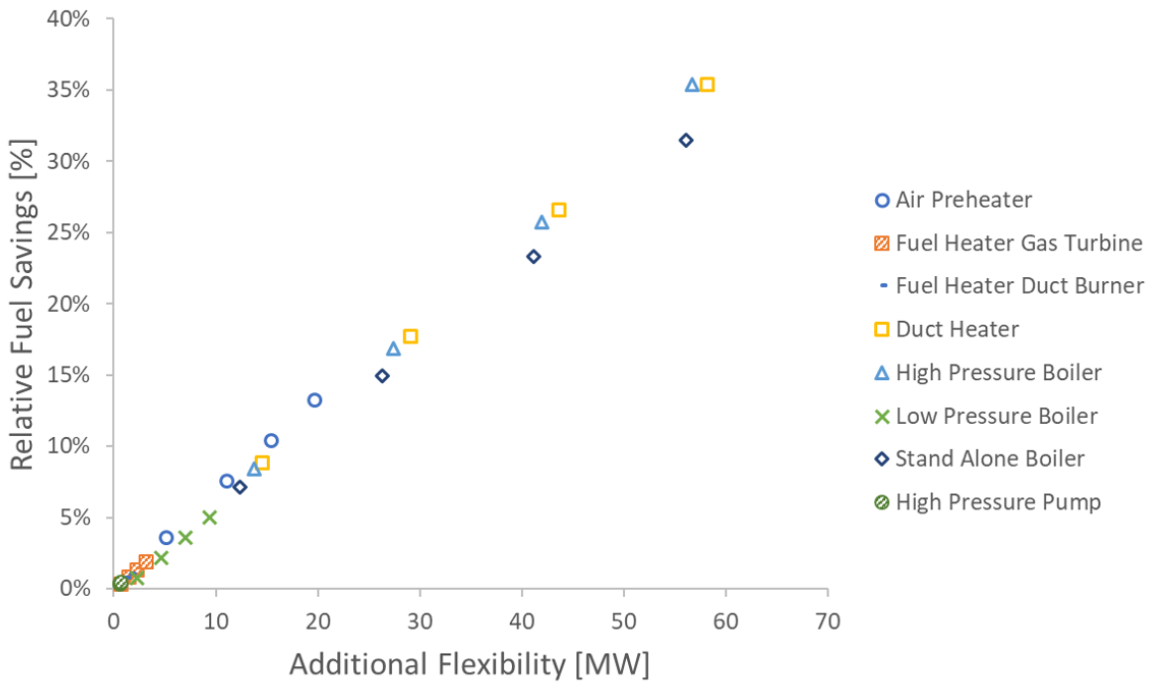

Figure A.4: Relative fuel savings of the electric heaters at process steam demand (140 t/h)

Effectiveness

See section 5.4.2.

Relative stack losses

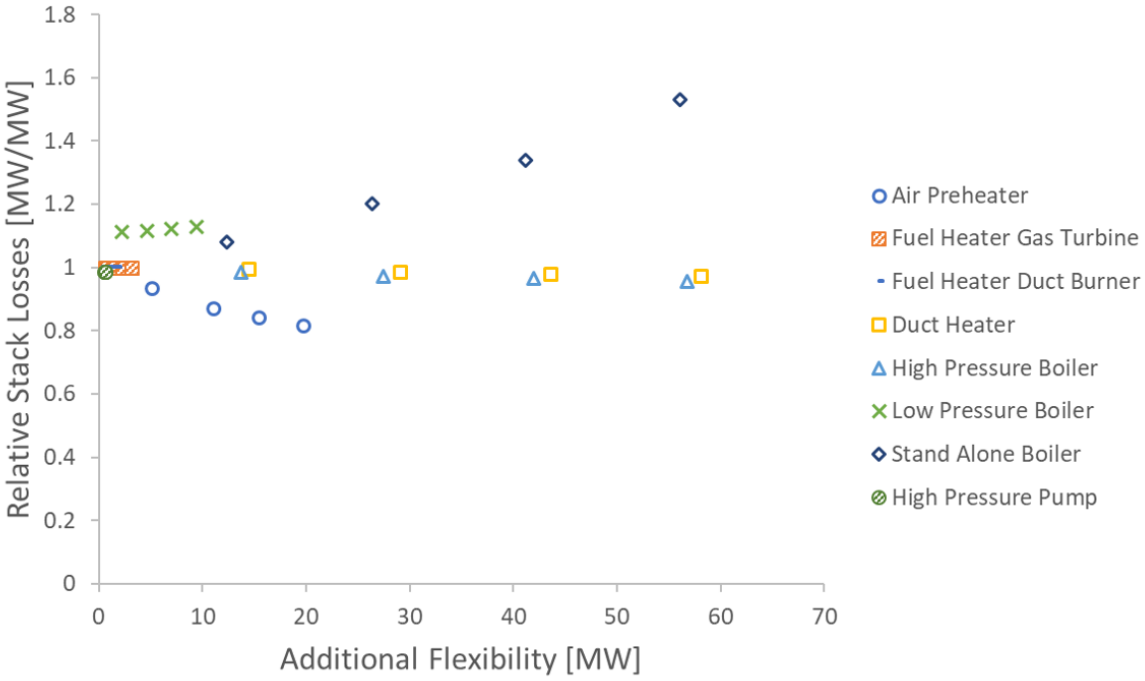

Figure A.5: Relative stack losses of the electric heaters at process steam demand (140 t/h)

B

Formulas to determine the Heat transfer in the heat exchangers of the dynamic model

In section 6.3.1 the conservation of energy is formulated. The heat transfer used in this section is calculated with the help of the equations described in this appendix. In section B.1 the equations used to determine the heat transfer from the flue gas path are given. In section B.2 the calculation method on the heat transfer to the superheated steam in the superheaters is elaborated on. In section B.3 the formulas to calculate the heat transfer to the evaporation process are given. In section B.4 the formulas to calculate the radiative heat transfer in the duct burner are presented.

B.1. The transfer of heat from the flue gas side flow path

The heat transfer from the flue gas to the tube walls of a heat exchanger is a function of the geometry of the heat exchanger, and the characteristics of the flow within. In this section, the calculation method for the convected heat transfer from the flue gases is shown. A distinction is made between a heat exchanger with and without fins, respectively section B.1.1 and B.1.2. The heat exchangers are set up in cross flow, with the flue gas duct horizontally oriented and the water tube banks oriented vertically. All the physical properties (such as dynamic viscosity , density and Prandtl number) of the flue gas discussed in this section are evaluated at the mean temperature.

$$T_m = \frac{T_E + T_L}{2} \tag{B.1}$$

B.1.1. Convective heat transfer in a duct with bare tubes in cross flow

The difference between an in-line and a staggered arrangement of tubes in a cross flow is shown in figure B.1.

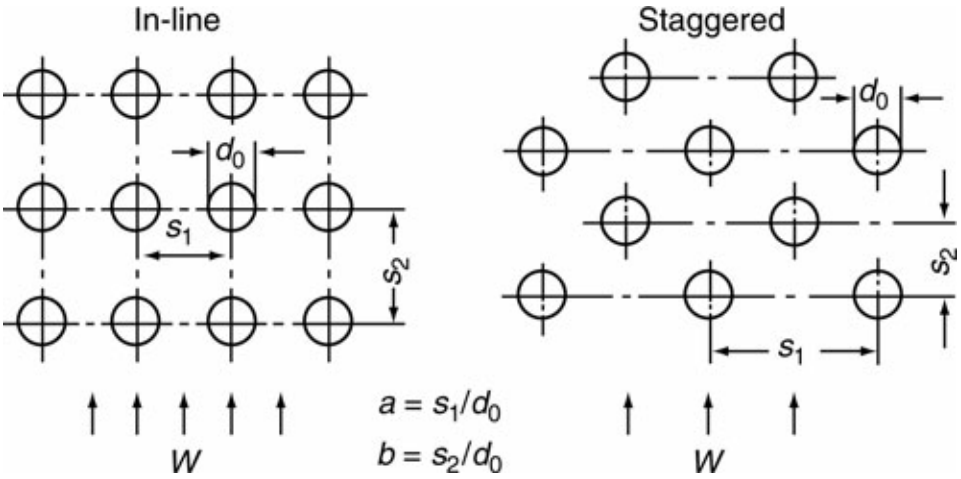

Figure B.1: In-line and staggered configuration of bare tubes in a cross flow.

The Nusselt number (Nu) is defined as the ratio between convective and conductive heat transfer. For a single row of tubes in a cross-flow heat exchanger is

$$\mathrm{Nu}_{single,row} = 0.3 + \sqrt{\mathrm{Nu}_{l,lam}^2 + \mathrm{Nu}_{l,tur}^2} \tag{B.2}$$

in which $\mathrm{Nu}_{l,lam}$ is calculated with B.3 and $\mathrm{Nu}_{l,tur}$ with B.4. The Prandtl number (Pr) characterises the ratio of the momentum and thermal diffusivity.

$$\mathrm{Nu}_{l,lam} = 0.664\sqrt{\mathrm{Re}_{\psi,l}}\sqrt[3]{\mathrm{Pr}} \tag{B.3}$$

$$\mathrm{Nu}_{l,tur} = \frac{0.037\,\mathrm{Re}_{\psi,l}\,\mathrm{Pr}}{1 + 2.443\,\mathrm{Re}_{\psi,l}^{-0.1}\left(\mathrm{Pr}^{2/3} - 1\right)} \tag{B.4}$$

The Reynold's number (Re) is described by equation B.5, in which w is the mass flux. It is corrected with the void fraction ψ, to obtain the mass flux at the smallest cross sectional area in the duct passage.

$$\mathrm{Re}_{\psi} = \frac{w\,l}{\psi\,\mu} \tag{B.5}$$

The characteristic length l used in equation B.5 is the flow path transverse over a tube: the streamed length l_s which is equal to half the circumference of a cylinder, $l_s = (\pi/2)d_o$. The void fraction is calculated with equation B.6. The definition of the transverse and longitudinal pitch ratio, respectively a and b are shown in figure B.1 .

$$\psi = \begin{cases} 1 - \frac{\pi}{4a}, & \text{if} \quad b \geq 1 \\ 1 - \frac{\pi}{4ab}, & \text{if} \quad b < 1 \end{cases} \tag{B.6}$$

The Nusselt number for multiple rows of tubes is calculated with equation B.7, in which r is the number of rows.

$$\mathrm{Nu}_{0,bundle} = \frac{1 + (r-1)f_A}{r}\,\mathrm{Nu}_{single-row} \tag{B.7}$$

The factor f_A is defined as in equation B.8 and B.9, respectively for an in-line and a staggered configuration of the tube banks.

$$f_A = 1 + \frac{0.7\,(b/a - 0.3)}{\psi^{1.5}\,(b/a + 0.7)^2} \tag{B.8}$$

$$f_A = 1 + \frac{2}{3b} \tag{B.9}$$

The heat transfer coefficient α_{fg} results from equation B.10. The thermal conductivity λ is evaluated at the mean temperature from equation B.1.

$$\mathrm{Nu}_{0,bundle} = \frac{\alpha_{fg}\,l}{\lambda} \tag{B.10}$$

B.1.2. Convective heat transfer in duct in cross flow with finned tubes

Not only does the heat transfer area increase with the implementation of fins, it also influences the heat transfer coefficient in the flue gas duct. Inside the system boundaries chosen in section 6.1, the SHII and the evaporator are the components with circular finned tubes. The approach of determining the heat transfer coefficient α_{fg} and consequently the heat transfer Q for finned tubes only adds to the method for the duct with bare tube banks. The void fraction of finned tubes will be different from bare tubes, shown in equation B.11. Using the method from section B.1.1 an uniform heat transfer coefficient can be obtained α_m. This represents the heat transfer coefficient between the bare tube and the fins. Together with the fin efficiency η_f the heat transfer coefficient of the complete tube could be established. The calculation method is explained in this section.

$$\psi = \frac{(s_2 - d_o)a + (s_2 - D)\delta}{s_2(a + \delta)} \tag{B.11}$$

After the heat transfer coefficient of the bundle with bare tubes α_m is established from equation B.10, it can be substituted in equation B.15. The efficiency in which the heat that enters the fins is transferred to the tube material is for circular finned tubes described with the equations B.12 to B.14, in which η_f is the efficiency, and X and φ are shape dependent operands and D is the diameter including the height of the fin.

$$\eta_f = \frac{\tanh X}{X} \tag{B.12}$$

$$X = \varphi \frac{d_o}{2} \sqrt{\frac{2\alpha_m}{\lambda_f \delta}} \tag{B.13}$$

$$\varphi = \left(\frac{D}{d_o} - 1\right)\left[1 + 0.35 \ln\left(\frac{D}{d_o}\right)\right] \tag{B.14}$$

A virtual heat transfer coefficient can now be established, equation B.15. This is the total heat transfer coefficient between the flue gases and the material of the tubes.

$$\alpha_v = \alpha_m \left[1 - (1 - \eta_f)\frac{A_f}{A}\right] \tag{B.15}$$

Where A_f / A is the ratio between fin surface and the total surface of the tube.

The heat transfer from the flue gas to the bare tube wall is described with equation B.16, in which A is the total outer surface area.

$$\dot{Q}_{fg} = \alpha_{fg} A \Delta T_{LM} \tag{B.16}$$

B.2. Heat transfer to the superheated steam path

In case the heat exchanger from section 6.3.1 is a superheater the heat transfer from the tube wall material to the water side flow path is discussed in this section. In case of an evaporator the calculation method is discussed in section B.3.

The Reynolds number is expressed in terms of the mass velocity flux w [kg s^{-1} m^{-2}], see equation B.17.

$$\mathrm{Re} = \frac{w\, d_i}{\mu} \tag{B.17}$$

All the fluid properties should be at the average temperature of the wall temperature T_{wall} and the bulk temperature T_B. The bulk temperature is $0.5(T_E + T_L)$.

$$T_m = \frac{T_{wall} + T_B}{2} \tag{B.18}$$

B.2.1. Nusselt number in a tube

The heat transfer from the tube wall material to the water side flow path depends on the characteristics of the flow. For the determination of the Nusselt number a distinction is made between laminar, turbulent and transitional flow regimes, all of which are discussed in this section. In all these regimes the main assumption is that the flow is hydrodynamic and thermal developed, which is valid for $L > d_i \geq 60$. The temperature of the material of the tubes are assumed to be constant, which fit the characteristic of the discretised system.

Nusselt number in Laminar flow regime (Re < 2300)

$$\mathrm{Nu}_{m,T} = \left\{\mathrm{Nu}_{m,T,1}^3 + 0.7^3 + (\mathrm{Nu}_{m,T,2} - 0.7)^3 + \mathrm{Nu}_{m,T,3}\right\}^{1/3} \tag{B.19}$$

with

$$\mathrm{Nu}_{m,T,1} = 3.66 \tag{B.20}$$

$$\mathrm{Nu}_{m,T,2} = 1.615 \sqrt[3]{\mathrm{Re}\,\mathrm{Pr} \cdot d_i / l} \tag{B.21}$$

$$\mathrm{Nu}_{m,T,3} = \left(\frac{2}{1 + 22\,\mathrm{Pr}}\right)^{1/6} (\mathrm{Re}\,\mathrm{Pr}\, d_i / l)^{1/2} \tag{B.22}$$

Nusselt number in Turbulent flow regime (Re > 10^4)

For a turbulent flow with $10^4 < Re < 10^6$ the Nusselt number follows from

$$\mathrm{Nu}_m = \frac{(\zeta/8)\,\mathrm{Re}\,\mathrm{Pr}}{1+12.7\sqrt{\zeta/8}(\mathrm{Pr}^{2/3}-1)}\left[1+(d_i/l)^{2/3}\right] \tag{B.23}$$

with the friction factor ζ, which is $\zeta = (1.8\log\mathrm{Re}-1.5)^{-2}$ for smooth pipes.

Nusselt number in transitional flow regime (2300 ≤ Re ≤ 10^4)

In the transitional regime, the Nusselt number is defined by

$$\mathrm{Nu} = (1-\gamma)\,\mathrm{Nu}_{lam,2300} + \gamma\,\mathrm{Nu}_{turb,10^4} \tag{B.24}$$

Where γ is the intermittency factor and is defined by

$$\gamma = \frac{\mathrm{Re}-2300}{10^4-2300} \tag{B.25}$$

$Nu_{lam,2300}$ is established by substituting Re = 2300 in equation B.19 for Re = 2300, and $\mathrm{Nu}_{turb,10^4}$ is calculated by substitution of Re = 10^4 in equation B.23.

The overall heat transfer coefficient in a tube

The average heat transfer coefficient α can now be calculated using:

$$\mathrm{Nu} = \frac{\alpha\, d_i}{\lambda} \tag{B.26}$$

where Nu is the appropriate Nusselt number in terms of the Reynolds number. The heat transfer is calculated with $Q = \alpha\, A\, \Delta T_{LM}$. The area over which heat is transfer effectively is $L\pi\, d_i$ per tube.

The logarithmic mean temperature difference ΔT_{LM} is defined by

$$\Delta T_{LM} = \frac{(T_{wall}-T_E)-(T_{wall}-T_L)}{\ln\frac{T_{wall}-T_E}{T_{wall}-T_L}} \tag{B.27}$$

B.3. The transfer of heat to the evaporation process

During the evaporation process the temperature of the saturated water stays constant. All the energy absorbed by the fluid is used to change the phase of the fluid, this energy is also known as the latent heat. Although the fluid is a bit subcooled, due to the increase in hydrostatic pressure in the downcomers, the assumption is made that the main process in the evaporator is convective flow boiling.

For vertical tubes the local heat transfer coefficient as function of the vertical distance to the start is calculated with equation B.28. The heat transfer coefficient is assumed to be uniform over the circumference of the tubes. The circulation ratio of the evaporator is the amount of passes through the evaporator a certain control volume has to make before it is completely vaporised. This theoretically results in a outlet quality of the steam of $1/CR$ for each tube in the evaporator. A linearly increase of quality in the tubes is assumed.

$$\alpha(z) = \alpha_{LO}\left\{(1-\dot{x})^{0.01}\left[(1-\dot{x})^{1.5}+1.9\dot{x}^{0.6}\left(\frac{\rho_L}{\rho_G}\right)^{0.35}\right]^{-2.2}+\dot{x}^{0.01}\left[\frac{\alpha_{GO}}{\alpha_{LO}}\left(1+8(1-\dot{x})^{0.7}\left(\frac{\rho_L}{\rho_G}\right)^{0.67}\right)\right]^{0.2}\right\}^{-0.5} \tag{B.28}$$

In this formula α_{LO} and α_{GO} are the heat transfer coefficient for respectively the liquid (with a vapour quality of 0) and the vapour (with a vapour quality of 1). For each z values are calculated with the following formula's.

For Laminar hydrodynamically developed flow in which the temperature of the tube walls is assumed constant the Nusselt number is described by equation

$$\mathrm{Nu}_z = \sqrt[3]{3.66^3+1.077^3\,\mathrm{Re}\,\mathrm{Pr}\cdot C} \tag{B.29}$$

$$C = \begin{cases} \frac{d_i}{z}, & \text{if } \frac{d_i}{z} < 1 \\ 1, & \text{otherwise} \end{cases} \tag{B.30}$$

In turbulent flow, for a constant wall temperature and hydrodynamically developed flow, the Nusselt number is calculated with B.31, in which the friction factor ζ is described by equation B.32.

$$\mathrm{Nu}_z = \frac{(\zeta/8)\,(\mathrm{Re}-1000)\,\mathrm{Pr}}{1+12.7\sqrt{(\zeta/8)}\left(\mathrm{Pr}^{2/3}-1\right)} \tag{B.31}$$

$$\zeta = \left(1.82\log_{10}(Re)-1.64\right)^{-2} \tag{B.32}$$

For α_{LO} the Reynolds number for saturated liquid is used and for α_{GO} the Reynolds number for saturated vapour is used. Using equation B.33 values can be determined for both the heat transfer coefficients for saturated liquid and vapour.

$$\mathrm{Nu}_z = \frac{\alpha(z)\,d_i}{\lambda} \tag{B.33}$$

As readily can be seen, for negligible inflow effects ($d_i/z > 1$) both α_{LO} and α_{GO} are constants in equation B.28. The vapour quality in equation B.28 is varied linearly between $\dot{x} = 0$ and $\dot{x} = 1/CR$.

The total heat transfer over the tube is the integral of the local heat transfer coefficients obtained from equation B.28 to z. Because of the piecewise discretization, this comes down to the sum of the values obtained for each z.

The heat transfer to the evaporation process is determined with equation B.34.

$$\dot{Q}_{H_2O} = A_i\,\alpha\,(T_w - T_{sat}) \tag{B.34}$$

B.4. Heat transfer in the duct burner

In the duct burner the temperature of the flue gases is elevated by means of combustion of natural gas. Heat is transferred from the flue gases to the evaporation screen and water walls. The function of these elements is to protect the material and the HRSG against the high temperature radiation. The convective heat transfer from the flue gases to the tubes is determined with method described in section B.1.1. The radiative heat transfer to the water walls and evaporation screen is reviewed in this section.

B.4.1. Radiative heat transfer to the Water walls

The water walls and evaporation screen are assumed to behave like one radiation surface . It is assumed that no accumulation of energy exists in the duct burner. The water in the tubes completes its phase change in one pass. The heat in the duct burner determines the mass flow in the water walls and the evaporation screen. Convection and Radiation happen in a simultaneous matter, in terms of heat transfer resistive network "parallel". The temperature, density and concentration are uniform over the first cell of the duct burner.

$$\dot{Q} = A_{rad}\,\sigma\,\frac{\varepsilon_w}{1-(1-\varepsilon_w)(1-A_v)}\left(\varepsilon_g T_g^4 - A_v T_w^4\right) \tag{B.35}$$

In equation B.35 subscripts w and g stand respectively for wall and gas. ε and A_v stand for emissivity and the absorptivity of the flue gas. The Stefan–Boltzmann constant is defined as $\sigma = 5.670\,40\times10^{-8}\,\mathrm{W/m^2/K^4}$, A_{rad} is the surface area which is 'seen' by the radiation, which is equal to $155\,\mathrm{m}^2$.

$$\varepsilon_g = \varepsilon_{\mathrm{H_2O}} + \varepsilon_{\mathrm{CO_2}} - (\Delta\varepsilon)_g \tag{B.36}$$

$$A_v = A_{v,\mathrm{H_2O}} + A_{v,\mathrm{CO_2}} - (\Delta\varepsilon)_w \tag{B.37}$$

The $\Delta\varepsilon$ terms are correction factors for the overlap in emission bands of the components involved [53]. They are used to account for the self-absorption taking place. See section B.4.2 for their determination.

The equivalent layer thickness (s_{eq}) seen in the following sections is a way to express that the radiation surface is not an ideal sphere surrounding the source. A very general way to estimate this s_{eq} is

$$s_{eq} = 0.9\frac{4V}{A} \tag{B.38}$$

Substituting values for the absorptivity and emissitivity and their correction from section B.4.3 and B.4.4 in equation B.35 result in the amount of heat transfered to the material of the water walls and evaporation screen.

B.4.2. Emission correction

To calculate a value for $(\Delta\varepsilon)_g$ equation B.39 is used [53].

$$(\Delta\varepsilon)_g = \left[\frac{\zeta}{10.7+101\zeta} - 0.0089\zeta^{10.4}\right] \log_{10}\left(\frac{(p_{H_2O}+p_{CO_2})s_{eq}}{(p\,s)_0}\right)^{2.76} \tag{B.39}$$

where

$$\zeta = \frac{p_{H_2O}}{p_{H_2O}+p_{CO_2}} \tag{B.40}$$

The correction factor for the absorptivity is calculated in a similar way, but is corrected for the wall temperature.

$$(\Delta\varepsilon)_w = \left[\frac{\zeta}{10.7+101\zeta} - 0.0089\zeta^{10.4}\right] \log_{10}\left(\frac{(p_{H_2O}+p_{CO_2})s_{eq}\cdot\frac{T_{wall}}{T_g}}{(p\,s)_0}\right)^{2.76} \tag{B.41}$$

For both equations holds that $(p\,s)_0 = 0.01\,\text{m bar}$.

B.4.3. The emissivity and absorptivity of CO_2

$$\varepsilon_{CO_2} = Z - \sum_{i=1}^{6} a_i\, e^{-k_i\, p_{CO_2}\, s_{eq}} \tag{B.42}$$

where:

$$Z = \begin{bmatrix} 0.27769 \\ 0.03869 \\ 1.4249\cdot10^{-5} \end{bmatrix} \cdot \begin{bmatrix} 1 \\ \frac{T_g}{1000\,\text{K}} \\ \left(\frac{T_g}{1000\,\text{K}}\right)^2 \end{bmatrix}, \quad \vec{k} = \begin{bmatrix} 0.036 \\ 0.3586 \\ 3.06 \\ 14.76 \\ 102.28 \\ 770.6 \end{bmatrix} \tag{B.43}$$

where

$$\vec{a} = \begin{bmatrix} 0.1074 & -0.10705 & 0.072727 \\ 0.027237 & 0.10127 & -0.04377 \\ 0.058438 & -0.00121 & 0.000656 \\ 0.019078 & 0.037609 & -0.01542 \\ 0.056993 & -0.025412 & 0.002617 \\ 0.002801 & 0.038826 & 0.020198 \end{bmatrix} \cdot \begin{bmatrix} 1 \\ \frac{T_g}{1000\,\text{K}} \\ \left(\frac{T_g}{1000\,\text{K}}\right)^2 \end{bmatrix} \tag{B.44}$$

The absorptivity A_{v,CO_2} is found by using T_{wall} instead of T_g in equation B.43 and B.44. These equations are valid for a total gas pressure of 1 bar, a partial pressure of $0.01\,\text{m bar} < p_{CO_2}\, s_{eq} < 10\,\text{m bar}$ and $300\,\text{K} < T_g < 1800\,\text{K}$.

B.4.4. The emissivity and absorptivity of H_2O

$$\varepsilon_{H_2O} = Z - a\, e^{-k\, p_{H_2O}\, s_{eq}} \tag{B.45}$$

with

$$Z = \begin{bmatrix} 0.66439 \\ -0.17389 \end{bmatrix} \cdot \begin{bmatrix} 1 \\ \frac{T_g}{1000\,\text{K}} \end{bmatrix}, \quad a = \begin{bmatrix} 0.4572 \\ -0.1317 \end{bmatrix} \cdot \begin{bmatrix} 1 \\ \frac{T_g}{1000\,\text{K}} \end{bmatrix} \text{ and } \quad k = 0.84652 \tag{B.46}$$

The absorptivity A_{v,H_2O} is found by using T_{wall} instead of T_g in equation B.46. These equations are valid for a total gas pressure of 1 bar, a partial pressure of $0.5\,\text{m bar} < p_{H_2O}\, s_{eq} < 0.5\,\text{m bar}$ and $700\,\text{K} < T_g < 1500\,\text{K}$.

C

Set of Ordinary Differential Equations used in the dynamic model

The oridnary differential equations set up in section 6.3 are collected in matrices. The mass conservation equations are all of the form $\mathbf{A} \cdot \vec{m} = \vec{0}$ and are shown in section C.1.1. The conservation equations of energy are of the form $\mathbf{A} \cdot \vec{m} + \vec{Q} = \frac{d\vec{U}}{dt}$ and are shown in section C.1.2.

C.1. Overview

C.1.1. ODE system of mass

Superheater II

$$\begin{bmatrix} 1 & -1 & 0 & 0 & 0 \\ 0 & 1 & -1 & 0 & 0 \\ 0 & 0 & 1 & -1 & 0 \\ 0 & 0 & 0 & 1 & -1 \end{bmatrix} \cdot \begin{bmatrix} \dot{m}_{SHII,fg,1} \\ \dot{m}_{SHII,fg,2} \\ \dot{m}_{SHII,fg,3} \\ \dot{m}_{SHII,fg,4} \\ \dot{m}_{SHII,fg,5} \end{bmatrix} = \vec{0} \tag{C.1}$$

$$\begin{bmatrix} -1 & 1 & 0 & 0 & 0 \\ 0 & -1 & 1 & 0 & 0 \\ 0 & 0 & -1 & 1 & 0 \\ 0 & 0 & 0 & -1 & 1 \end{bmatrix} \cdot \begin{bmatrix} \dot{m}_{SHII,w,1} \\ \dot{m}_{SHII,w,2} \\ \dot{m}_{SHII,w,3} \\ \dot{m}_{SHII,w,4} \\ \dot{m}_{SHII,w,5} \end{bmatrix} = \vec{0} \tag{C.2}$$

Superheater I

$$\begin{bmatrix} 1 & -1 & 0 & 0 & 0 & 0 & 0 & 0 & 0 \\ 0 & 1 & -1 & 0 & 0 & 0 & 0 & 0 & 0 \\ 0 & 0 & 1 & -1 & 0 & 0 & 0 & 0 & 0 \\ 0 & 0 & 0 & 1 & -1 & 0 & 0 & 0 & 0 \\ 0 & 0 & 0 & 0 & 1 & -1 & 0 & 0 & 0 \\ 0 & 0 & 0 & 0 & 0 & 1 & -1 & 0 & 0 \\ 0 & 0 & 0 & 0 & 0 & 0 & 1 & -1 & 0 \\ 0 & 0 & 0 & 0 & 0 & 0 & 0 & 1 & -1 \end{bmatrix} \cdot \begin{bmatrix} \dot{m}_{SHI,fg,1} \\ \dot{m}_{SHI,fg,2} \\ \dot{m}_{SHI,fg,3} \\ \dot{m}_{SHI,fg,4} \\ \dot{m}_{SHI,fg,5} \\ \dot{m}_{SHI,fg,6} \\ \dot{m}_{SHI,fg,7} \\ \dot{m}_{SHI,fg,8} \\ \dot{m}_{SHI,fg,9} \end{bmatrix} = \vec{0} \tag{C.3}$$

$$\begin{bmatrix} -1 & 1 & 0 & 0 & 0 & 0 & 0 & 0 & 0 \\ 0 & -1 & 1 & 0 & 0 & 0 & 0 & 0 & 0 \\ 0 & 0 & -1 & 1 & 0 & 0 & 0 & 0 & 0 \\ 0 & 0 & 0 & -1 & 1 & 0 & 0 & 0 & 0 \\ 0 & 0 & 0 & 0 & -1 & 1 & 0 & 0 & 0 \\ 0 & 0 & 0 & 0 & 0 & -1 & 1 & 0 & 0 \\ 0 & 0 & 0 & 0 & 0 & 0 & -1 & 1 & 0 \\ 0 & 0 & 0 & 0 & 0 & 0 & 0 & -1 & 1 \end{bmatrix} \cdot \begin{bmatrix} \dot{m}_{SHI,w,1} \\ \dot{m}_{SHI,w,2} \\ \dot{m}_{SHI,w,3} \\ \dot{m}_{SHI,w,4} \\ \dot{m}_{SHI,w,5} \\ \dot{m}_{SHI,w,6} \\ \dot{m}_{SHI,w,7} \\ \dot{m}_{SHI,w,8} \\ \dot{m}_{SHI,w,9} \end{bmatrix} = \vec{0} \tag{C.4}$$

Evaporator

Desuperheater and Duct Burner

$$\begin{bmatrix} -1 & 1 & 1 & 0 & 0 \\ 0 & 0 & 0 & 1 & -1 \end{bmatrix} \cdot \begin{bmatrix} \dot{m}_{DSH,w,in} \\ \dot{m}_{DSH,w,add} \\ \dot{m}_{DSH,w,out} \\ \dot{m}_{DB,w,1} \\ \dot{m}_{DB,w,2} \end{bmatrix} = \vec{0} \tag{C.5}$$

C.1.2. ODE system of energy

The ODE systems are all of the form $A \cdot \vec{m} + \vec{Q} = \frac{\vec{dU}}{dt}$.

Superheater II

$$\mathbf{A}_{SHII,fg} = \begin{bmatrix} h_{SHII,fg,1} & -h_{SHII,fg,2} & 0 & 0 & 0 \\ 0 & h_{SHII,fg,2} & -h_{SHII,fg,3} & 0 & 0 \\ 0 & 0 & h_{SHII,fg,3} & -h_{SHII,fg,4} & 0 \\ 0 & 0 & 0 & h_{SHII,fg,4} & -h_{SHII,fg,5} \end{bmatrix}$$

$$\vec{m}_{SHII,fg} = \begin{bmatrix} \dot{m}_{SHII,fg,1} \\ \dot{m}_{SHII,fg,2} \\ \dot{m}_{SHII,fg,3} \\ \dot{m}_{SHII,fg,4} \\ \dot{m}_{SHII,fg,5} \end{bmatrix}, \quad \vec{Q}_{SHII,fg} = \begin{bmatrix} \dot{Q}_{SHII,fg,c1} \\ \dot{Q}_{SHII,fg,c2} \\ \dot{Q}_{SHII,fg,c3} \\ \dot{Q}_{SHII,fg,c4} \end{bmatrix}, \quad \frac{\vec{dU}}{dt}_{SHII,fg} = \begin{bmatrix} \frac{dU}{dt}_{SHII,fg,2} \\ \frac{dU}{dt}_{SHII,fg,3} \\ \frac{dU}{dt}_{SHII,fg,4} \\ \frac{dU}{dt}_{SHII,fg,5} \end{bmatrix}$$

$$\mathbf{A}_{SHII,w} = \begin{bmatrix} -h_{S-hII,w,1} & h_{S-hII,w,2} & 0 & 0 & 0 \\ 0 & -h_{S-hII,w,2} & h_{S-hII,w,3} & 0 & 0 \\ 0 & 0 & -h_{S-hII,w,3} & h_{S-hII,w,4} & 0 \\ 0 & 0 & 0 & -h_{S-hII,w,4} & h_{S-hII,w,5} \end{bmatrix}$$

$$\vec{m}_{SHII,w} = \begin{bmatrix} \dot{m}_{SHII,w,1} \\ \dot{m}_{SHII,w,2} \\ \dot{m}_{SHII,w,3} \\ \dot{m}_{SHII,w,4} \\ \dot{m}_{SHII,w,5} \end{bmatrix}, \quad \vec{Q}_{SHII,w} = \begin{bmatrix} \dot{Q}_{SHII,w,c1} \\ \dot{Q}_{SHII,w,c2} \\ \dot{Q}_{SHII,w,c3} \\ \dot{Q}_{SHII,w,c4} \end{bmatrix}, \quad \frac{\vec{dU}}{dt}_{SHII,w} = \begin{bmatrix} \frac{dU}{dt}_{SHII,w,1} \\ \frac{dU}{dt}_{SHII,w,2} \\ \frac{dU}{dt}_{SHII,w,3} \\ \frac{dU}{dt}_{SHII,w,4} \end{bmatrix}$$

Superheater I

$$\mathbf{A}_{SHI,fg} = \begin{bmatrix} h_{SHI,fg,1} & -h_{SHI,fg,2} & 0 & 0 & 0 & 0 & 0 & 0 & 0 \\ 0 & h_{SHI,fg,2} & -h_{SHI,fg,3} & 0 & 0 & 0 & 0 & 0 & 0 \\ 0 & 0 & h_{SHI,fg,3} & -h_{SHI,fg,4} & 0 & 0 & 0 & 0 & 0 \\ 0 & 0 & 0 & h_{SHI,fg,4} & -h_{SHI,fg,5} & 0 & 0 & 0 & 0 \\ 0 & 0 & 0 & 0 & h_{SHI,fg,5} & -h_{SHI,fg,6} & 0 & 0 & 0 \\ 0 & 0 & 0 & 0 & 0 & h_{SHI,fg,6} & -h_{SHI,fg,7} & 0 & 0 \\ 0 & 0 & 0 & 0 & 0 & 0 & h_{SHI,fg,7} & -h_{SHI,fg,8} & 0 \\ 0 & 0 & 0 & 0 & 0 & 0 & 0 & h_{SHI,fg,8} & \end{bmatrix}$$

$$\vec{\dot{m}}_{SHI,fg} = \begin{bmatrix} \dot{m}_{SHI,fg,1} \\ \dot{m}_{SHI,fg,2} \\ \dot{m}_{SHI,fg,3} \\ \dot{m}_{SHI,fg,4} \\ \dot{m}_{SHI,fg,5} \\ \dot{m}_{SHI,fg,6} \\ \dot{m}_{SHI,fg,7} \\ \dot{m}_{SHI,fg,8} \\ \dot{m}_{SHI,fg,9} \end{bmatrix}, \quad \vec{\dot{Q}}_{SHI,fg} = \begin{bmatrix} \dot{Q}_{SHI,fg,c1} \\ \dot{Q}_{SHI,fg,c2} \\ \dot{Q}_{SHI,fg,c3} \\ \dot{Q}_{SHI,fg,c4} \\ \dot{Q}_{SHI,fg,c5} \\ \dot{Q}_{SHI,fg,c6} \\ \dot{Q}_{SHI,fg,c7} \\ \dot{Q}_{SHI,fg,c8} \end{bmatrix}, \quad \frac{d\vec{U}}{dt}_{SHI,fg} = \begin{bmatrix} \frac{dU}{dt}_{SHI,fg,2} \\ \frac{dU}{dt}_{SHI,fg,3} \\ \frac{dU}{dt}_{SHI,fg,4} \\ \frac{dU}{dt}_{SHI,fg,5} \\ \frac{dU}{dt}_{SHI,fg,6} \\ \frac{dU}{dt}_{SHI,fg,7} \\ \frac{dU}{dt}_{SHI,fg,8} \\ \frac{dU}{dt}_{SHI,fg,9} \end{bmatrix}$$

$$\mathbf{A}_{SHI,w} = \begin{bmatrix} -h_{SHI,w,1} & h_{SHI,w,2} & 0 & 0 & 0 & 0 & 0 & 0 & 0 \\ 0 & -h_{SHI,w,2} & h_{SHI,w,3} & 0 & 0 & 0 & 0 & 0 & 0 \\ 0 & 0 & -h_{SHI,w,3} & h_{SHI,w,4} & 0 & 0 & 0 & 0 & 0 \\ 0 & 0 & 0 & -h_{SHI,w,4} & h_{SHI,w,5} & 0 & 0 & 0 & 0 \\ 0 & 0 & 0 & 0 & -h_{SHI,w,5} & h_{SHI,w,6} & 0 & 0 & 0 \\ 0 & 0 & 0 & 0 & 0 & -h_{SHI,w,6} & h_{SHI,w,7} & 0 & 0 \\ 0 & 0 & 0 & 0 & 0 & 0 & -h_{SHI,w,7} & h_{SHI,w,8} & 0 \\ 0 & 0 & 0 & 0 & 0 & 0 & 0 & -h_{SHI,w,8} & h_{SHI,w,9} \end{bmatrix}$$

$$\vec{\dot{m}}_{SHI,w} = \begin{bmatrix} \dot{m}_{SHI,w,1} \\ \dot{m}_{SHI,w,2} \\ \dot{m}_{SHI,w,3} \\ \dot{m}_{SHI,w,4} \\ \dot{m}_{SHI,w,5} \\ \dot{m}_{SHI,w,6} \\ \dot{m}_{SHI,w,7} \\ \dot{m}_{SHI,w,8} \\ \dot{m}_{SHI,w,9} \end{bmatrix}, \quad \vec{\dot{Q}}_{SHI,w} = \begin{bmatrix} \dot{Q}_{SHI,w,c1} \\ \dot{Q}_{SHI,w,c2} \\ \dot{Q}_{SHI,w,c3} \\ \dot{Q}_{SHI,w,c4} \\ \dot{Q}_{SHI,w,c5} \\ \dot{Q}_{SHI,w,c6} \\ \dot{Q}_{SHI,w,c7} \\ \dot{Q}_{SHI,w,c8} \end{bmatrix}, \quad \frac{d\vec{U}}{dt}_{SHI,w} = \begin{bmatrix} \frac{dU}{dt}_{SHI,w,1} \\ \frac{dU}{dt}_{SHI,w,2} \\ \frac{dU}{dt}_{SHI,w,3} \\ \frac{dU}{dt}_{SHI,w,4} \\ \frac{dU}{dt}_{SHI,w,5} \\ \frac{dU}{dt}_{SHI,w,6} \\ \frac{dU}{dt}_{SHI,w,7} \\ \frac{dU}{dt}_{SHI,w,8} \end{bmatrix}$$

Desuperheater

$$\begin{bmatrix} -h_{DSH,w,in} & -h_{DSH,w,add} & -h_{DSH,w,out} \end{bmatrix} \begin{bmatrix} \dot{m}_{DSH,w,in} \\ \dot{m}_{DSH,w,add} \\ \dot{m}_{DSH,w,out} \end{bmatrix} + \vec{0} = \vec{0}$$

Duct Burner

$$\begin{bmatrix} h_{DB,fg,1} & -h_{DB,fg,2} & 0 & H \\ 0 & h_{DB,fg,2} & -h_{DB,fg,3} & 0 \end{bmatrix} \cdot \begin{bmatrix} \dot{m}_{DB,fg,1} \\ \dot{m}_{DB,fg,2} \\ \dot{m}_{DB,fg,3} \\ \dot{m}_{DB,fuel} \end{bmatrix} + \begin{bmatrix} 0 \\ \dot{Q}_{fg,1} \end{bmatrix} = \vec{0}$$

D

PI-controller

The temperature at the exit of SHII is controlled by the added mass flow in the desuperheater $\dot{m}_{DSH}$. In the model, a feedback loop with a Proportional Integral (PI) controller will determine the mass flow, its set up is shown in figure D.1. In this model the reference signal r is not time dependent and will be kept constant

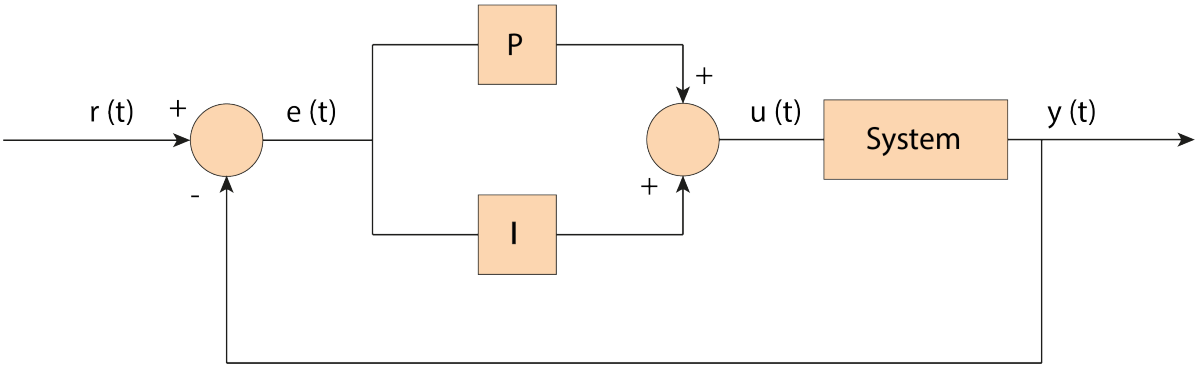

Figure D.1: PI controller

at 505 °C . $\hat{y}$ is the output signal after it has been filtered and does depend on time. The error between the reference signal and the filtered output signal is described with equation D.1.

$$e(t) = r - \hat{y}(t) \tag{D.1}$$

D.0.1. Gains of the PI controller

The PI controller consists of a Proportional, an Integral, and a Derivative component in parallel, see figure D.1. The Proportional Component evaluates the absolute error (equation D.2). The Integral component assesses the time the error exists (equation D.3). In this way, even if a continuous error is small it can be acted upon. The Derivative term does assess the rate of change of the error, and will work to minimise this rate. These three terms in parallel result in the control output signal of equation D.4.

$$P = K_p\, e(t) \tag{D.2}$$

$$P = K_i \int_0^t e(t^*)\, dt^* \tag{D.3}$$

$$u(t) = K_p\, e(t) + K_i \int_0^t e(t^*)\, dt^* \tag{D.4}$$

The discrete form of equation D.4 used in the dynamic model is given in equation D.5. For the purpose of the desuperheater a proportional gain of $K_p = 1$ and an integral gain of $K_i = 1$ is used.

$$u^n = K_p\, e^n + K_i \Delta t \sum_{j=1}^{n} e^j \tag{D.5}$$

E

Results of the dynamic model

E.1. Time derivative of the header temperature

E.1.1. Air preheater

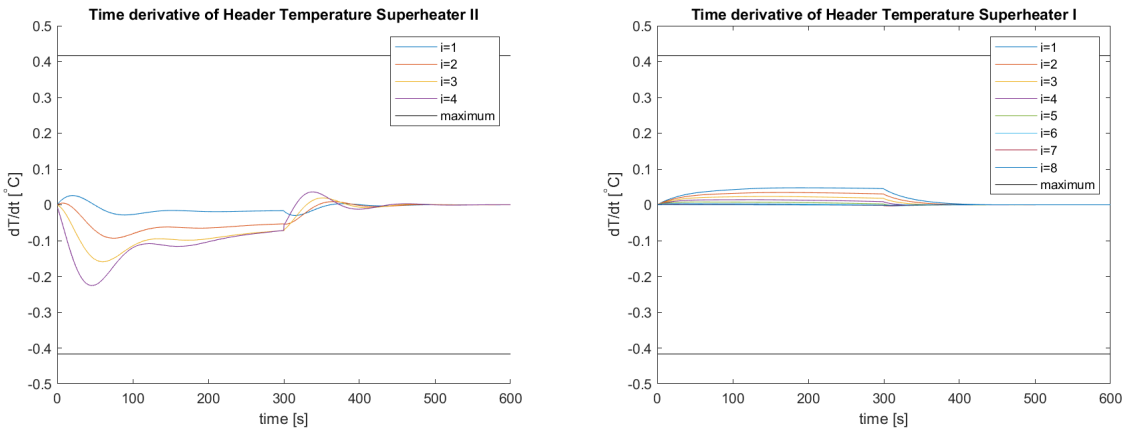

(a) Superheater II

(b) Superheater I

Figure E.1: Time derivative of the temperature of the steam in the headers of superheater II and superheater I at a ramp up time of the AP of 5 minutes

E.1.2. Duct heater

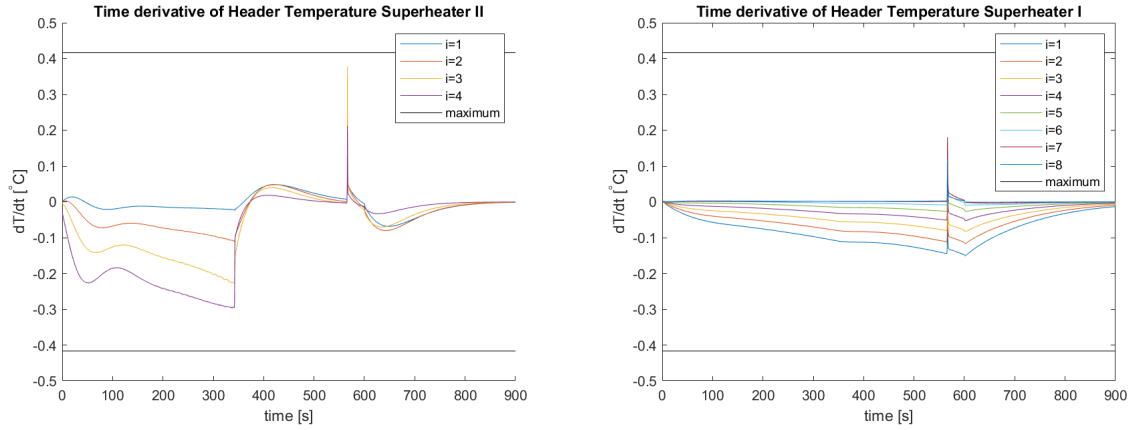

(a) Superheater II **(b)** Superheater I

Figure E.2: Time derivative of the temperature of the steam in the headers of superheater II and superheater I at a ramp up time of the DH of 10 minutes

E.1.3. Stand-alone boiler

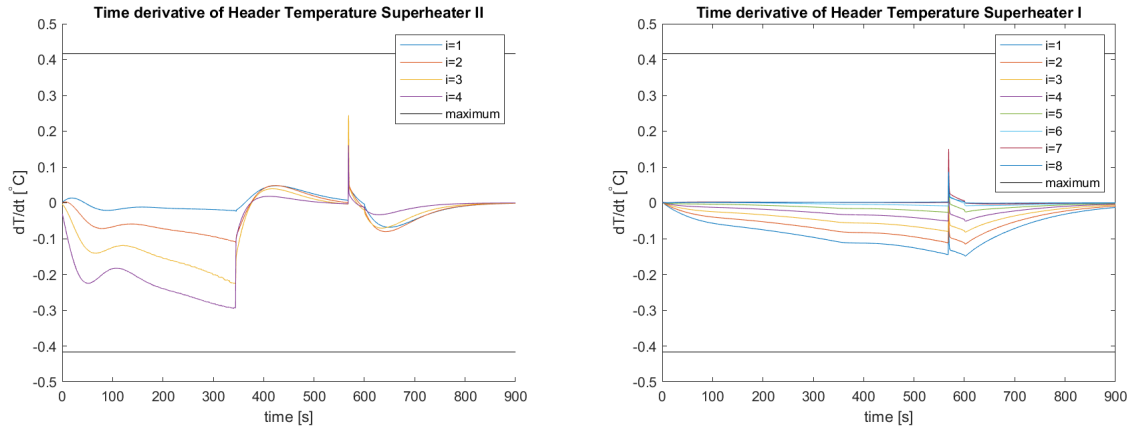

(a) Superheater II **(b)** Superheater I

Figure E.3: Time derivative of the temperature of the steam in the headers of superheater II and superheater I at a ramp up time of the SB of 10 minutes

E.1.4. Air preheater - duct heater

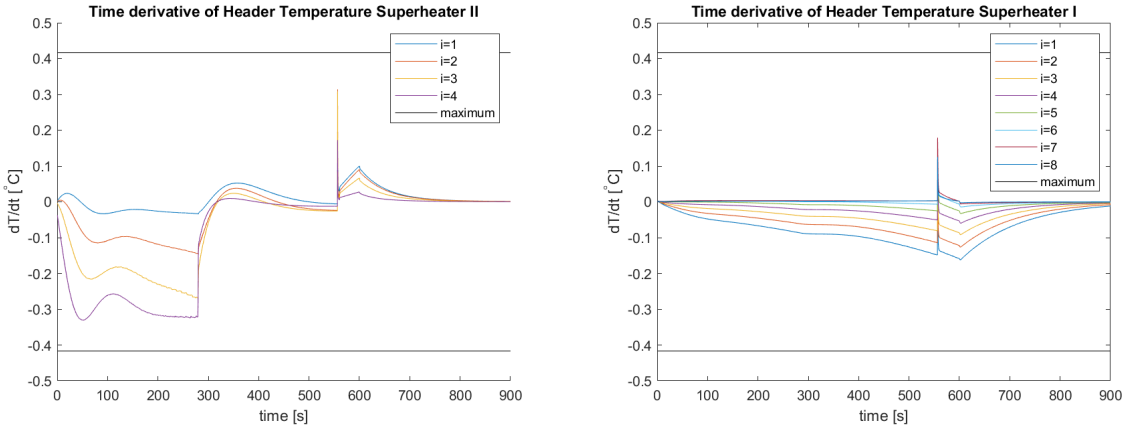

(a) Superheater II

(b) Superheater I

Figure E.4: Time derivative of the temperature of the steam in the headers of superheater II and superheater I at a ramp up time of the APDH of 10 minutes

E.1.5. Air preheater - high pressure boiler

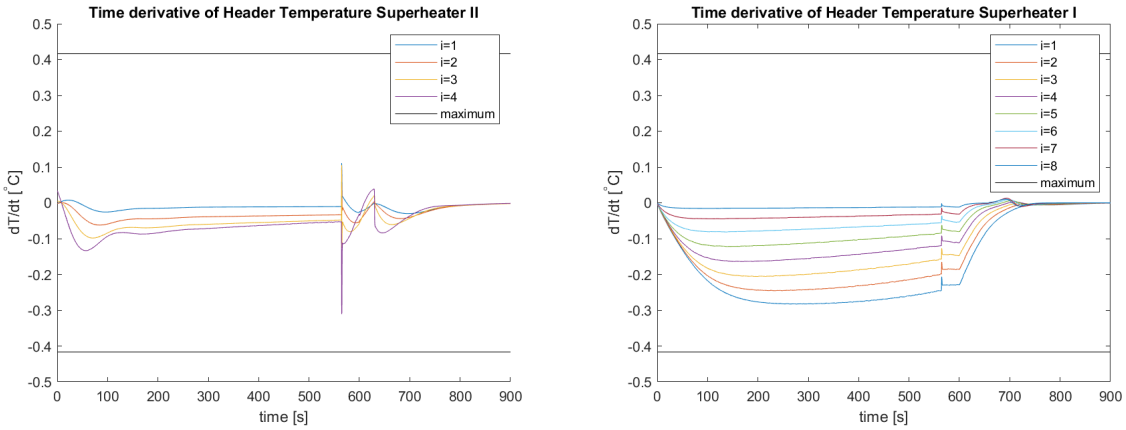

(a) Superheater II

(b) Superheater I

Figure E.5: Time derivative of the temperature of the steam in the headers of superheater II and superheater I at a ramp up time of the APHPB of 10 minutes

E.1.6. Air preheater - Stand-alone boiler

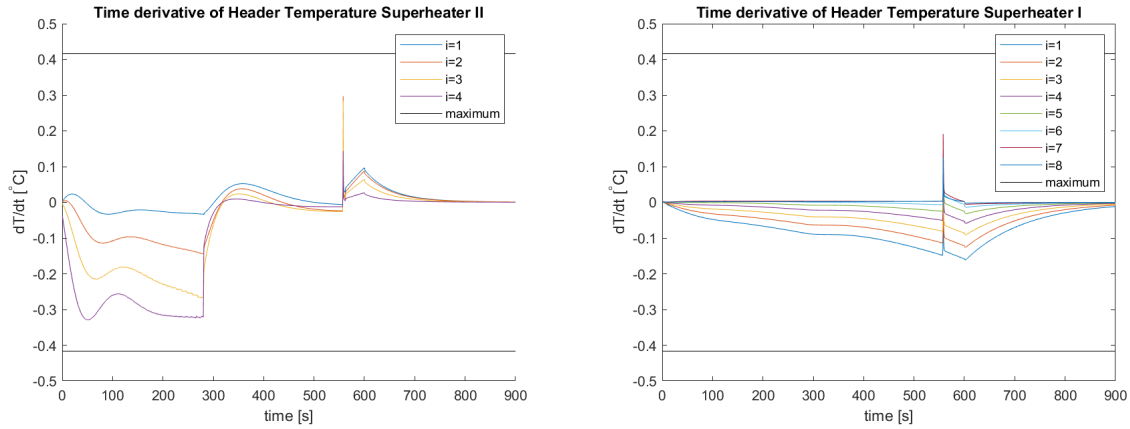

(a) Superheater II **(b)** Superheater I

Figure E.6: Time derivative of the temperature of the steam in the headers of superheater II and superheater I at a ramp up time of the APSB of 10 minutes

E.2. Coil-to-coil temperature difference

E.2.1. Air preheater

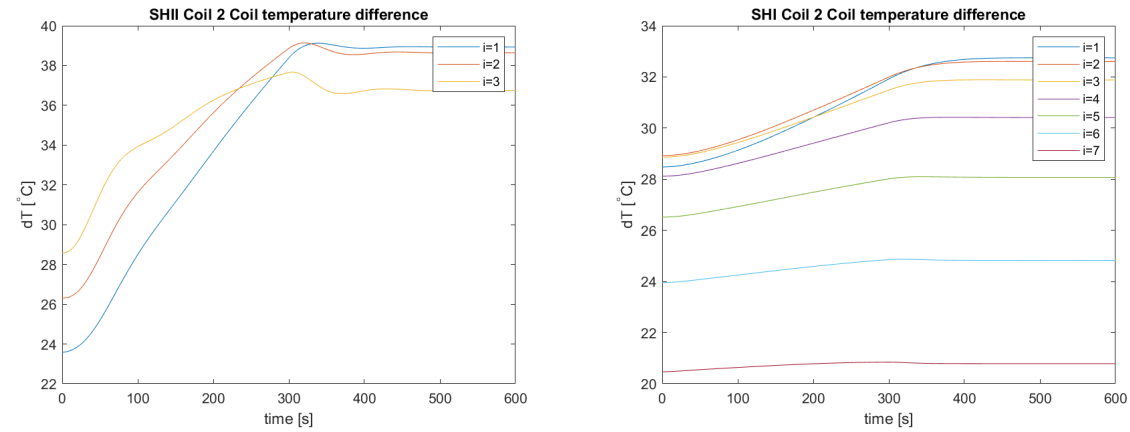

(a) Superheater II **(b)** Superheater I

Figure E.7: Coil-to-coil temperature difference over time of the superheater II and superheater I at a ramp up time of the AP of 5 minutes

E.2.2. Duct heater

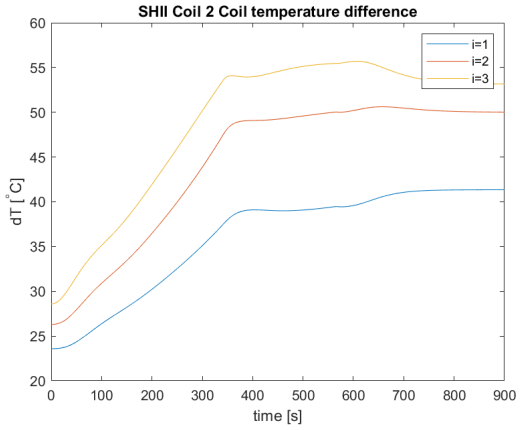

(a) Superheater II

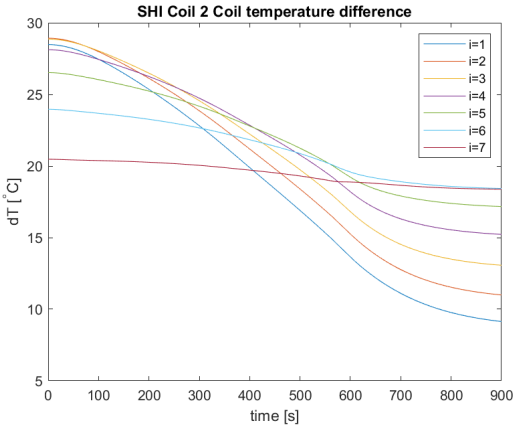

(b) Superheater I

Figure E.8: Coil-to-coil temperature difference over time of the superheater II and superheater I at a ramp up time of the DH of 10 minutes

E.2.3. Stand-alone boiler

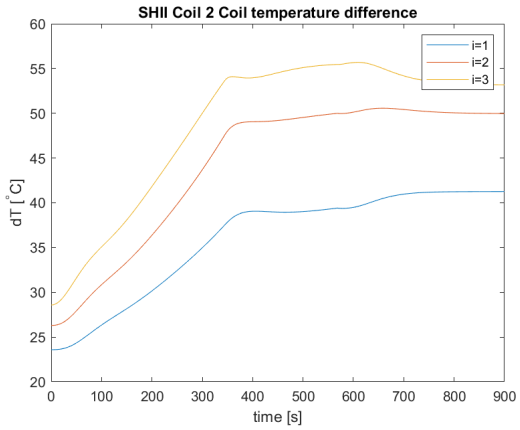

(a) Superheater II

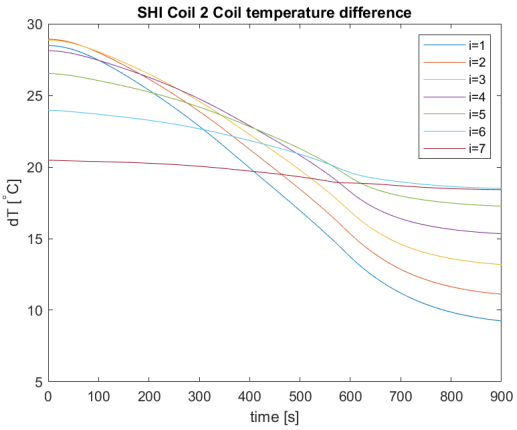

(b) Superheater I

Figure E.9: Coil-to-coil temperature difference over time of the superheater II and superheater I at a ramp up time of the SB of 10 minutes

E.2.4. Air preheater - duct heater

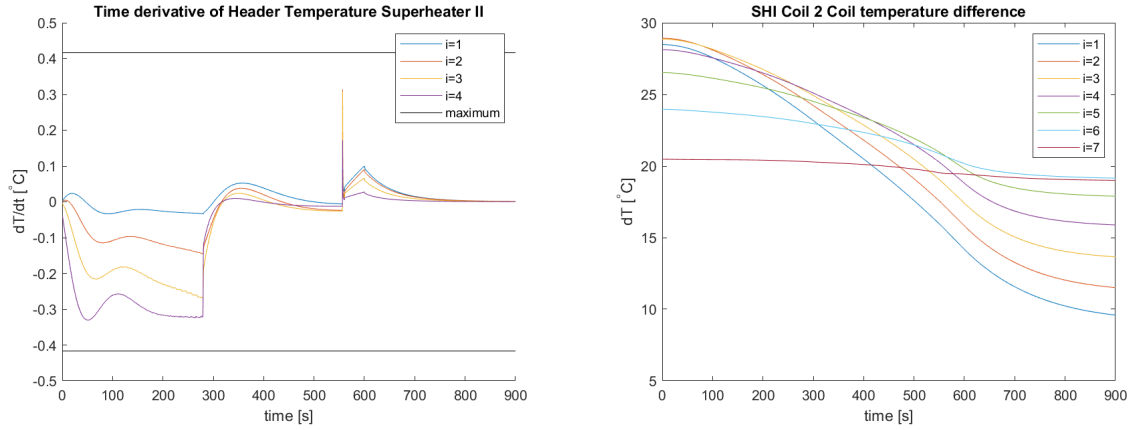

(a) Superheater II **(b)** Superheater I

Figure E.10: Coil-to-coil temperature difference over time of the superheater II and superheater I at a ramp up time of the APDH of 10 minutes

E.2.5. Air preheater - high pressure boiler

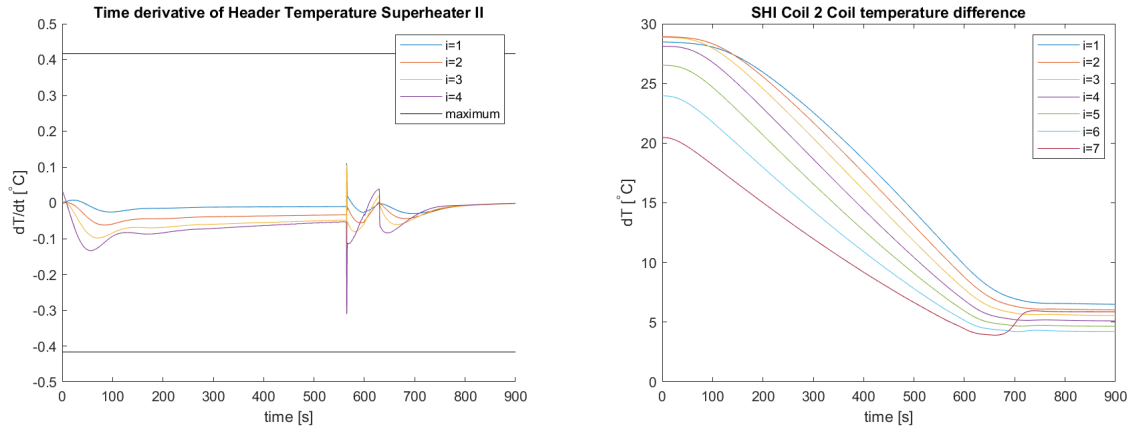

(a) Superheater II **(b)** Superheater I

Figure E.11: Coil-to-coil temperature difference over time of the superheater II and superheater I at a ramp up time of the APHPB of 10 minutes

E.2.6. Air preheater - Stand-alone boiler

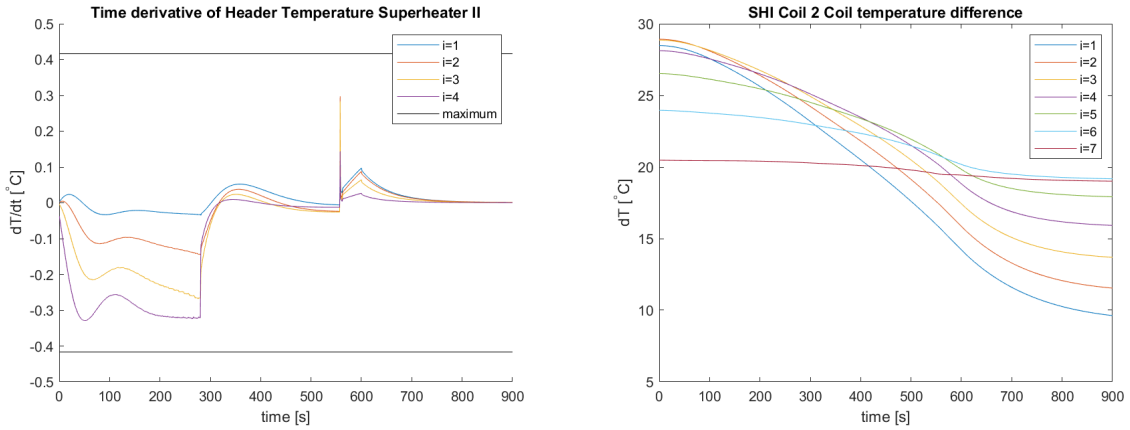

(a) Superheater II

(b) Superheater I

Figure E.12: Coil-to-coil temperature difference over time of the superheater II and superheater I at a ramp up time of the APSB of 10 minutes

F

Financial summary of the electric heaters

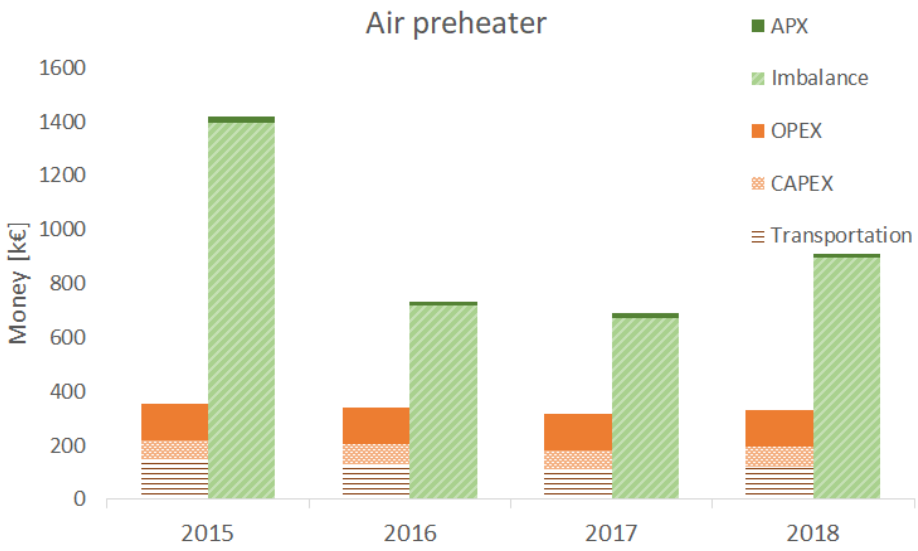

Figure F.1: Approximated income and expenses for the air preheater from 2015 to 2018

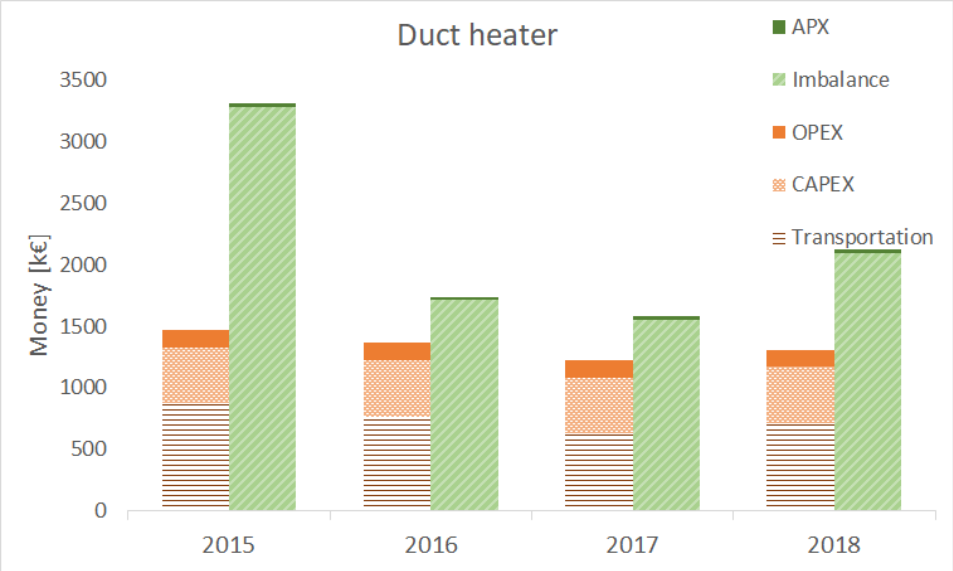

Figure F.2: Approximated income and expenses for the duct heater from 2015 to 2018

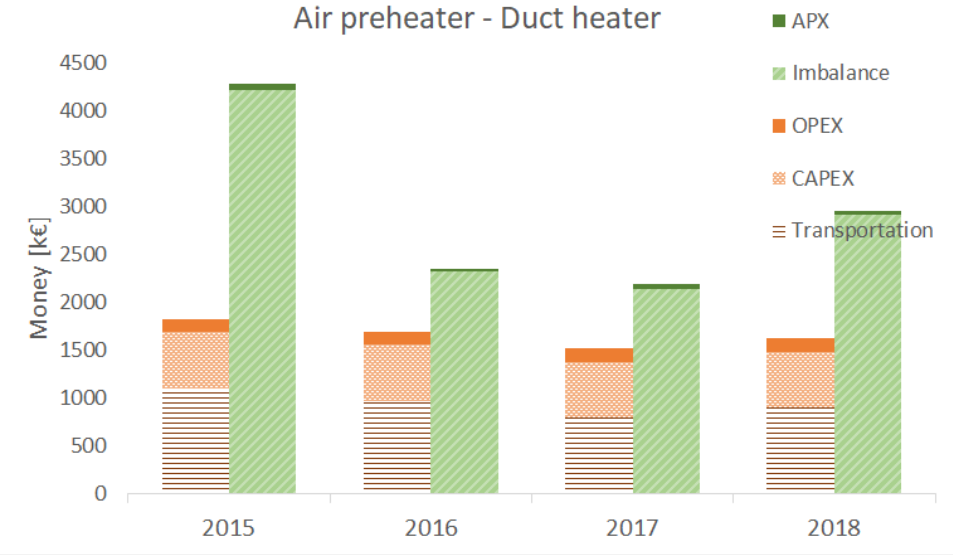

Figure F.3: Approximated income and expenses for the air preheater - duct heater from 2015 to 2018

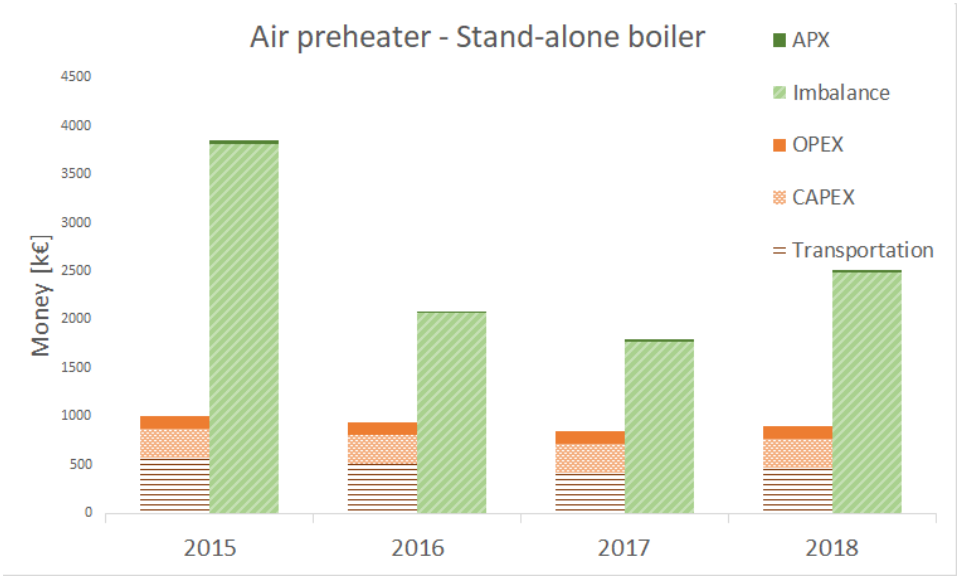

Figure F.4: Approximated income and expenses for the air preheater - stand-alone boiler from 2015 to 2018